NASA CR-137471

APPLIED SCIENCE ASSOCIATES, INC.

105 EAST CHATHAM STREET
POST OFFICE BOX 949
APEX, NORTH CAROLINA 27502
PHONE (919) 362-7256

GULF STREAM MODEL

FINAL REPORT
September, 1974

Prepared Under

NASA CONTRACT NO. NAS6-2307

for

NATIONAL AERONAUTICS AND SPACE ADMINISTRATION

WALLOPS STATION

WALLOPS ISLAND, VIRGINIA 23337

FOREWORD

This report was prepared for the National Aeronautics and Space Administration by the Applied Science Associates, Inc., under Contract NAS6-2307. C. D. Leitao acted as NASA coordinator.

The study was performed at Applied Science Associates, Inc. N. E. Huang served as project director. Professor L. J. Pietrafesa of the North Carolina State University at Raleigh served as consultant and contributed heavily to this report. Mr. J. H. Boone and Mrs. N. Beyer also assisted in the study.

ABSTRACT

This report presents the results of the study of surface elevation deviations in the Gulf Stream region off the eastern coast of the United States between Wallops Island, Virginia and Miami, Florida. The main causes of surface elevation deviations are geoid perturbations due to the continental shelf and the geostrophic adjustment of the density field due to the Gulf Stream. Quantitative surface elevation profiles were calculated based on geophysical measurements of gravity anomalies and hydrographic data. The results are presented graphically along with contemporaneous weather data. Comparisons are made between the profiles based on hydrographic data and a mean theoretical model. The agreement is generally good. The theory of geostrophic flows including some classical Gulf Stream models is also presented briefly.

CONTENTS

1. INTRODUCTION AND SUMMARY OF RESULTS

1.1 INTRODUCTION

The objectives of the Gulf Stream model study are (a) to find out the locations and magnitudes of surface elevation deviations due to water movement and other causes, (b) to use such results to interpret the satellite altimeter data, and finally, (c) to calculate water movement based solely on satellite altimeter measurements. Due to the limiting scope of the present phase of the study, this report presents the results of a study of surface elevation deviation due to water movement and gravity anomalies along the Gulf Stream between Miami, Florida, and Wallops Island, Virginia.

In Chapter 2, a brief discussion of the relation between surface elevation deviation and the water movement is presented. This includes theory of geostrophic flow, numerical procedure used to calculate the surface elevation based on hydrographic data, classical Gulf Stream models, and a mean numerical model of the Gulf Stream using all the existing hydrographic data in the North Atlantic Ocean.

Chapter 3 presents all of the surface elevation profiles calculated by the method discussed in Chapter 2 and based on data published by the National Oceanographic Data Center, NOAA, covering all of the ship bound surveys from 1912 to 1972. Together with the profiles, wind data are presented whenever available. The profiles are also compared with the results of the mean numerical model of the Gulf Stream. The agreement is generally, and in a mean sense, good.

Chapter 4 deals with the calculation of geoid perturbation at the continental shelf. Due to the lack of data, an approximation method has been used. The procedures of approximation, calculation and the results are presented.

1.2 CONCLUSIONS

The results of this study indicate that:

(a) A mean Gulf Stream model can be constructed but such a model can only be used as an estimate of the location and the strength of the Gulf Stream. Individual cases may deviate substantially from such a model by perhaps 100% in strength as a result of seasonal fluctuations and also due to local meteorological conditions.

(b) The mean location of the Gulf Stream south of Cape Hatteras generally follows the continental shelf break where large geoid perturbations exist due to the continental rise. The change of the geoid elevation varies from one location to another, but, in general, the magnitude is larger than that produced by the Gulf Stream. However, the location and the magnitude of the geoid perturbation are fixed in space and time. Such features can be easily filtered out of observational data.

(c) Due to the high mobility of the Gulf Stream, shipbound surveys alone are definitely insufficient to determine the nature of the motion. Remote sensing methods have to be used, not in lieu of, but rather in complement to the standard hydrographic method.

2. THEORY AND CALCULATION OF DYNAMIC HEIGHTS AND GULF STREAM MODELS

2.1 INTRODUCTION

The distribution of temperature, salt, density and pressure within and motion of any body or part therein of water is approximately governed by a system of seven non-linear partial differential equations, i.e.,

$$\rho\frac{\partial u_i}{\partial t} + \rho u_j \frac{\partial u_i}{\partial x_j} + 2\rho\,\varepsilon_{ijk}\Omega_j u_k = -\frac{\partial p}{\partial x_i} - g\rho\delta_{3i} + \frac{\partial}{\partial x_j}\left\{\mu\left(\frac{\partial u_j}{\partial x_i} + \frac{\partial u_i}{\partial x_j}\right)\right\} \quad (2.1,2,3)$$

$$\frac{\partial u_j}{\partial x_j} = 0 \quad (2.4)$$

$$\frac{\partial S}{\partial t} + u_j\frac{\partial S}{\partial x_j} = \frac{\partial}{\partial x_j}\left(D_{ij}\frac{\partial S}{\partial x_i}\right) \quad (2.5)$$

$$\frac{\partial T}{\partial t} + u_j\frac{\partial T}{\partial x_j} = \frac{\partial}{\partial x_j}\left(K_{ij}\frac{\partial T}{\partial x_i}\right) \quad (2.6)$$

$$\rho = \rho_0\,(1 + \beta S - \alpha T) \quad (2.7)$$

where u is the velocity, Ω the earth's rotational vector, P the pressure, g the gravitation acceleration, ρ the density, δ_{3i} the Kronecker delta, S the salinity, T the temperature, μ the molecular viscosity, ε the cyclic tensor, D the eddy diffusivity, K the eddy conductivity, α the coefficient of thermal expansion, β the coefficient of volumetric expansion and the subscripts i, j, k are each equal to 1, 2 and 3. These equations describe the behavior of a baroclinic fluid in an arbitrarily shaped basin on a spherical earth with boundary, bottom, side and surface, conditions which are consistent with the physical effects and subsequent constraints of the surrounding environment.

The complete system of equations (2.1 through 2.7) is impossible to solve given the present state of mathematical art. Under certain conditions however, simplifications based on appropriate physical considerations can be made to reduce the equations to a more manageable, tractible form. In the case of major ocean current systems, the motions are rather steady and to a lower order approximation, it can be assumed that the ratio of the non-linear acceleration to the rotational force, i.e., the vertical component of relative vorticity, is rather small. Since molecular friction and vertical accelerations can always be neglected in the steady state and furthermore because we may assume that turbulent stresses change slowly over distances which are short compared to the characteristic length of the flow, then we are permitted to simulate a particular class of motions called "geostrophic currents." As long as the current system under investigation is not in a lateral frictional boundary layer, where sharp horizontal gradients of velocity can be generated or in either one or two vertical frictional boundary layers which include strong vertical velocity gradients, the geostrophic assumption can yield useful approximations to the actual current system. In such cases, the governing momentum equations (the reduced Navier-Stokes' system) become:

$$\rho (\underset{\sim}{\Omega} \times \underset{\sim}{v}) = - \nabla_H p \quad , \tag{2.8}$$

$$\frac{\partial p}{\partial z} = - g \rho \quad , \qquad \text{and} \tag{2.9}$$

$$\nabla \cdot \underset{\sim}{v} = 0 \quad , \tag{2.10}$$

where the subscript H denotes horizontal components.

We can integrate (2.9) in z and combine with (2.8) to get

$$\underset{\sim}{\Omega} \times \underset{\sim}{v}_H = g \nabla_H \eta \tag{2.11}$$

where η is the deviation of the free surface from mean sea level. Obvious factors influencing departures of sea surface elevation from a level of constant z are implicitly evident in equation (2.11).

Initially the current field will cause the density field of sea water to adjust to the apparent rotational force. The density field adjustment can be evaluated using hydrographic data through the dynamic height method (Fomin, 1964; Neuman, 1968). In addition to geostrophic adjustment, surface slope can also change in response to gravitational anomalies, i.e., local changes in the value of the gravitational acceleration function. Gravitational anomalies can become especially significant for two reasons. Firstly, we are interested in obtaining information about the current systems based on surface slope measurements only and therefore any departures from a flat surface are interpreted as having been caused by geostrophic adjustment (or winds, etc.) if no other correction has been made. Secondly, the Gulf Stream between Florida and Cape Hatteras generally follows the continental shelf break countour which is a region of rather abrupt changes in the gravitational acceleration value and subsequently in the gravimetric geoidal height. At the continental shelf break, there are changes in depth of the order of a hundred meters to five thousand meters over horizontal distances of the order of several to several tens of kilometers.

These two facts, i.e., the existence of intense current systems along the shelf break of western oceanic boundaries, in the Northern hemisphere, coupled with the dramatic change in gravimetric geoidal height transverse to the western boundary make for extremely difficult complexities in the solution of the problem of interest to the ocean dynamicist as it is coupled to the primary problem of interest of the gravity minded marine geophysicist. Both problems, that of sea surface slope associated with winds, currents and hydrography and that of determining the crustal and subcrustal structure of the earth can be attacked

most directly and synoptically through the use of satellite imagery versus the laborious, time consuming, unsynoptic (without the co-ordinated use of several ocean research vessels) direct sea surface, single ship effort. Unfortunately the problems become coupled in actual satellite observations so that initial interpretation and future decoupling of the data are problems which must be addressed directly.

Sea level also varies along continental boundaries as well as transverse to the margins. Along the eastern Atlantic coast of the U.S., sea surface height drops approximately one-half meter between the latitudes 20°N to 40°N. It has been demonstrated (Sturges, 1974) that this meridional slope along the inshore lateral boundary of the Gulf Stream has the correct sign and magnitude to be balanced by the cross-stream gradient of the alongstream current. This is an extremely important finding concerning the dynamics of the Gulf Stream and furthermore may help to explain why sea level on the Pacific coast stands higher than that on the Atlantic coast.

Corrections for changes in the gravitational potential can result in sea surface height differences of several meters across the Gulf Stream as a function of its path. Because of the afore-mentioned complications, initial surface slope calculations will have to be based on hydrographic, current and wind data and adjusted with geophysical gravity data including Free-air, Bouguer corrections and a variety of isotatic and hydrostatic compensation adjustments.

The change of the surface height across the Gulf Stream may be of the order of one to several meters resulting in a cross-stream slope of at most 10^{-6}. This gradient is too small to be realized by conventional oceanographic methods. Consequently, previous to the introduction of remote sensing, the only sea surface work was done with tide gauges and hydrography. The data from tide gauges is direct but of itself yields only longshore slope. The hydrography data, though

difficult to obtain can be used, with appropriate reservation, to indirectly compute of sea currents and sea surface slope. This method was generated by Helland-Hansen (1903) on the basis of the Bjerknes circulation theorem (Bjerknes, 1900) and makes it possible to indicate surface topography without direct measurement. The technique was, in its initiation, accepted as truth but it must be pointed out that the so-called dynamic method cannot be used to compute the wind driven current because frictional forces that are not considered in the dynamic method, do play a role in the set-up of the pure drift currents. So, though the pure drift component of velocity maintains the sea surface slope, it cannot be computed from hydrographic methods.

In a baroclinic ocean, i.e., an ocean in which constant pressure surfaces and surfaces of constant density are allowed to intersect, the horizontal pressure gradient and current velocity become zero at some depth at and below which the baroclinic and barotropic pressure gradients become equal and opposite in magnitude and direction. This level of no motion may extend below the bottom so that the pressure gradients due to inhomogeneities in the field of mass are not in mutual compensation with the free surface slope pressure gradient. From the following equation

$$f v = \frac{g}{\rho_0} \int_{\eta}^{z} \frac{\partial \rho}{\partial x} dz - g \frac{\rho(\eta)}{\rho_0} \frac{\partial \eta}{\partial x} \quad , \tag{2.12}$$

it becomes explicitly obvious that at some depth, at which $v = 0$, the two terms on the righthand side are equal in magnitude and opposite in direction so that mutual compensation occurs.

The sections to follow explain more fully the theory and actual use of the dynamic method.

2.2 BASIC GEOSTROPHY AND THE DYNAMIC METHOD

The opposition of the pressure gradient force and the apparent rotational force, the Coriolis force, is the general dynamic constraint observed by steady flow. It is generally acknowledged that steady flow in the ocean has meaning only as an average with respect to time, especially ocean currents such as the Gulf Stream which observes an extensive range of frequencies (Fuglister, 1951, and Wertheim, 1954). Near oceanic boundaries, the geostrophic assumption breaks down since sharp horizontal and vertical velocity gradients can require lateral and vertical friction to play important dynamic roles. Still it is possible to assume geostrophy, with informed reservation in a phenomenon such as the Gulf Stream.

Vectorial gravitational acceleration can be expressed in terms of a scaler potential function. The difference in the potential function between two points lying along the vertical co-ordinate, which is aligned parallel to the direction of gravitational acceleration, is equivalent to the amount of work that it takes to move a unit mass from one point to the other point. This scaler potential function is related to the vertical spatial variable by

$$dz = \frac{1}{g}\, d\phi \quad , \text{ so that} \tag{2.13}$$

levels of constant geopotential correspond to levels of unchanging z.

In terms of the density inverse, i.e., the specific volume of sea water, the potential function can then be written as

$$d\phi = \alpha\, dp \quad , \tag{2.14}$$

by combining 2.9 and 2.13. Thus the geopotential is directly determined by the pressure and specific volumes functions, which are in multiplicative association,

in an environment where all vertical accelerations are insignificant relative to gravitational acceleration.

In the absence of winds and topographic boundaries, the equations defining geostrophic velocity are

$$-\rho f v = -\frac{\partial p}{\partial x} \quad \text{and} \tag{2.15}$$

$$+\rho f u = -\frac{\partial p}{\partial y} \tag{2.16}$$

which can be written in terms of the potential function ϕ by introducing the transformation

$$\left(\frac{\partial p}{\partial x}\right)_{\phi} = -\frac{\left(\frac{\partial \phi}{\partial x}\right)_p}{\left(\frac{\partial \phi}{\partial p}\right)_{x,y}} = \rho\left(\frac{\partial \phi}{\partial x}\right)_p , \tag{2.17}$$

and

$$\left(\frac{\partial p}{\partial y}\right)_{\phi} = -\frac{\left(\frac{\partial \phi}{\partial y}\right)_p}{\left(\frac{\partial \phi}{\partial p}\right)_{x,y}} = \rho\left(\frac{\partial \phi}{\partial y}\right)_p , \tag{2.18}$$

so that the geostrophic equations become

$$-fv = -\left(\frac{\partial \phi}{\partial x}\right)_p , \tag{2.19}$$

and

$$+fu = -\left(\frac{\partial \phi}{\partial y}\right)_p . \tag{2.20}$$

If equation 2.19 is now integrated then we obtain

$$\phi(p) - \phi(p_0) = -\int_{p_0}^{p} \alpha \, dp \tag{2.21}$$

which can then be written as

$$\phi(p) = \phi(p_\circ) - \int_{p_\circ}^{p} \alpha_\circ \, dp - \int_{p_\circ}^{p} \delta \, dp , \tag{2.22}$$

where $\alpha_\circ$ is a reference density inverse of sea water and δ is the specific volume anomaly.

Equations 2.19 and 2.20 can now be rewritten as

$$-fv = -\frac{\partial \phi(p_\circ)}{\partial x} + \frac{\partial \Delta D(p)}{\partial x} , \tag{2.23}$$

and

$$fu = -\frac{\partial \phi(p_\circ)}{\partial y} + \frac{\partial \Delta D(p)}{\partial y} , \tag{2.24}$$

where the dynamic height, ΔD, is defined by

$$\Delta D = \int_{p_\circ}^{p} \delta \, dp , \tag{2.25}$$

if we next consider the geostrophic relations at the ocean surface to be

$$-fv(o) = -\frac{\partial \phi(o)}{\partial x} , \tag{2.26}$$

and

$$fu(o) = -\frac{\partial \phi(o)}{\partial y} , \tag{2.27}$$

then equations 2.23 and 2.24 can be rewritten as

$$-f\left\{v(0)-v(p)\right\} = -\frac{\partial \Delta D(p)}{\partial x}\,, \tag{2.28}$$

and

$$f\left\{u(0)-u(p)\right\} = -\frac{\partial \Delta D(p)}{\partial y}\,, \tag{2.29}$$

or if the velocity on an isobaric surface, P_R is known then the velocity at any other surface is given by

$$f\left\{v(p)-v(P_R)\right\} = \frac{\partial}{\partial x}\left\{\Delta D(P_R)-\Delta D(p)\right\}\,. \tag{2.30}$$

The actual construct of a sea surface picture occurs after the depth of the nearly zero gradient current has been determined. Measurements in the region of the Gulf Stream vary considerably in depth of actual observation but there are sufficient measurements made at depths of two to three thousand meters to insure that we've satisfied the criteria of the dynamic method.

Defant (1941) examined the departures in isobaric surface dynamic depth, from a constant value, for a considerable number of station pairs and determined that for the Atlantic Ocean, the one thousand to sixteen hundred layer be considered the no-motion reference layer. Unfortunately, there is not yet any method which applies to all oceans, so one must approach this problem on a case by case basis with a belief in relative values.

Fomin (1964) examined the accuracy of the dynamic method and showed that, owing to the accumulation of random errors, computed dynamic heights differed from actual isobaric surface dynamic height by errors of the order of twenty dynamic millimeters in water depths of a thousand meters off of the Kamchatka coast.

The accuracy of sea water temperature, salinity and denisty calculations should be evaluated, since errors in these measurements give an initial biasing to the results. The extent to which surface topography, as indicated by dynamic methods, departs from true topo is a function not only of the reference surface and on the magnitude of horizontal motion at this depth but also, and very directly, on the precision of the devices used in actual data collection and [illegible]. This precision includes the number of vertical and horizontal data points, i.e., levels and stations occupied, as well as the more obvious concern of instrument scale division. Moreover, the reference surface cannot be located at too great a depth because of the immediate increase in computational errors which results. It should be noted though, that in cases where computational errors are large, it may be of some use to use a shallower reference surface in a trade-off of the loss of absolute values versus more exact computation.

Temperature is usually measured directly in the ocean with reversing thermometers while salinity is implied from chlorine measurements and a chemical table (Zubov, 1957). The reading accuracy of deep-water reversing thermometers is plus or minus two-hundredth's of a degree celsius while the accuracy of the chemical method used to determine salt content is about plus or minus fourteen thousands of a part per mille.

It must also be observed that the hydrological profiles across the Gulf Stream occasionally extend from abyssal plain ocean depths to continental shelf depths, where the depth is less than the reference surface depth. In such a case dynamic analyses have been performed (Helland-Hansen, 1934, Mohn, 1885) by replacing the earth's crust of the continental shelf and slope by a fictitious water mass and by then extending the ocean density field into the fictitious water mass with artistic license.

2.3 Calculations Using the Dynamic Method

In order to make a computation of dynamic height and or of geostrophic flow, one must first calculate the anomaly of specific volume, δ , which is related to the density of sea water. The density of sea water is determined by its temperature (T), salinity (S) and, to a much lesser degree, its pressure (P), so that $\rho = \rho(S,T,P)$.

Changing the temperature of a parcel of sea water results in a change in the density of sea water by an amount $\Delta\rho_T$. Similarly $\Delta\rho_S$ is the density change due to a change in the salinity within the parcel of sea water. By changing both the temperature and the salinity within the parcel of water results in a new volumetric density of

$$\rho_{ST} = \rho_{S_0T_0} + \Delta\rho_T + \Delta\rho_S + \Delta\rho_{ST} \quad , \tag{2.31}$$

where the subscript zero denotes the original values of S and T. Note that the separate effects of salinity and temperature are not simply superpositional in nature. There is also an interaction term $\Delta\rho_{ST}$ which must be considered. If we now introduce the parameter pressure, then

$$\rho_{STP} = \rho_{S_0T_0P_0} + \Delta\rho_S + \Delta\rho_T + \Delta\rho_P + \Delta\rho_{ST} + \Delta\rho_{SP} + \Delta\rho_{PT} + \Delta\rho_{STP} . \tag{2.32}$$

This relation can be reduced by considering the definition of a quantity called sigma -T (σ_T), so that

$$\rho_{STP} = 1 + \sigma_T + \Delta\rho_P + \Delta\rho_{SP} + \Delta\rho_{TP} . \tag{2.33}$$

Using an alternate notation, the specific volume (α) can be written as

$$\alpha_{STP} = \frac{1}{\rho_{STP}} = \alpha_{S_o T_o P_o} + \delta_{ST} + \delta_{SP} + \delta_{TP} + \delta_{STP} + \delta_P \ , \qquad (2.34)$$

and using standard notation, a calculation of α may be done using the reduced, or simplified, equation

$$\alpha_{STP} = \alpha_{35,0,P} + \Delta_{ST} + \delta_{SP} + \delta_{TP} \ , \qquad (2.35)$$

where Δ_{ST} is called the "thermosteric anomaly." The last three terms contain the departure of α from the value $\alpha_{35,0,P}$ and are known as the anomaly of specific volume

$$\delta = \delta_{SP} + \delta_{TP} + \Delta_{ST} \ . \qquad (2.36)$$

Now variations in δ indicate the so-called "relative field of mass" within the ocean and are used to calculate geostrophic flow.

To reiterate, the calculation of $\delta(z)$ at two stations must be done before the geostrophic flow can be computed. From the beginning though, it should be emphasized that derived sea surface heights and slopes, velocities and transports are only arbitrary. The choice of a level-of-no-motion above which the mass field and the sea surface are in perfect adjustment, is open to conjecture and becomes rather an art based on our present state of knowledge.

After the values of $\delta(z)$ have been computed using hydrographic tables, then the procedure for calculating the dynamic height anomalies is as follows:

First calculate an average δ, $\bar{\delta} = \frac{(\delta_{z_1} + \delta_{z_2})}{2}$ between two depths, say the surface, z = 0, and another depth, say z = h meters, at two different stations. One can then calculate the dynamic height anomalies (ΔD) for both stations, where in each case $\Delta D = \delta_{\Delta z}$. Then the cumulative dynamic height anomaly can be assessed by summing the ΔD values at each station as $\Sigma \Delta D$. Geostrophic velocities and sea surface slopes between stations a and b can be computed. Geostrophic velocities are obtained by the relationship

$$V_{z_1} - V_{z_2} = -\frac{10}{f} \frac{[\Delta D_a (Z_1 - Z_2) - \Delta D_b (Z_1 - Z_2)]}{L} \ , \qquad (2.37)$$

where V denotes velocities and L the distance between stations a and b.

If one wants to interpret relative flow from isopycnals, then one could consider the formula

$$\frac{\Delta V}{\Delta z} = -\frac{g}{\rho f}\frac{\partial \rho}{\partial z}\left(\tan\gamma - \tan\beta\right), \text{ where } V = g \tan B \qquad (2.38)$$

Equation (2.38) defines a relationship between geostrophic velocity and the slope of an isobar (a line of constant density). In the northern hemisphere, if the isobars slope up to the East, then the velocity of the water along the isobaric surface is to the North. The steeper the slope, the higher is the velocity. In the case where $\frac{\Delta V}{\Delta z} = 0$ (barotropic flow) then $\gamma \gg \beta$ and equation (2.38) may be written in its approximate form

$$\frac{\Delta V}{\Delta z} = -\frac{g}{\rho f}\frac{\partial \rho}{\partial z}\tan\gamma \qquad (2.39)$$

Equation (2.39) defines a relationship between the slope of the isopycnals and the velocity shear. For a stably stratified water column, $\frac{\partial \rho}{\partial z} > 0$, in the northern hemisphere, the isopycnals slope down to the East when the northern component of velocity decreases with depth. Equivalently, we could say that the velocity becomes more southerly in character with increased depth. A pictoral representation of this, which represents the Gulf Stream, is shown in Figure 2.1.

The computer program given in Appendix 1 will now be explained. As mentioned above, it is the convention to compute dynamic dpeth in terms of a standard chunk of seawater, in which T = 0°C, S = 35°/₀₀, plus an anomaly. Thus we have the $\alpha_{P,0°C,35°/_{00}}$ term plus the δ term. So each parcel of sea water at each depth is composed of two volumes, i.e., each unit volume so at

z = 0 meters

and at

z = 100 meters

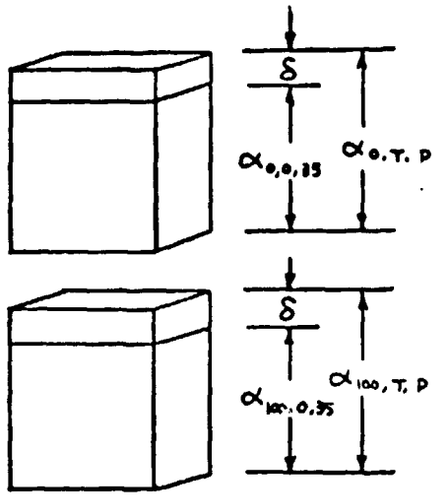

Since the $\alpha_{P,0,35}$ is a standard and since we are only interested in differences from stations then this program follows the convention of summing only the anomalies.

If we rewrite the anomaly as composed of terms $\delta_T, \delta_S, \delta_{ST}, \delta_{TP}, \delta_{SP}$ and δ_{STP} then

$$\delta = \delta_T + \delta_S + \delta_{ST} + \delta_{TP} + \delta_{SP} + \delta_{STP} \quad . \tag{2.40}$$

Now in standard oceanographic tables, the first three terms are combined and the last is assumed small, i.e.,

$$\Delta_{ST} = \delta_T + \delta_S + \delta_{ST} \quad , \tag{2.41}$$

$$\delta_{STP} \sim 0 \quad . \tag{2.42}$$

The program works directly with the equation of state and use the relationship

$$\alpha_{STP} = \alpha_{35\,‰\,,\,0°C\,,\,P} + \delta \qquad \text{where} \tag{2.43}$$

$$\alpha_{35,0,0} = 0.97264 \, .$$

The anomaly in dynamic depth is then the integration (2.25) $\Delta D = \int_0^P \delta \, dp$. On paper the calculation goes something like this:

Depth				$\Sigma\delta = \Delta_{S,T} + \delta_{T,P} + \delta_{S,P}$			Sum of all three	Average value for this depth interval	$\bar{\delta} \times P$	
Z	P	T	S	Δ_{ST}	$\delta_{T,P}$	$\delta_{S,P}$	$\Sigma\delta$	$\bar{\delta}$	ΔD	$\Sigma\Delta D$
0	0	0.89	34.23	62.9	0	0	62.9	63.10	631.0	0
10	10	0.88	34.22	63.3	0	0	63.3			631.0
20										

Anomaly of dynamic depth for each depth interval

Anomaly of dynamic depth referred from surface down

$\times 10^5$

where in the program, the following is used:

DIMENSION

D depth on specific data

T temperature of data

S salinity of data

DD, TT, SS	values used by computer in calculating specific volume for dynamic calculations.
D1, T1, S1	values interpolated to standard intervals, i.e., 0-10-20, etc.
K1	a counting parameter
P	pressure
DYN	dynamic meters, $D = \int \alpha_{p,T,S}\, dP$
ALPH	specific volume, $\alpha_{T,S,P}$
NSTA	station number
FLA	latitude
FLO	longitude
ALP	$\alpha_{0°C,35°/_{oo},P}$
ANOM	anomaly summation, $\Delta D = \int \delta\, dP$
DYA	dynamic meters, $D = \int \alpha_{p,0,35}\, dP$
DEAN	specific volume anomaly
SIGT	sigma -t

FORMAT

100	data cards
101	master card for each station
102	printer heading
1021	" "
1022	" "
103	printout format for depth and velocity
104	printer heading

105 space

106 printer heading

197 " "

108 print-out format for depth, temperature, salinity, sigma -t, dynamic meters, anomaly, anomaly sum

DIN=10 an interpolation interval in meters--could be changed to a more convenient spacing

II = 0

1. II = II + 1 determines that we start with first station--do the interpolations, then look at second station

INTERPOLATION

The integration of the specific volume anomaly given later in the program uses all the observed data, but a value for S and T must be specified at the surface and at standard depth intervals.

This part of the program assigns the shallowest observation to be the surface value. Usually this will mean that the first observation at say 0.5 to 2.0 meters depth will be moved to the surface. Observations between the "surface" and the first standard depth are then assigned new index numbers. An interpolated T,S value is then found at the first standard depth and so on down the water column until observations run out.

2. Read 100,D(I),T(I),S(I)
   IF (S(1)) 4,4,3
3. I = I + 1
   GO TO 2

Reads all the data cards--a blank data card at the end gives S = 0, so the computer senses that the last card has been read.

4. MAXI = I - 1

This is the number of data cards.

DD(1) = DI(1) = 0.0
TT(1) = TI(1) = T(1)
SS(1) = SI(1) = S(1)

This tells the machine that the surface (z = 0) values are equivalent to the first observations.

```
      K = 1                          counter-index parameter
      L1 = 2                         counter-index parameter
      DMAS = D(MAX1)                 maximum observed depth
      NINT = DMAX/DIN + 1            number of interpolation intervals
      XNINT = NINT                   real number
      IF (···) 11,12,11
11.   LAST = NINT + 1
      GO TO 13                       checks for round-off errors
12.   LAST = NINT
13.   DI (LAST) = D (MAX1)
      TI (LAST) = T (MAX1)           Assigns to last interpolated depth the T,S
      SI (LAST) = S (MAX1)           values at the deepest observed depth
```

See the following example, which relates to Figure (2.2) for an explanation of the Do Loops.

Example:

Suppose we have the following STD trace:

S(1) = 34.1 D(1) = 1

S(2) = 34.2 D(2) = 2

S(3) = 34.2 D(3) = 3

S(4) = 34.4 D(4) = 4

S(5) = 34.5 D(5) = 7

S(6) = 34.6 D(6) = 8

S(7) = 34.8 D(7) = 9

S(8) = 35.0 D(8) = 11

S(9) = 35.0 D(9) = 14

S(10) = 35.0 D(10) = 15

S(11) = 0 (blank card)

MAX1 = 11 - 1 = 10 data cards

DI(1) = 0.0

SI(1) = S(1) = 34.1

DMAX = D(10) = 15 meters

N1NT = 15/10 + 1 = 2 (integer)

XN1NT = 2.0 (real)

DMAX/D1N + 1.0 - XN1NT = 0.5 (positive)

LAST = N1NT + 1 = 3

DI(3) = D(MAX1) = 15

SI (3) = S(MAX1) = 35.0

DO I = 2,2

X1M = 2-1 = 1

D1NT = X1M·D1N = 1·10 = 10 meters

MAX1 = L1 = 10-2 = positive (to 61)

61. DO 6 J = 2,10

(D(2) - D1NT) = 2-10 = NEGATIVE (to 7)

7. K = K + 1 = 2

DD(2) = D(2)

SS(2) = S(2) (to 6)

6. J = 3

continue

6. J = 8

D(8) - D1NT = 11 - 10 = positive (to 9)

9. K = 7 + 1 = 8

DD(8) = D1NT = 10 meters

SS(8) = ((35.0 - 34.8) (10-9))/(11-9)) + 34.8

= ((0.2) (1)/2)) + 34.8 = 34.9

S1(2) = 34.9

K1(2) = 8

IF (MAX1 - L1) (is 10 - 8, positive)

DO 10 J = 8 - 10

K = 9

DD(9) = D(8)

SS(9) = S(8)

52. KI(1) = 1

KI(3) = 11

DYNAMIC CALCULATIONS

P(1) = 0.0 set sea level pressure = 0

DEAN(1) = 0.0 let anomaly at surface = 0

ANOM(1) = 0.0 anomaly sum (or vertical integration)

ALP(1) = ALPHA (0.0,0.0,35.0) is specific volume at the surface

DYA(1) = 0

ALPH(1) = ALPHA(P(1),TT(1),SS(1)) is total specific volume at the surface computed from function ALPHA

SIGT(1) = $(1./\text{ALPH}(1) - 1.)\cdot 10^3$ is σ_T at the surface

DYN(II,I) = 0.0 dynamic meters

Do 15 I = 2, LAST

Do Loops 15 and 16 do a stepwise integration of the equation of state to obtain the anomaly of dynamic depth.

The specific volume is

$\alpha_{P,T,S} = \alpha_{P,0°C,35°/..} + \delta$ where δ = DEAN(I)

and dynamic depth

$$D = \int \alpha_{P,T,S} dP$$

$$D = \int \alpha_{P,0°C,35°/..} dP + \int \delta dP$$

so the anomaly of dynamic depth $\Delta D = \int \delta dP = \int \alpha_{P,T,S} dP - \int \alpha_{P,0°C,35°/..} dP$

or

ANOM(1) = DYN(II,I) - DYA(I)

2.4 ADVANCED GEOSTROPHY AND GULF STREAM THEORY

It is convenient here to introduce the concepts of baroclinic and barotropic velocities since the former indicates relative geostrophic currents and the field of mass while the latter is related to deep water velocities and sea surface slope. To differentiate fully between the two termonological concepts as they apply to a western boundary current such as the Gulf Stream, it is of benefit to develop some theory explaining the use and meaning of the concepts. To more fully appreciate the nature of the Gulf Stream it would also be of worth to consider not just the dynamics of rotation balancing horizontal pressure gradients but also the effects of winds and bottom topography (see section on Gulf Stream models) since presumably (see the section on Results) winds and topography do modify the intensity, shape and position of the Gulf Stream.

If we consider the steady system of equations

$$-\rho f v = -\frac{\partial p}{\partial x} + \frac{\partial}{\partial z}\tau_{xz} \tag{2.44}$$

$$\rho f u = -\frac{\partial p}{\partial y} + \frac{\partial}{\partial z}\tau_{yz} \tag{2.45}$$

and

$$\frac{\partial p}{\partial z} = -g\rho \tag{2.46}$$

where τ_{xz} and τ_{yz} are Reynold's stress terms and we've a right-handed cartesian co-ordinate system with x east and y north.

Next we define mass transport as:

$$U = \int_{z_b}^{\eta} \rho u \, dz \tag{2.47}$$

and

$$V = \int_{z_b}^{\eta} \rho v \, dz \qquad \text{where b} \tag{2.48}$$

indicates the bottom depth. Then evaluating the stress difference from top, η, to bottom, z_b, we integrate the central region equations over depth, so we obtain

$$-fV = -\int_{z_b}^{\eta} \frac{\partial p}{\partial x} dz + \tau_{xz}\Big|_{z_b}^{\eta} , \tag{2.49}$$

and

$$fU = -\int_{z_b}^{\eta} \frac{\partial p}{\partial y} dz + \tau_{yz}\Big|_{z_b}^{\eta} , \tag{2.50}$$

where a portion of the velocity components, individually, balances the pressure gradient (geostrophic part) and a portion of the velocity balances the stress (Ekman part).

Next we can break the geostrophic flow into both barotropic and baroclinic parts but we must first reformulate the pressure gradient. Consider the continuity condition to be

$$\frac{\partial \rho u}{\partial x} + \frac{\partial \rho v}{\partial y} + \frac{\partial \rho w}{\partial z} = 0 . \tag{2.51}$$

Then integrate equation (2.51) in z to get

$$\int_{z_b}^{\eta} \frac{\partial \rho u}{\partial x} dz + \int_{z_b}^{\eta} \frac{\partial \rho v}{\partial y} dz + \rho(\eta) w(\eta) - \rho(z_b) w(z_b) = 0. \tag{2.52}$$

Now if we assume that the volume of water passing through unit width in a vertical cross section in unit time is constant with the same condition holding for the other two directions, i.e., that

$$\rho(\eta)u(\eta)\frac{\partial \eta}{\partial x} - \rho(z_b)u(z_b)\frac{\partial z_b}{\partial x} = 0 \quad , \tag{2.53}$$

and

$$\rho(\eta)v(\eta)\frac{\partial \eta}{\partial y} - \rho(z_b)v(z_b)\frac{\partial z_b}{\partial y} = 0 \quad , \tag{2.54}$$

then we get:

$$\frac{\partial U}{\partial x} + \frac{\partial V}{\partial y} = 0 \quad , \tag{2.55}$$

so there is no mass flux through the bottom or the surface and continuity is satisfied by the horizontal mass flux.

Now, for a re-formation of the pressure gradient, we must investigate the term

$$-\int_{z_b}^{\eta} \frac{\partial P}{\partial x}\, dz \tag{2.56}$$

which is equal to

$$-\int_{z_b}^{\eta} \frac{\partial P}{\partial x}\, dz = -\frac{\partial}{\partial x}\int_{z_b}^{\eta} P\, dz + P_{atm}\frac{\partial \eta}{\partial x} - P_b\frac{\partial z_b}{\partial x} \quad . \tag{2.57}$$

As is evident, part of the pressure, P, is independent of the density distribution and part is not so we must get a reference pressure and get an anomaly from that reference where this anomaly does vary with position. Define

$$P = g\int_{z}^{\eta} \rho\, dz \tag{2.58}$$

which is the hydrostatic condition, and

$$E_p = \int_{z_b}^{\eta} p\,dz \quad , \tag{2.59}$$

which is the potential energy of a column of water of unit horizontal area. It thus becomes obvious that we get potential energy anomalies where we have pressure anomalies. Combining (2.58) and (2.59) then yields

$$E_p = \frac{1}{g}\int_{P_{atm}}^{P_b} p\alpha_o\,dp + \frac{1}{g}\int_{P_{atm}}^{P_b} p\,\delta\,dp \quad , \tag{2.60}$$

where α_o is a function of pressure (P) but not a function of temperature (T) or salinity (S). Note that α_o is taken at T = 0°C, S = 35°/$_{oo}$ or $\alpha_{35,0,P}$ and δ is the specific volume anomaly. With these we can go back and rewrite equation 2.57 as

$$-\int_{z_b}^{\eta} \frac{\partial P}{\partial x}\,dz = \underbrace{-\frac{\partial}{\partial x}\int_0^{P_b} \frac{D}{C}\,dp}_{\text{where this is a function of bottom pressure only}} \underbrace{-\frac{\partial}{\partial x}\int_0^{P_b} \frac{p\delta}{g}\,dp}_{\text{where the integral can be called the potential energy anomaly, } \psi.} - P_b\frac{\partial z_b}{\partial x} \quad , \tag{2.61}$$

where $P_{atm} = 0$, so we obtain

$$-\int_{z_b}^{\eta} \frac{\partial P}{\partial x}\,dz = -\frac{\partial P_b}{\partial x} P_b \underbrace{\alpha_o(P_b)}_{\text{i.e., } \alpha_o = \alpha_{35,0,P} \text{ is a function of bottom pressure}} - \frac{\partial \phi}{\partial x} - P_b\frac{\partial z_b}{\partial x} \quad . \tag{2.62}$$

Now, $\frac{\partial \phi}{\partial x}$ is the only term dependent on the T,S distribution directly although P_b (bottom pressure) does depend on water density above the bottom as well. We can now combine terms to get

$$-\int_{z_b}^{\eta} \frac{\partial P}{\partial x}\,dz = \underbrace{-\frac{\partial \phi}{\partial x}}_{\text{represents the baroclinic part}} - P_b\underbrace{\left(\frac{\alpha_o(P_o)}{g}\frac{\partial P_b}{\partial x} + \frac{\partial z_b}{\partial x}\right)}_{\text{represents the barotropic part}} \quad , \tag{2.63}$$

where both parts of the barotropic term are related to the bottom slope. $\frac{\partial z}{\partial x}$ is the bottom slope directly and $\frac{\partial P_b}{\partial x}$ is equivalent to slope since it is the change of height of the water column above the bottom. The terms are essentially of opposite sign since P_b increases down and z increases up. These are both big terms but the difference between them may be small. If we now assume that $z \approx z_b$, i.e., a reference level near the bottom, then we'll be able to get rid of a large part of the P_b term. Recall that,

$$P_b = P_z + g \int_{z_b}^{z} \rho \, dz \tag{2.64}$$

where the first term is written as a reference pressure term near the bottom. Thus,

$$\frac{\partial P_b}{\partial x} = \frac{\partial P_z}{\partial x} + g \int_{z_b}^{z} \frac{\partial \rho}{\partial x} dz - g \rho_b \frac{\partial z_b}{\partial x} \tag{2.65}$$

where the upper limit of integration z is independent of x, so at $z = z_b$

$$\left.\frac{\partial P_b}{\partial x}\right|_{z=z_b} = \left.\frac{\partial P_z}{\partial x}\right|_{z=z_b} - g \rho_b \frac{\partial z_b}{\partial x} . \tag{2.66}$$

If we now multiply through by $\frac{\alpha_o(P_b)}{g}$ and substitute the result into we obtain

$$\int_{z_b}^{\eta} \frac{\partial \rho}{\partial x} dz = \frac{\partial \phi}{\partial x} - P_b \left[\frac{\alpha_o(P_b)}{g} \left.\frac{\partial P_z}{\partial x}\right|_{z=z_b} \right] - P_b \left\{ \left[1 - \rho_b \alpha_o(P_b) \right] \frac{\partial z_b}{\partial x} \right\} , \tag{2.67}$$

where if we have a bottom where T and S are essentially uniform and use this as a reference, i.e., take α_o at the S,T of the bottom of the ocean, then the last term on the right cancels out since $\alpha_o(P_b) = \frac{1}{\rho_b}$. Unfortunately, this decoupling breaks down where there are significant intrusions of deep water near the surface. Finally we obtain

$$\int_{z_b}^{\eta} \frac{\partial p}{\partial x}\, dz = \underbrace{\frac{\partial \phi}{\partial x}}_{\text{baroclinic part}} - \underbrace{\frac{p_b}{g\rho_b}\frac{\partial p_z}{\partial x}}_{\text{barotropic part}} , \tag{2.68}$$

where $\frac{\partial p_z}{\partial x}$ is depth independent. If integrated, this indicates a uniform velocity from top to bottom with a magnitude equal to that at the bottom as shown in Figure 2.3. We can now write the integrated equations as:

the Ekman transport relations,

$$-fV_E = \tau_x = \tau_{xz}\Big|_{z=\eta} \tag{2.69}$$

and

$$fU_E = \tau_y = \tau_{yz}\Big|_{z=\eta} \quad ; \tag{2.70}$$

the Baroclinic Geostrophic relations,

$$-fV_g = -\frac{\partial \phi}{\partial x} \tag{2.71}$$

and

$$fU_g = -\frac{\partial \phi}{\partial y} \quad ; \tag{2.72}$$

and the barotropic geostrophic transport as

$$-fV_B = -\frac{p_b}{g\rho_b}\frac{\partial p_z}{\partial x} \tag{2.73}$$

and

$$fU_B = -\frac{p_b}{g\rho_b}\frac{\partial p_z}{\partial y} \quad , \tag{2.74}$$

where the subscripts B,g and E denote baroclinic, barotropic, and Ekman transport, respectively.

Summed up, we have a velocity satisfying the total relation

$$U = U_E + U_g + U_B. \tag{2.75}$$

The 2-D continuity equation is not satisfied by any of these velocities separately except in special cases. Rather, in general, the continuity condition is

$$\frac{\partial U}{\partial x} + \frac{\partial V}{\partial y} = 0 \quad . \tag{2.76}$$

In the case of Baroclinic Geostrophic Transport (BCLT), there is a divergence because of the Coriolis parameter's dependence on latitude. In the case of Barotropic Geostrophic Transport (BTT), there can be a divergence due to changes in depth. So we can get a number of variations depending on how we drive this with wind stress. We can drive it such that the wind driven part satisfies continuity alone or such that we need the geostrophic part, i.e., if $\nabla_H U_E = 0$ nothing happens but if $\nabla_H U_E \neq 0$ then we get the balance from other components (geostrophic).

The break up of motion into such parts is not quite complete but it includes what we use in ocean circulation studies.

There are exceptional cases where a bottom Ekman is important. This occurs where a bottom stress causes a significant transport in the bottom layer and occurs in cases where Barotropic flow is dominant over Baroclinic.

We can have the motion composed purely of one component when the divergence of that component is zero. Otherwise, we need enough of the other components to satisfy the continuity balance for the total motion.

Please note that in the open ocean, the only way to get an Ekman transport is to have a non-zero curl of the wind stress.[a]

---

[a] Note that f will be assumed a function of latitude as $f = f_{local} + \beta y$, where f_{local} and β are constants ($\beta = 10^{-13}$).

Thus, by cross-differentiating the component equations, we can form vorticity relations which contain terms that are the horizontal divergence of the particular component of motion. So, for the Ekman Transport, we have

$$\underbrace{f\left(\frac{\partial U_E}{\partial x}+\frac{\partial V_E}{\partial y}\right)}_{(a)}+\underbrace{\beta V_E}_{(b)}=\underbrace{\frac{\partial \tau_{yz}}{\partial x}-\frac{\partial \tau_{xz}}{\partial y}}_{(c)} \tag{2.77}$$

where (a) is the rate of change of vorticity due to stretching,

(b) is the advective change of vorticity, and

(c) is the production of vorticity due to torque (or curl) of the wind stress applied to the sea surface.

This equation can also be written as:

$$\underbrace{\frac{\partial U_E}{\partial x}+\frac{\partial V_E}{\partial y}}_{\text{horizontal divergence}}=\underbrace{\frac{\partial}{\partial x}\left(\frac{\tau_{yz}}{f}\right)-\frac{\partial}{\partial y}\left(\frac{\tau_{xz}}{f}\right)}_{\text{curl of }\left(\frac{\text{wind stress}}{f}\right)}, \tag{2.78}$$

so we can have the Ekman velocity in pure form only when the curl of $\left(\frac{\text{wind stress}}{f}\right) = 0$.

By cross-differentiating the BCLT we obtain

$$f\left(\frac{\partial U_g}{\partial x}+\frac{\partial V_g}{\partial y}\right)+\beta \cdot V_g = 0 \quad , \tag{2.79}$$

which says that the horizontal divergence is equal to zero only when there is:

(1) no meridional velocity component, and

(2) no dependence of the rotational parameter on latitude.

The curl of the BTT yields

$$f\left(\frac{\partial U_B}{\partial x}+\frac{\partial V_B}{\partial y}\right)-\beta V_B=-\frac{P_b}{g\rho_b}\left(\frac{\partial^2 P_z}{\partial x\partial y}-\frac{\partial^2 P_z}{\partial y\partial x}\right)-\underbrace{\frac{\partial P_z}{\partial y}\frac{\partial}{\partial x}\left(\frac{P_b}{g\rho_b}\right)}_{(a)}+\underbrace{\frac{\partial P_z}{\partial x}\frac{\partial}{\partial y}\left(\frac{P_b}{g\rho_b}\right)}_{(b)} \tag{2.80}$$

where (a) and (b) must be considered non-zero terms since we may not have a zero change in depth and since bottom pressure can change significantly with position. In (a), $\frac{\partial p_z}{\partial y}$ is proportional to $-U_b$ and in (b), $\frac{\partial p_z}{\partial x}$ is proportional to V_b so the right-hand side ((a) + (b)) represents an advective change.

This Barotropic Geostrophic balance can also be written as:

$$\underbrace{f\left(\frac{\partial U_g}{\partial x} + \frac{\partial V_g}{\partial y}\right)}_{(a)} + \underbrace{\beta V_g}_{(b)} \approx -f\underbrace{\left(U_g \frac{\partial z_b}{\partial x} - V_g \frac{\partial z_b}{\partial y}\right)}_{(c)},$$

where (a) is stretching due to advection,

(b) is stretching due to local change of earth's rotation, and

(c) is stretching due to change of total depth,

so the horizontal divergence is zero when either there is no meridional component and no change of f with latitude and no change in depth.

Ekman transport takes place within a certain distance from the boundary which is essentially the Ekman depth. This depth is dependent on the eddy viscosity and the coriolis parameter.

The boundary generates shear waves which propagate into the fluid. This is the same kind of boundary as with an oscillating plate--but the boundary is rotating versus oscillating. So the velocity decays with depth. The problem is made time independent by eliminating the time dependence on the rotating plane where the time dependence really is. Note that we can obtain the meridional component of velocity directly from the wind stress curl. This is the vertical vorticity balance with no stretching.

If there is zero wind stress curl then we have only one velocity component which is in the x-direction and will be a function of y only. Since if the wind stress curl is zero then $V_E = 0$, which indicates that $U = U(y)$ only so

$\frac{\partial U_E}{\partial x} = 0$. Thus we get a zonal flow varying with latitude for zero wind stress curl in the pure Ekman case.

For the above we have no boundary effects. When we have boundaries, then this type of motion (flow) doesn't satisfy the boundary conditions so we may need another type of flow which is also divergenceless in the interior regions to satisfy the boundary conditions. Such a flow is called coastal upwelling.

We can have pure baroclinic only in cases of pure zonal flow, i.e., flow only along contours of constant coriolis parameter f. If $V_g = 0$ then $U_g \neq U_{g(x)}$, but $U_g = U_{g(y)}$ only. But when we introduce boundaries, then this is no longer possible. Pure baroclinic flow is valid in the atmosphere, the interior of the ocean and in zonal canals (such as the Antarctic Ocean).

Then, for pure geostrophic barotropic transport,

$$\frac{\partial}{\partial x}\left(\frac{f}{h} U_g\right) - \frac{\partial}{\partial y}\left(\frac{f}{h} V_g\right) = 0 \qquad (2.81)$$

and the flow must be along lines (contours) of (f/h), otherwise the flow is an arbitrary function of (f/h), so if the bottom is level then the flow is zonal (along constant f) and if f doesn't change much, then the flow follows the bottom contours. Since (f/h) is constant along a streamline, for this case, then the flow goes towards the equator in crossing a ridge and towards the North or South Poles in crossing a trough in the ocean.

We can also have combinations of ET, BCLT and BTT such as: Stress-driven Barocline Transport.

This is the type of problem that is considered for most ocean circulation studies. We have both the ET and the BCLT systems of equations which are combined to yield the Sverdrup Equation:

$$\beta\left(V_E + V_g\right) = \frac{\partial \tau_{yz}}{\partial x} - \frac{\partial \tau_{xz}}{\partial y} \qquad (2.82)$$

So, for the Sverdrup Equation, we require the condition that

$$\frac{\partial U_E}{\partial x} + \frac{\partial V_E}{\partial y} = -\left(\frac{\partial U_g}{\partial x} + \frac{\partial V_g}{\partial y} \right) \tag{2.83}$$

which is the continuity equation for the total flow.

$$\beta \left(V_E + V_g \right) = -\frac{\partial \tau_{yz}}{\partial x} - \frac{\partial \tau_{xz}}{\partial y} \tag{2.84}$$

which is known as the Sverdrup Equation.

There is also the possibility of an ET and BTT type of flow represented by the following balance

$$\beta V_E - \left(\frac{\partial \tau_{yz}}{\partial x} - \frac{\partial \tau_{xz}}{\partial y} \right) = -h \underbrace{\left[U_B \frac{\partial}{\partial x}\left(\frac{f}{h}\right) + V_B \frac{\partial}{\partial y}\left(\frac{f}{h}\right) \right]}_{\text{the change in vorticity from the barotropic position due to streamlines crossing contours of (f/h).}} . \tag{2.85}$$

There is a limit on doing this kind of flow because in most oceans bottom friction may be small-since most of the current is normally picked up in the baroclinic portion. But, neglecting baroclinic flow does require the inclusion of a bottom stress.

In applying these concepts to actual Gulf Stream models, it is proper to consider first, Sverdrup's Theory of Wind Generated Transport. The equations of motion governing the system are

$$-\rho f v = -\frac{\partial P}{\partial x} + \frac{\partial}{\partial z}\left(A_z \frac{\partial u}{\partial z} \right) \tag{2.86}$$

and

$$\rho f u = -\frac{\partial P}{\partial y} - \frac{\partial}{\partial z}\left(A_z \frac{\partial v}{\partial z} \right) \tag{2.87}$$

which are integrated from depth $z = -h$ to the surface, where $z = \eta \simeq 0$. It is next assumed that the stress at $z = -h$ is zero, in accordance with the

assumption of zero current below some depth, z_{nomo}. So,

$$-fV = -\frac{\partial P}{\partial x} + \tau_{xs} \tag{2.88}$$

and

$$fU = -\frac{\partial P}{\partial y} + \tau_{ys} \tag{2.89}$$

where the subscript s implies the seasurface value of the wind stress. Then taking the curl of the equations of motion and adding the resultant relations with the continuity condition, the following results

$$\beta V = \frac{\partial \tau_{ys}}{\partial x} - \frac{\partial \tau_{xs}}{\partial y} \tag{2.90}$$

which says that the North-South transport is completely determined by the curl of the wind stress. If this relationship is now substituted into the continuity equation and an integration with respect to x is performed, then

$$U = -\frac{1}{\beta}\int \frac{\partial}{\partial y}(\nabla \times \underset{\sim}{\tau})_z \, dx + g(y) \tag{2.91}$$

where g(y) is a constant of integration, now g(y) is an arbitrary function of y which must be evaluated. The equations are of first order so we can satisfy only one boundary condition but by the nature of observations, we know that in the western part of the Atlantic Ocean, there is a narrow band of intense current occurring, so this solution will probably not apply to the western boundary region, or at least the distance ϵ away from the boundary which is at x = 0.

Though this early model of wind generated transport seems inappropriate to a Gulf Stream model, it did establish a theoretical basis from which to proceed.

So we've solved a circulation problem with U being zero at one coast (Eastern) but we were unable to satisfy a condition on the other coast (Western). The dynamics of the problem were not of a high enough order to permit a closed

basin solution.

What we really have here is a divergence of the Ekman wind drift, produced by the convergence of the geostrophic flow (or vice versa convergence by divergence). Thus the picture is of a coupled flow comprised of the Ekman layer responding to the wind and the underlying geostrophic layer which adjusts itself.

We'll next look at a "closed" circulation in a bounded basin--something not possible in the Sverdrup approximations. Stommel (1948) introduced a frictional term or rather, a mechanism for dissipation. The friction is introduced in the form of a drag on the bottom of the ocean--which may or may not be a realistic dissipation source--to show that closed basin circulation with western intersification are possible. Consider a rectangular basin, $0 \le x \le L$, $0 \le y \le W$, and a wind stress given by $\tau(y) = -F \cos(\frac{\pi y}{b})$. We now have

$$\int_{-h}^{\eta} \frac{\partial}{\partial z}\left(A_z \frac{\partial u}{\partial z}\right) dz = \left(A_z \frac{\partial u}{\partial z}\right)\Big|_{-h}^{\eta} = \tau_{xs} - \tau_{xb} \qquad (2.92)$$

and

$$\int_{-h}^{\eta} \frac{\partial}{\partial z}\left(A_z \frac{\partial v}{\partial z}\right) dz = \left(A_z \frac{\partial v}{\partial z}\right)\Big|_{-h}^{\eta} = \tau_{ys} - \tau_{yb} \qquad (2.93)$$

If we next choose

$$\frac{\tau_{xs}}{\rho} = \frac{\tau(y)}{\rho} = -F \cos(\pi y/b)$$

$$\frac{\tau_{ys}}{\rho} = 0$$

$$\frac{\tau_{xb}}{\rho} = R\bar{u} \qquad \bar{u} = \frac{1}{h}\int_{-h}^{\eta} u \, dz$$

$$\frac{\tau_{yb}}{\rho} = R\bar{v} \qquad v = \frac{1}{h}\int_{-h}^{\eta} v\,dz$$

and R is a constant measuring the bottom drag. Stommel then integrated from $z = -h$ to $z = \eta$ using, by definition:

$$\int_{-h}^{\eta} u\,dz = \bar{u}(h+\eta) \simeq h\bar{u}$$

$$\int_{-h}^{\eta} v\,dz = \bar{v}(h+\eta) \simeq h\bar{v}$$

and noting that

$$-\int_{-h}^{\eta}\frac{1}{\rho}\frac{\partial p}{\partial x}\,dz = -\frac{1}{\rho}\int_{-h}^{\eta} g\rho\frac{\partial \eta}{\partial x}\,dz = -g\frac{\partial \eta}{\partial x}\int_{-h}^{\eta} dz$$

$$= -g\frac{\partial \eta}{\partial x}(h+\eta) \simeq -gh\frac{\partial \eta}{\partial x}$$

and

$$-\int_{-h}^{\eta}\frac{1}{\rho}\frac{\partial p}{\partial y}\,dz = -\frac{1}{\rho}\int_{-h}^{\eta} g\rho\frac{\partial \eta}{\partial y}\,dz = -g\frac{\partial \eta}{\partial y}\int_{-h}^{\eta} dz$$

$$= -g\frac{\partial \eta}{\partial y}(h+\eta) \simeq -gh\frac{\partial \eta}{\partial y}$$

so the main equations become:

$$-fh\bar{v} = -gh\frac{\partial \eta}{\partial x} + [-F\cos(\pi y/b)] - R\bar{u} \qquad (2.94)$$

$$fh\bar{u} = -gh\frac{\partial \eta}{\partial y} - R\bar{v} \qquad (2.95)$$

$$\frac{\partial \bar{u}}{\partial x} + \frac{\partial \bar{v}}{\partial y} = 0 \qquad (2.96)$$

Taking the curl of the equations of motion and summing yields in terms of a stream function Ψ' such that

$$\bar{v} = \frac{\partial \psi'}{\partial x} \quad , \quad -\bar{u} = \frac{\partial \psi'}{\partial y}$$

results in the following equation

$$\frac{hB}{R}\frac{\partial \psi'}{\partial x} - \frac{\pi F}{bR}\sin\left(\frac{\pi y}{b}\right) + \frac{\partial^2 \psi'}{\partial x^2} + \frac{\partial^2 \psi'}{\partial y^2} = 0 \qquad (2.97)$$

to be solved.

If it is now assumed that the y-dependence for ψ' is of the form $\sin(\pi y/b)$ and if we assume that ψ' can be written as $\psi'(x,y) = G(x)\sin(\pi y/b)$, then substituting this into the ψ' equation yields

$$\frac{d^2G}{dx^2} + \alpha\frac{dG}{dx} - \left(\frac{\pi}{b}\right)^2 G = \gamma \quad , \qquad (2.98)$$

where

$$\alpha = \frac{hb}{R} \quad \text{and} \quad \gamma = \frac{\pi F}{bR} \quad .$$

Now, the general solution to the homogeneous equation 2.97, with

$$A = -\frac{\alpha}{2} + \left(\frac{\alpha^2}{4} + \frac{\pi^2}{b^2}\right)^{1/2} \qquad \text{and}$$

$$B = -\frac{\alpha}{2} - \left(\frac{\alpha^2}{4} + \frac{\pi^2}{b^2}\right)^{1/2} \qquad \text{is}$$

$$G = C_1 e^{Ax} + C_2 e^{Bx}$$

where C_1 and C_2 are the constants of integration, so

$$\psi'(x,y) = \gamma\frac{b^2}{\pi^2}\left(C_4 e^{Ax} + C_5 e^{Bx} - 1\right)\sin\left(\frac{\pi y}{b}\right) \qquad (2.99)$$

where

$$C_4 = \frac{C_1}{\left(\gamma\frac{b^2}{\pi^2}\right)} \quad , \quad C_5 = \frac{C_2}{\left(\gamma\frac{b^2}{\pi^2}\right)} \quad .$$

For the $\wedge\psi'$ equation, the boundary conditions are that

$$\wedge\psi' = 0 \quad \text{at} \quad y = 0, b$$
$$\text{and} \quad x = 0, L$$

so that

$$\wedge\psi'(0,y) = \psi'(L,y) = \wedge\psi'(x,0) = \psi'(x,b) = 0.$$

The condition on $y = 0, b$ is met immediately since the result is a function of $\sin \frac{\pi y}{b}$. The condition on $x = 0, L$ yields that

$$C_4 = \frac{1 - e^{BL}}{e^{AL} - e^{BL}} \qquad \text{and} \qquad C_5 = \frac{e^{AL} - 1}{e^{AL} - e^{BL}}$$

so the Stommel solution is that

$$\psi' = \left\{ \frac{\gamma \wedge b^2}{\pi^2 \left[e^{\left(-\frac{\alpha}{2} + \left(\frac{\alpha^2}{4} + \frac{\pi^2}{b^2}\right)^{1/2} L\right)} - e^{\left(-\frac{\alpha}{2} - \left(\frac{\alpha^2}{4} + \frac{\pi^2}{b^2}\right)^{1/2} L\right)} \right]} \right\}$$
$$\left\{ \left[1 - e^{\left(-\frac{\alpha}{2} - \left(\frac{\alpha^2}{4} + \frac{\pi^2}{b^2}\right)^{1/2}\right) L} \right] e^{\left(-\frac{\alpha}{2} + \left(\frac{\alpha^2}{4} + \frac{\pi^2}{b^2}\right)^{1/2}\right) x} \right. \tag{2.100}$$
$$\left. + \left[e^{\left(-\frac{\alpha}{2} + \left(\frac{\alpha^2}{4} + \frac{\pi^2}{b^2}\right)^{1/2}\right) L} - 1 \right] e^{\left(-\frac{\alpha}{2} - \left(\frac{\alpha^2}{4} + \frac{\pi^2}{b^2}\right)^{1/2}\right) x} \right\} \sin \frac{\pi y}{b}$$

and thus

$$\bar{u} = -\frac{\partial \psi'}{\partial y} = -\gamma \wedge \frac{b}{\pi} \left[C_4 e^{Ax} + C_5 e^{Bx} - 1 \right] \cos \frac{\pi y}{b} \tag{2.101}$$

and

$$\bar{v} = \frac{\partial \psi'}{\partial x} = \gamma \wedge \frac{b^2}{\pi^2} \left[A C_4 e^{Ax} + B C_5 e^{Bx} \right] \sin \frac{\pi y}{b} . \tag{2.102}$$

In interpreting this, Stommel chose (rather arbitrarily, to say the least),

$$L = 10^9 \text{ cm}$$
$$b = 2 \ (10^8) \text{ cm}$$

$h = 2(10^4)$ cm

$R = 0.02$

$F = 1$ dyne/cm^2.

Now if the ocean is not rotating, i.e.,

$$f_o = \beta = 0$$

then

$$C_4 = e^{-\pi L/b} \quad , \quad C_5 = 1$$

and

$$\Psi' = \gamma \frac{b^2}{\pi^2} \sin\left(\frac{\pi y}{b}\right)\left(e^{(x-L)\frac{\pi}{b}} + e^{-\frac{x\pi}{b}} - 1 \right) .$$

a solution depicted in Figure 2.4.

The sea surface is given by

$$\eta(x,y) = -\left(\frac{F}{gh}\right)\left(\frac{C_4}{A} e^{Ax} + \frac{C_5}{B} e^{Bx} \right) - \frac{b^2}{\pi^2}\frac{F}{gh}\left(C_4 A e^{Ax} + C_5 B e^{Bx}\right)\left(\cos\frac{\pi y}{b} - 1\right)$$

$$- \left\{ \frac{f\gamma}{g}\frac{b^2}{\pi^2} \sin\frac{\pi y}{b} - \frac{\beta\gamma}{g}\frac{b^3}{\pi^3}\cos\frac{\pi y}{b} \right\} \cdot \left(C_4 e^{Ax} + C_5 e^{Bx} - 1\right) \qquad (2.103)$$

and depicted in Figure 2.5. Now when the Coriolis parameter is a constant ($0.25\ (10^{-4})$) then the streamline diagram remains the same as the $\beta = f_o = 0$ case but the η diagram changes as shown in Figure 2.6. Next, when the Coriolis parameter is a linear function of latitude, i.e., $f = f_o + \beta y$ then Figure 2.7 results for Ψ' and Figure 2.8 is the sea surface topography depiction.

The obvious feature of the f = constant case is the crowding of streamlines on the western side of the basin. The velocity along the Southern border is ~ 20 cm/sec and along the Western border is ~ 240 cm/sec. The band width of the intensified current is ~ 100 km. The implication is then, because f changes as a function of latitude, then there is a concentration of streamlines along

the western boundaries of oceans .. ulting in such phenomena as the Gulf Stream and the Kuroshio.

We'll now consider the Munk (1950) frictional theory of the ocean with a model structure similar to that of Stommel's. Munk's motivation to do this problem was that Stommel made the assumption of a non-zero drag at the bottom, which might be rather unrealistic, so Munk solved a problem using the assumptions that at some depth $z = -z_{nomo}$, the currents vanish and the stress is assumed negligible and that lateral friction is not negligible. The equations of motion are now

$$-\rho f v = -\frac{\partial P}{\partial x} + K_x \left(\frac{\partial^2 u}{\partial x^2} + \frac{\partial^2 u}{\partial y^2} \right) + \frac{\partial}{\partial z} \left(K_z \frac{\partial u}{\partial z} \right) \qquad (2.104)$$

and

$$\rho f u = -\frac{\partial P}{\partial y} + K_x \left(\frac{\partial^2 v}{\partial x^2} + \frac{\partial^2 v}{\partial y^2} \right) + \frac{\partial}{\partial z} \left(K_z \frac{\partial v}{\partial z} \right). \qquad (2.105)$$

Munk then used the concept of vertically integrated mass transport which was introduced by Sverdrup. After integrating in z, cross-differentiating in x and y and combining the equations in ψ', where $V = \frac{\partial \psi'}{\partial x}$ and $U = -\frac{\partial \psi'}{\partial y}$ then the equation to be solved is

$$K_x \left(\frac{\partial^4}{\partial x^4} + \frac{2\,\partial^4}{\partial x^2 \partial y^2} + \frac{\partial^4}{\partial y^4} \right) \psi' - \beta \frac{\partial \psi'}{\partial x} = \frac{\partial \tau_{xs}}{\partial y} - \frac{\partial \tau_{ys}}{\partial x} \qquad (2.106)$$

for singular boundary region

for the interior region

This equation is now applied to the rectangular ocean.

The boundary constraints are that both ψ' and its derivatives normal to

the boundaries must varnish. Note that we've assumed only an east-west wind system so $\tau_{ys}=0$.

Munk's rational was to look for a boundary layer solution of 2.106. The motivation to do this comes from the problem's physics which implies that friction may play a small role in the interior of the ocean so in the interior K_x may be small.

From Figure 2.9 , τ_{xs} can be represented by

$$\tau_{xs} = -\tau \cos \frac{\pi y}{b} \tag{2.107}$$

A change in variables such that

$$\psi^* = \frac{\beta \psi'}{\pi \tau} \quad , \quad x' = \frac{x}{b} \quad , \quad y' = \frac{y}{b} \quad \text{and} \quad r = \frac{a}{b}$$

is now introduced.

Then if we assume that ψ' is of the form $\sin \pi y'$ as a y' variation, then we can write the x'-dependent part of 2.106 as

$$\lambda \left(\frac{d^4\psi^*}{dx'^4} + 2\pi \frac{d^2\psi^*}{dx'^2} + \pi^4 \psi^* \right) - \frac{d\psi^*}{dx'} = 1. \tag{2.108}$$

and furthermore, if we call ψ_i^* the interior solution then $\psi_i^* = -x' + c$. Near the boundary, frictional terms are important and since the boundary layer is small we can stretch the x co-ordinate in this region by introducing the variable ξ defined as $x' = \lambda^m \xi$ where m is a constant determined from 2.108. Since we require the balance in the boundary region to retain the $\frac{d^4\psi^*}{dx'^4}$ term, then we would like this term to be of order unity in the boundary region. We now match this term with all others in the equation which are of order unity. If this is done then we find that $\frac{d^4\psi^*}{d\xi^4}$ and $\frac{d\psi^*}{d\xi}$ balance each other fairly well. Equation (2.108) then becomes

$$\lambda^{(1-4m)} \frac{d^4\psi^*}{d\xi^4} - 2\pi \lambda^{(1-2m)} \frac{d^2\psi^*}{d\xi^2} + \lambda \pi^4 \psi^* - \lambda^{-m} \frac{d\psi^*}{d\xi} = 1 \tag{2.109}$$

and the balance in 2.109 implies that

$$1 - 4m = -m$$

$$\text{so } m = 1/3$$

so we have

$$\frac{d^4\psi^*}{d\xi^4} - 2\pi^2\lambda^{2/3}\frac{d^2\psi^*}{d\xi^2} + \lambda^{4/3}\pi^4\psi^* - \frac{d\psi^*}{d\xi} = \lambda^{1/3} \tag{2.110}$$

and to an order of $\lambda^{1/3}$, this equation can be approximated by

$$\frac{d^4\psi^*}{d\xi^4} - \frac{d\psi^*}{d\xi} = 0 \tag{2.111}$$

for the boundary layer.

The final solution of 2.111 is

$$\psi^* = \psi^*_{bd\,(x'=0)} + \psi^*_{bd\,(x'=r)} + \psi^*_i \tag{2.112}$$

and if we apply the boundary conditions that $\psi' = 0$ on all boundaries and that $\frac{\partial\psi'}{\partial x} = 0$ at $x = 0$, a then the complete solution is

$$\psi' = \sin\pi y \left\{ -x + r - \lambda^{1/3} + \lambda^{1/3} e^{(x-r)\lambda^{-1/3}} + \left[(\lambda^{1/3} - r)\cos\frac{x\sqrt{3}\lambda^{-1/3}}{2} + (\sqrt{3}\lambda^{1/3} - \frac{r}{\sqrt{3}})\sin\frac{x\sqrt{3}\lambda^{-1/3}}{2} \right] e^{\frac{-x\lambda^{-1/3}}{2}} \right\}. \tag{2.113}$$

So using the mean annual zonal winds only, the solution shows that the integrated oceanic wind-driven circulation is divided into closed circulatory systems called "gyres." The gyres are bounded at latitudes where the curl$\underset{\sim}{\tau} = 0$ and are centered at latitudes where curl$\underset{\sim}{\tau}$ is an extremum.

So for the zonal wind case given here, the dividing lines between the gyres are given by

$$\frac{\partial \tau_{xs}}{\partial y} = \frac{\pi}{b} \tau \sin \frac{\pi y}{b} = 0.$$

and the maxima or the axes of the gyres are at

$$\frac{d}{dy}\left(\frac{1}{\beta}\frac{\partial \tau_{xs}}{\partial y}\right) = \frac{1}{\beta}\frac{\pi^2}{b^2}\tau \cos\frac{\pi y}{b} = 0$$

The form of the streamlines is as shown in Figure 2.10. If we define $K = (\beta/K_L)^{1/3}$, then the region between x = 0 and x = 4/K corresponds to the Gulf Stream. Now if the solution that we have is written as

$$\psi' = \frac{r}{\beta} \cdot \frac{\partial \tau_{xs}}{\partial y} \cdot F \qquad (2.114)$$

where

$$F = -G e^{-kx/2}\cos\left(\frac{\sqrt{3}}{2}kx + \frac{\sqrt{3}}{2kr} - \frac{\pi}{6}\right) + 1 - \frac{1}{kr}\left(kx - e^{-k(r-x)} - 1\right) \qquad (2.115)$$

and

$$G = \frac{2kr - 3}{\sqrt{3}\ kr} \qquad (2.116)$$

then $F(x_1)$ is the total northward transport between x = 0 and x = x, and

$$\frac{dF}{dx} = kG e^{-kx/2}\sin\left(\frac{\sqrt{3}}{2}kx - \frac{\sqrt{3}}{2kr}\right) - \frac{1}{r}\left(1 - e^{-k(r-x)}\right), \qquad (2.117)$$

is the total northward transport per unit width between x = 0 and x = x. Now when F and $\frac{dF}{dx}$ are evaluated then we find that the ocean falls into the three parts (as a function of x) which were used in the solution development, so at the western boundary then $x \ll r$ and $r \gg 1$, and for any fixed latitude, varies with F(x) only, so

$$F_{west} = -\frac{2\sqrt{3}}{3} e^{-Kx/2} \cos\left(\frac{\sqrt{3}}{2} Kx - \frac{\pi}{6}\right) + 1 \qquad (2.118)$$

and

$$\frac{dF_{west}}{dx} = \frac{2\sqrt{3}\,K}{3} e^{-Kx/2} \sin\frac{\sqrt{3}}{2} Kx \quad . \qquad (2.119)$$

This represents an underdamped oscillation with wavelength

$$L = \frac{4\sqrt{3}\,\pi}{3} \left(\frac{K_L}{\beta}\right)^{1/3} .$$

Note also that the form of ψ' results in a counter-current outside of the western boundary region and for $K_L \sim 5(10^7)\text{cm}^2/\text{sec}$ $L \sim 200\text{-}250$ km.

Recent data suggests that the Gulf Stream is 50-60 km wide, so $K_L \sim 10^6$ cm^2/sec is a more reasonable characteristic lateral frictional transfer coefficient magnitude.

Away from either the east-west boundary, x is comparable to r and

$$\left.\begin{aligned} F_{central} &= 1 - \frac{x}{r} \\ \frac{dF_{central}}{dx} &= -\frac{1}{r} \end{aligned}\right\}$$ which give a broad constant drift

which corresponds to the Sverdrup solution where $\frac{\partial \psi'}{\partial x} = \nabla \times \frac{\underset{\sim}{\tau}}{\beta}$ where $\underset{\sim}{\tau}$ is zonal. On or along the eastern coastal strip then $x \simeq r$ or $(r-x) \ll r$ and

$$F_{eastern} = 1 - \frac{x}{r} + \frac{1}{kr}\left(e^{k(x-r)} - 1\right) \qquad (2.120)$$

$$\frac{dF_{eastern}}{dx} = \frac{1}{r}\left(e^{k(x-r)} - 1\right) \qquad (2.121)$$

so the width is small, the current is weak and in the real world a local meridional wind may obscure the current.

Munk found that the countercurrent east of the Gulf Stream was in good agreement with theory but there is also a counterflow observed also between the coast and the strong meridional current which is not predicted by Munk's viscous boundary layer theory.

Although the frictional baroclinic models are quite good there are problems such as: it is assumed that sufficient potential energy is available to allow the circulation to exist as a baroclinic mode, but it may not be true that for every distribution of wind stress, the density field will respond with a distribution of potential energy that is determined by the wind stress.

Since the non-linear terms are neglected, friction acts the same up and down stream along the western boundary. and the question remains "why does the western boundary current separate from the coast."

2.5 NUMERICAL MODELS

Though the analytical Munk (1950) model successfully predicts, to varying measure, the gross stationary features of the Gulf Stream, it is evident from ocean station data as well as present VHRR (Very High Resolution Radiometer) data that such a model is a simple approximation at best. There have been a multitude of models either in extension of the Munk work or with non-linear approaches to the problem, such as those of Fofonoff (1954), Morgan (1956), Charney (1955) and Stommel (1961), but no one has yet constructed a theoretical model in which one can have more than reserved confidence.

In all of the above models, non-linearities are not considered contemporaneously with lateral and or vertical friction. Furthermore, temporal variations and baroclinicity are neglected entirely. It thus becomes implicit, from the lack of good reproduction of nature by theory that the stationary barotropic assumption is not a very complete form of truth in approach to an investigation of the Gulf Stream nature.

It was, in fact, not until Lineykin's (1957) work appeared that the "diffusion of density" equations appeared in any of the mathematics systems approaches to the problem of solving the complete system of coupled equations (Nos. 2.1 through 2.7).

Sarkisyan (1969) indicates the more obvious shortcomings of barotropic oceanic circulation models. He demonstrates that failure to include baroclinicity and bottom topography are perhaps the most serious omissions. It is clear from his discussion that the density field, more than any other variable, defines the current field, so flow-field calculations are only as accurate as our knowledge of the field of mass. Consequently, Bryan and Cox (1967), Bryan and Cox (1968), Bryan (1969), Sarkisyan and Keondzhyan (1972), and Keondzhyan (1973) took the

numerical methods approach to calculating sea level, mass transport and flow fields using numerical, versus purely analytical, techniques. The latter two works furthered the numerical predictions with a diagnostic approach to the problems.

The present state of the numerical modeling art is not sufficient in terms of computer storage space, time limits, mesh grid and finances, to solve equations 2.1 through 2.7. Presumably with the advent of larger and faster computers, we'll be able to more adequately predict the velocity and density fields but presently the straightforward numerical approach has glaring shortcomings.

The diagnostic approach to numerical modeling prediction has been taken by several investigators based on the realization that there is a considerable amount of ocean station data which has been collected over the last sixty years in the near vicinity of the Gulf Stream. Given this data, Keondzhyan has reconstructed the density fields as a function of time and then directly computed the velocity and pressure fields which are contemporary with the STD field observables. With such an approach, one is not burdened with non-linearities in the equations of salt and heat and in the non-linear coupling of S and T with the horizontal equations of motion by way of the quasi-hydrostatic assumption. Keondzhyan notes that the results can be assumed to be a multilayered model, which in the limit of zero layer thickness becomes a representation of a continuously stratified fluid. This approach is further supported also since no layer--interfacial conditions need be imposed other than the continuity condition.

In the actual model, Keondzhyan imposes a wind stress and supposes the conditions of no flow normal or tangential to the lateral or vertical boundaries. With a basin defined laterally as $\Gamma(\theta,\lambda)$ and on the bottom by $H(\theta,\lambda)$, where θ and λ are latitude and longitude respectively, the author then specifies the

density field $\rho(\theta,\lambda,z)$ and numerically solves a modified version of the system of hydrodynamic equations 2.1 through 2.3 with a horizontal step spacing of 1.25°. The calculation results yield velocity profiles which are in reasonable agreement with present knowledge of the multiyear averages for the summer season for the direction and strength of circulation in the North Atlantic. The cyclonic nature of the lowest order circulation is evident with the East Greenland and Laborador currents and a strong Gulf Stream showing up quite clearly. Figure 2.11 depicts the field surface elevation as computed from the predicted field of pressure anomaly of Keondzhyan. The predicted change in sea surface elevation across the Gulf Stream is then used in a one by one comparison of surface elevations computed by the dynamic height methods from actual station data, as discussed earlier, along identical transects of the Gulf Stream. These comparative results are shown in all figures entitled Sea Level Elevations in this report.

A startling fact arises from these results, as evidenced in the figures, the Keondzhyan (K) numerical model, though only useful in a time-averaged sense, shows remarkable resemblence to the dynamic height calculations generated by Huang and Pietrafesa (H-P) in this report. The curves are never identical and the departures of the H-P curves from the K curve are not well correlated to the contemporaneous wind magnitudes and directions. It must be remembered here that the K curve includes a seasonally averaged surface wind so that departures of the mechanical forcing function from the mean should be the rule rather than the exception.

The results of the Keondzhyan work depict the following features of the North Atlantic ocean: the well-known counter-clockwise Northern cell; the East Greenland and a substantial Laborador current; the clockwise rotational circulation at mid-latitudes; an intense western boundary current, the Gulf Stream, which separates at approximately 50° west longitude and 40° north latitude into a

northeastward flowing branch, a continuation of the Gulf Stream and a part which turns, in a clockwise fashion to the south, to become a current counter to and beyond the eastern lateral boundary of the Gulf Stream.

The numerical models also substantiate the baroclinic ocean work of Lineykin (1955a, 1955b, 1955c, 1956, 1957a, 1957b, 1957c) in contrast to the classical theories based on the Sverdrup relation. The results of Keondzhyan also show, rather conclusively, that the meridional and zonal transports are not independent of one or the other, as is suggested by the Sverdrup theory, and extensions thereof, but depend, in a coupled way, on wind stress, bottom topography and the baroclinicity of the ocean regime. This diagnostic approach offers a powerful tool for future work in ocean dynamics.

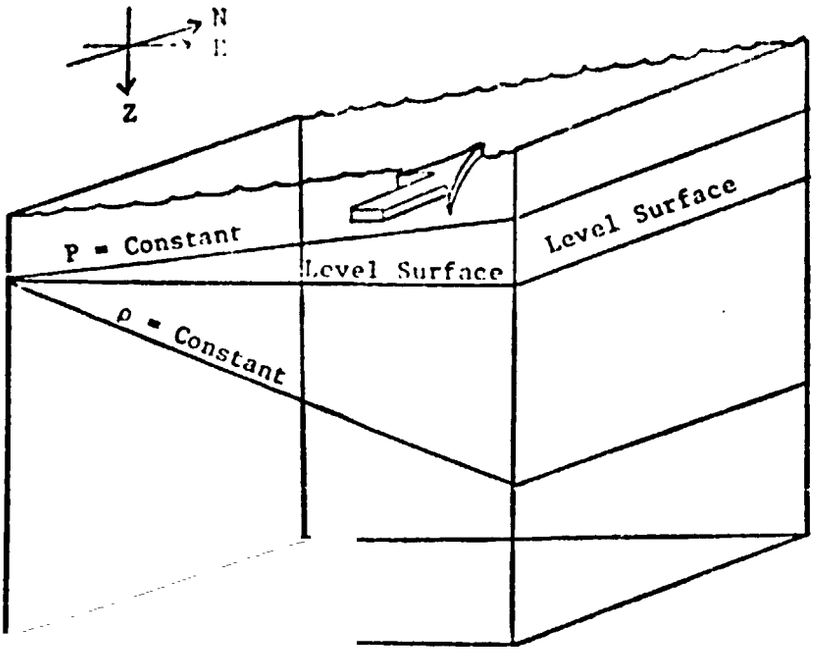

Figure 2.1 Dynamic configuration of Gulf Stream cross-section.

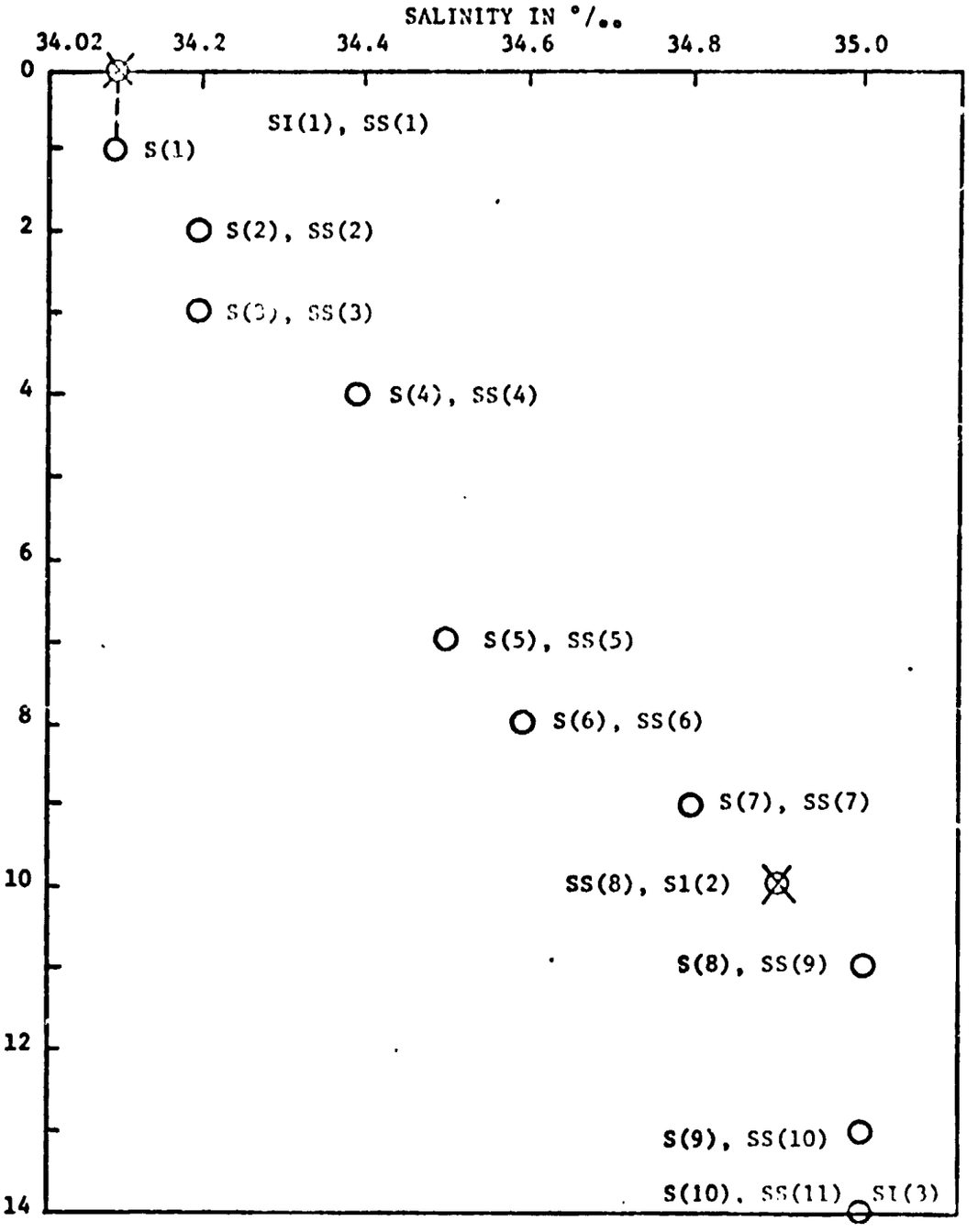

Figure 2.2 Salinity versus depth for example given in Section 2.3.

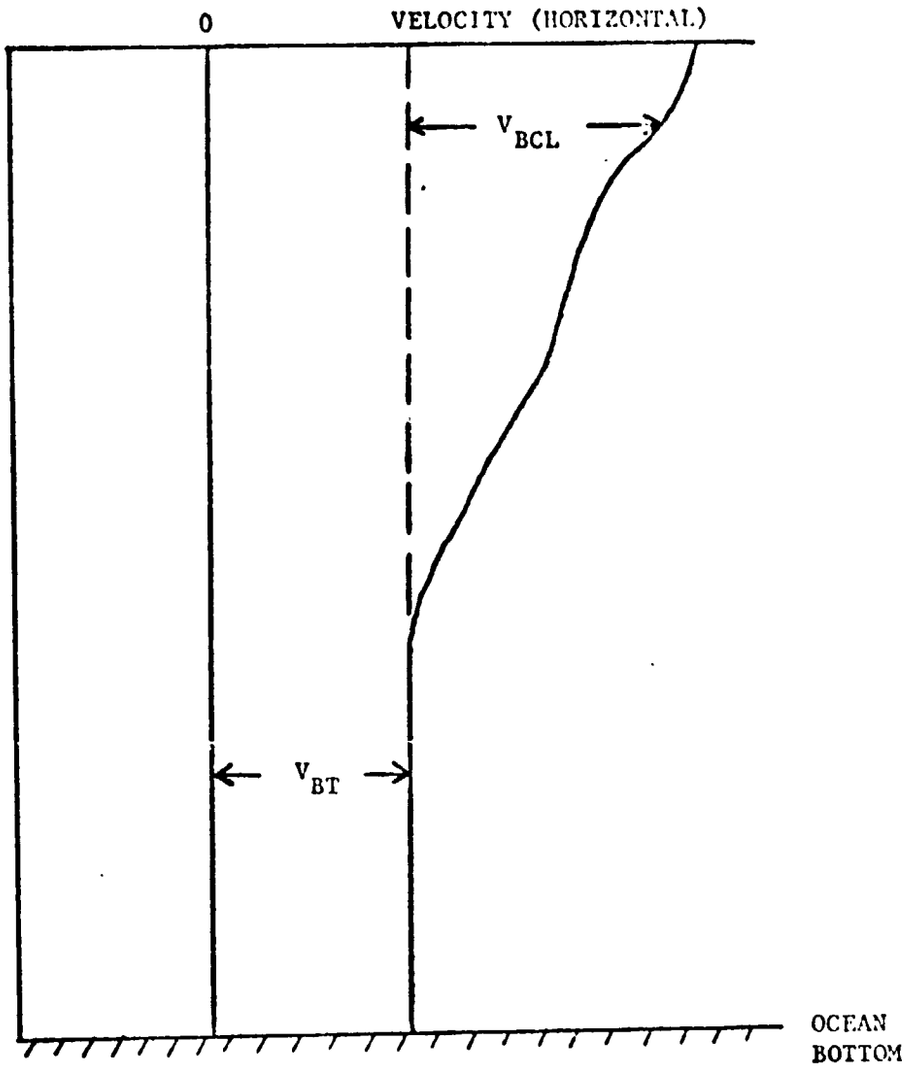

Figure 2.3 A diagram showing the decomposition of the horizontal velocity into Barotropic, V_{BT}, and Baroclinic, V_{BCL}, components as a function of depth in the ocean.

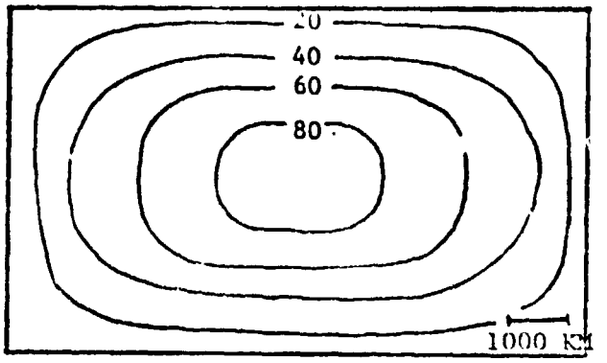

Figure 2.4 Streamlines of a non-rotating ocean (Stommel, 1948, Fig. 2).

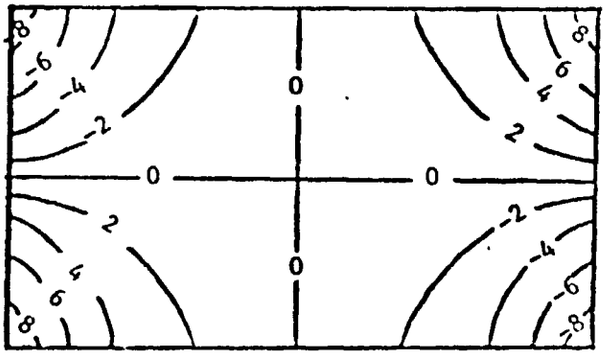

Figure 2.5 Contours of sea surface height in a non-rotating ocean (Stommel, 1948, Fig. 3).

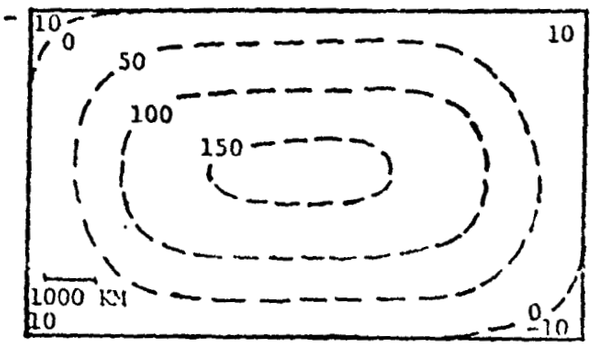

Figure 2.6 Contours of sea surface height in cm. in a uniformly rotating ocean (Stommel, 1948, Fig. 4).

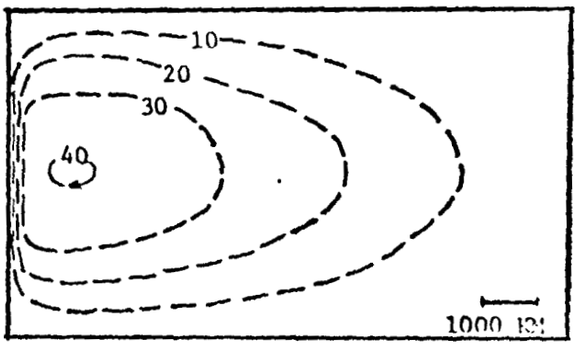

Figure 2.7 Streamlines for case in which Coriolis parameter varies linearly as a function of latitude (Stommel, 1948, Fig. 5).

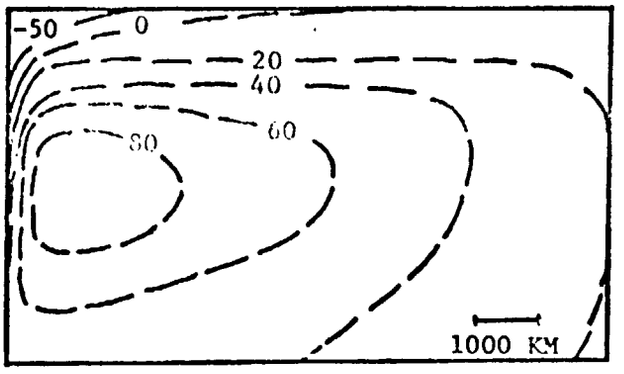

Figure 2.8 Contours of sea surface height in cm. in an ocean where the Coriolis parameter is a linear function of latitude (Stommel, 1948, Fig. 6).

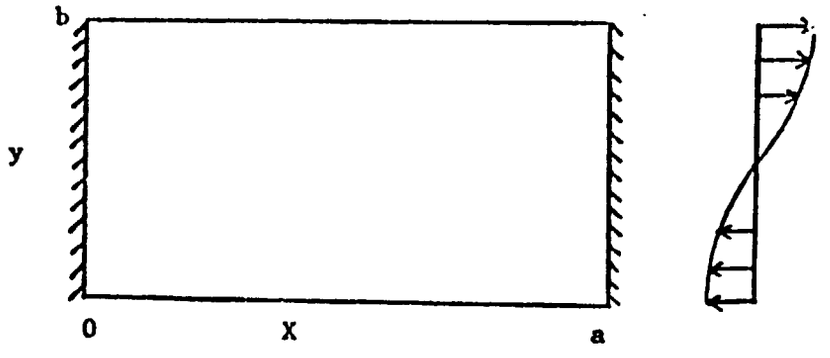

Figure 2.9 Rectangular ocean and wind stress, as applied latitudinally over the ocean, in Munk (1950) model.

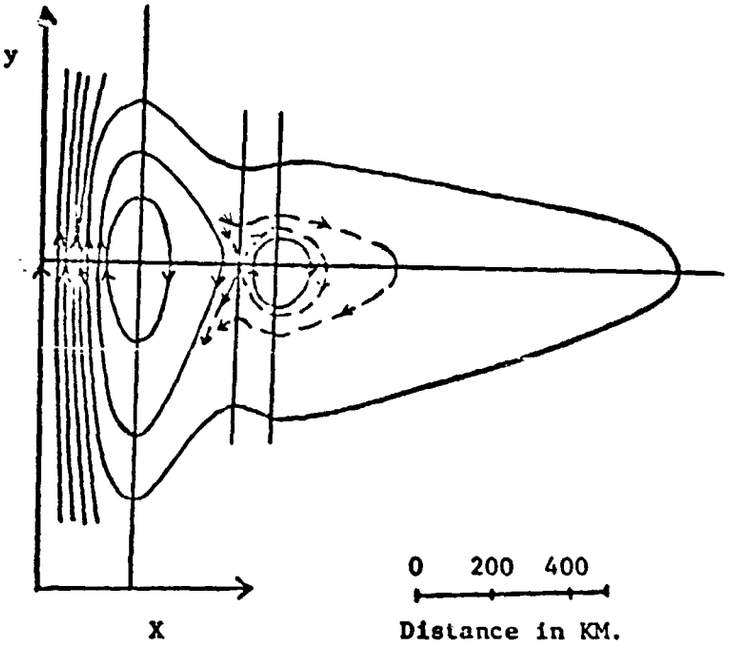

Figure 2.10 Mass transport streamfunction in units of 10^{12} gram sec^{-1} for the Munk (1950) model of the Gulf Stream (Munk, 1950, Fig. 5).

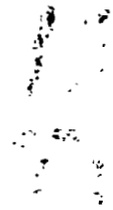

Figure 2.11 Theoretical Model of Gulf Stream Surface Elevation by Keondzhyan (1973).

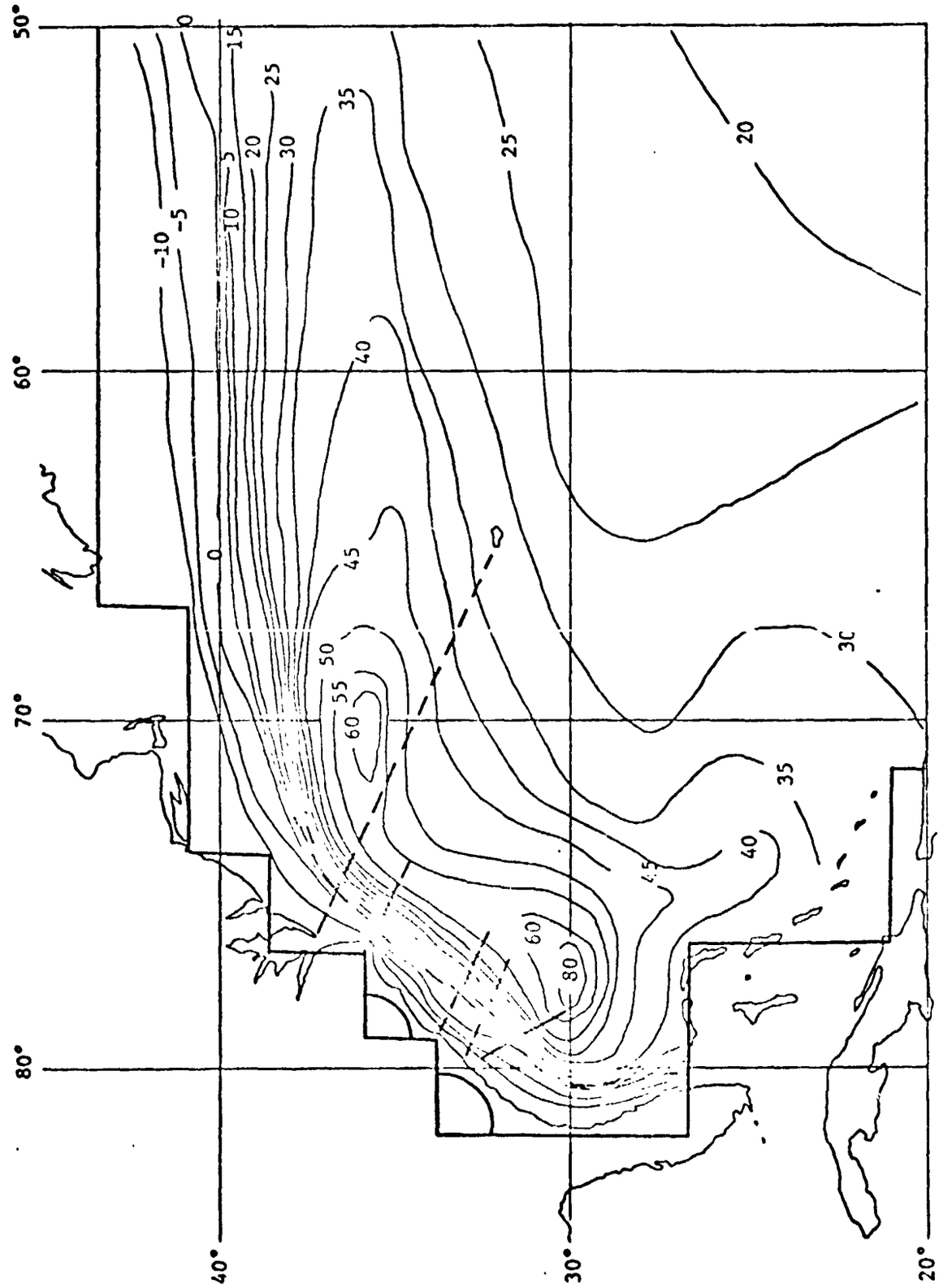
50°
60°
70°
80°
40°
30°
20°
-10
-5
0
5
10
15
20
25
30
35
40
45
50
55
60
80
25
20
35
40
45
60
35

3. SURFACE PROFILES BASED ON HYDROGRAPHIC DATA

As discussed in the previous chapter, the surface elevation of the ocean can be related to water movement directly through the geostrophic equations. Accepting the approximations of the model, we have calculated the ocean surface elevation profiles based on hydrographic data tabulated by National Oceanographic Data Center (NODC), NOAA along the Gulf Stream path off of the eastern coast of the United States. The data are arranged by ship tracks covering the period from 1912 to 1972. The location of each station is first plotted on a map with time of the survey indicated so that the ship track of each individual cruise can be identified. All of the stations taken on a particular cruise are then fed into the computer as described in Chapter 2 so that dynamic heights can be calculated.

From the station data, one finds that there are many cruises designed to study continental shelf water only. On such cruises, ship tracks stop as soon as the edge of the Gulf Stream is reached. Since our interest is, however, in the location as well as the magnitude of the surface elevation deviation caused by the Gulf Stream, any ship track that does not completely traverse the Gulf Stream is discarded. Thus the data from a number of very closely spaced stations collected mainly by Duke University (Stefannson, Atkinson, 1967) is unfortunately, of no use in this study. Also, since one of the basic assumptions of geostrophic modeling is the existence of a layer of no motion, models based solely on shallow water data will become increasingly inaccurate when the depth becomes too shallow. As a result, we exclude all of the stations with a total depth less than 30 meters. As for the layer of no motion, an arbitrary depth of 1000^{m} is used throughout the present study. When the total water depth is less than 1000^{m}, the bottom is used as the layer of no motion. This may not be the best choice, but it is adopted as a compromise

so that the vast amount of data collected by different ships at different times and locations can have a uniform reference.

All of the results are presented in graphs on a one for one graph to cruise basis. Sometimes when a single cruise covers two tracks, the profiles of both tracks are plotted together to show the difference of surface elevation over the short time period between the two transects. Wind data are presented together with the profiles whenever available. The wind speed is measured in knots and the direction in degrees with zero pointing to the north. Together with most of the profiles, Keondzhyan (1973), mean Gulf Stream model results are plotted as a common reference. The results are grouped by geographic locations and are presented as follows.

Figure 3.1 indicates the ship tracks of the survey conducted in 1932. Figures 3.2, 3.3, 3.4, 3.5 are the earliest complete profiles available from the NODC data. The ship tracks followed the line between Cape Charles and Bermuda. The profiles show considerable fluctuations in Gulf Stream strength, but the location of the Gulf Stream is rather stable at 200 nautical miles off of the coast. Unfortunately no wind data are available for these cruises.

Figure 3.6 indicates another eight ship tracks in the same general area off the coast of Virginia covering the years 1953 to 1966. Again, the agreement between the profiles based on the hydrographic data and the mean Gulf Stream model of Keondzhyan is acceptable. In figures 3.8, 3.11, 3.13 the ship tracks started and ended in the middle of the ocean. An arbitrary station in each cruise is picked as the reference station. The distance from land marks to such reference stations is indicated on the graph.

Figure 3.15 indicates ship tracks of all the stations south of Cape Hatteras covering the years from 1955 to 1970. Figures 3.16 to 3.30 show the profiles, the available wind conditions and the profiles from Keondzhyan's mean model.

Of special interest are the stations indicated in Figure 3.31. These are rather closely spaced stations both in the time and space domains. Figures 3.32 to 3.36 show the ten profiles surveyed in eleven days in June, 1968. According to the accepted theory, the Gulf Stream path will not change much in such a short time span as this (see, for example, Stommel, 1966). However, the hydrographic data showed that dramatic changes could occur over a very short time. Figure 3.32 presents two different profiles obtained over the same transect within a three day period. The remarkable thing is that surface elevation increased by half an order of magnitude from one curve to the other leading to inevitable questions concerning the accuracy of shipbound surveys spanning months during a single cruise. Similar features of short period changes have also been observed by recent remote sensing techniques. Such phenomena undoubtedly deserve further scrutiny.

Another group of closely spaced station cruises are presented in Figures 3.37 to 3.45. There are nine cruises transecting 17 tracks surveyed from August to December of 1965. Though the profiles in general agree very well during any single cruise, the differences between cruises are still substantial. This again indicates the mobility and transient nature of the Gulf Stream even south of Cape Hatteras.

In general, there seems to be no direct correlation between the local wind condition and the Gulf Stream strength. This is supported by Stommel's (Stommel, 1966) energy argument. This leaves rapid changes in Gulf Stream strength still not accountable. Another interesting point is that most of the profiles in the group covered by Figures 3.37 to 3.45 generally show weaker Gulf Stream intensity than the mean model of Keondzhyan. This is probably due to the weakened flow in the fall as reported by Iselin (1940) and Fuglister (1951).

The last group of profiles presented in Figures 3.46 to 3.50 is for the Miami area. The profiles are grouped by seasons. Some fluctuations can be detected but the variations are not substantial.

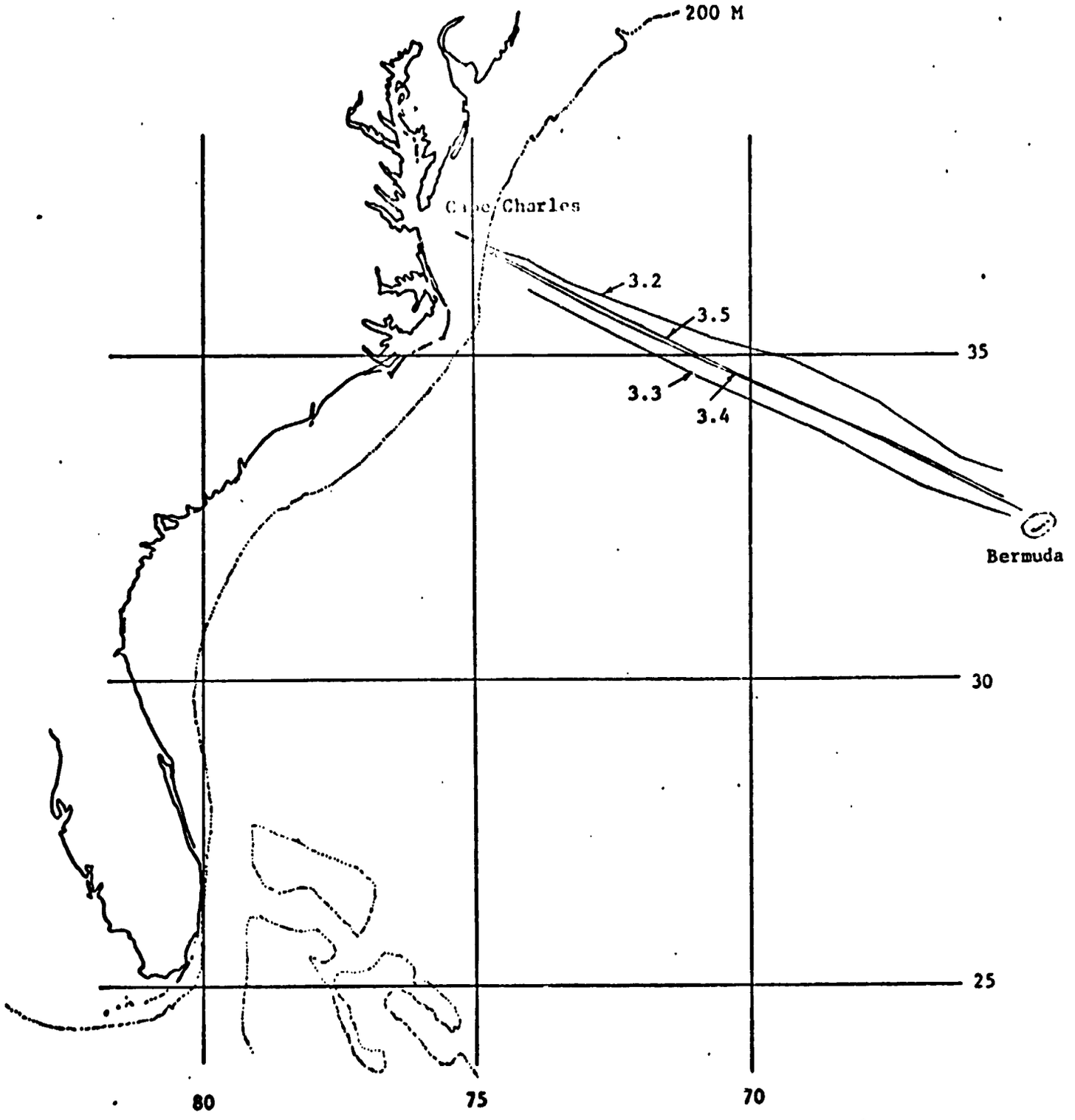

Fig. 3.1 Ship tracks for Figs. 3.2 to 3.5

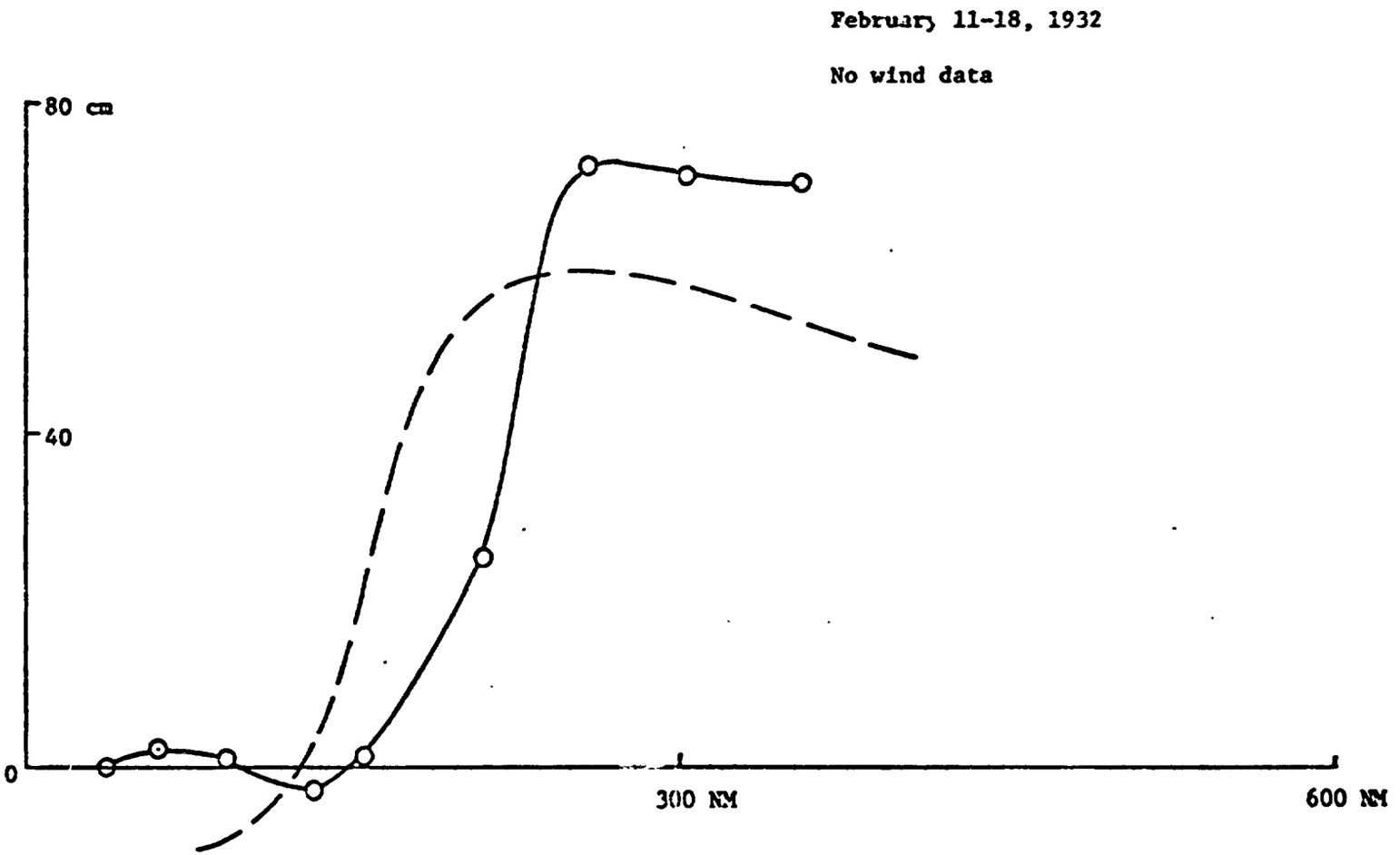

Fig. 3.2 Surface profile based on hydrographic data. Dashed line Keondaliyan Model.

April 17-23, 1932

No wind data.

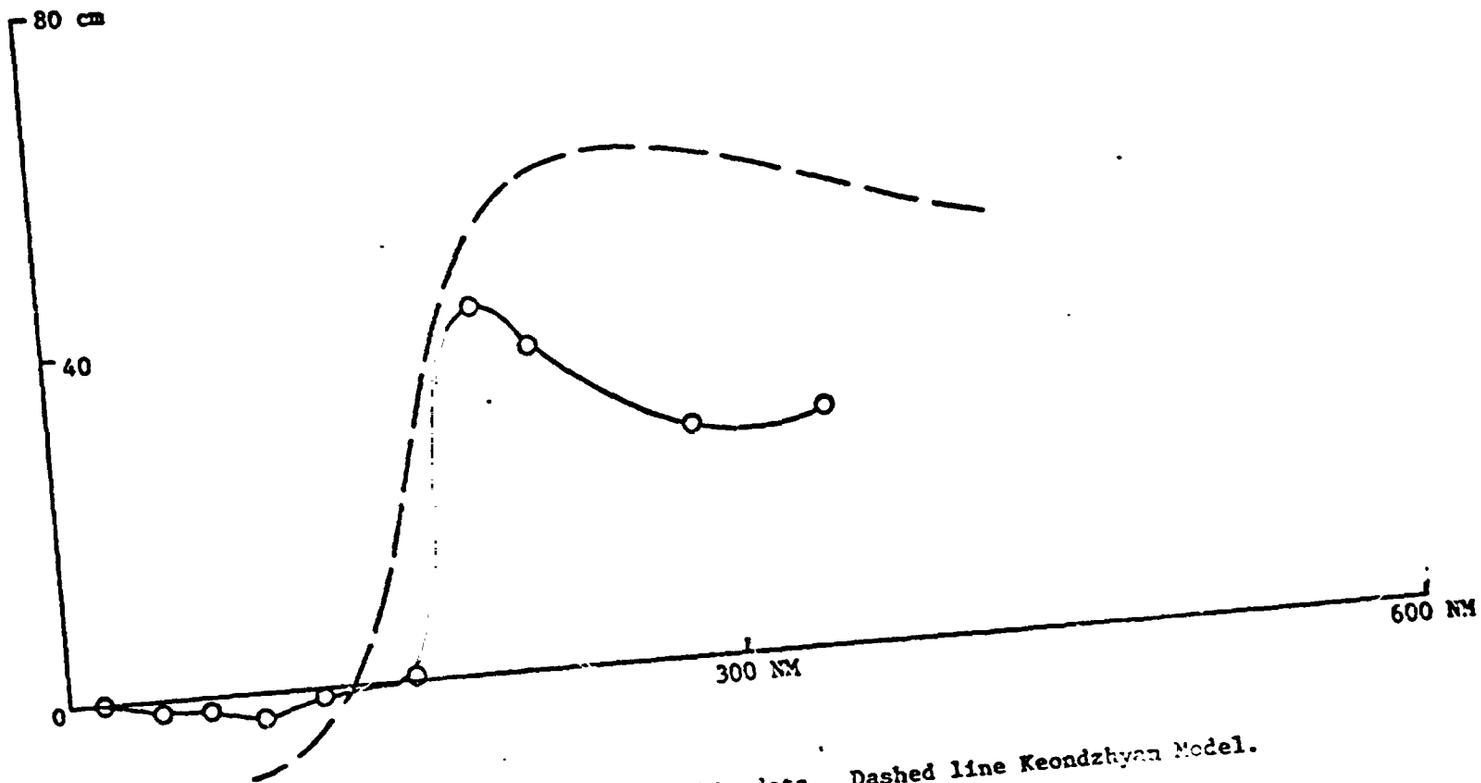

Fig. 3.3 Surface profile based on hydrographic data. Dashed line Keondzhyan Model.

August 28 to September 3, 1932

No wind data.

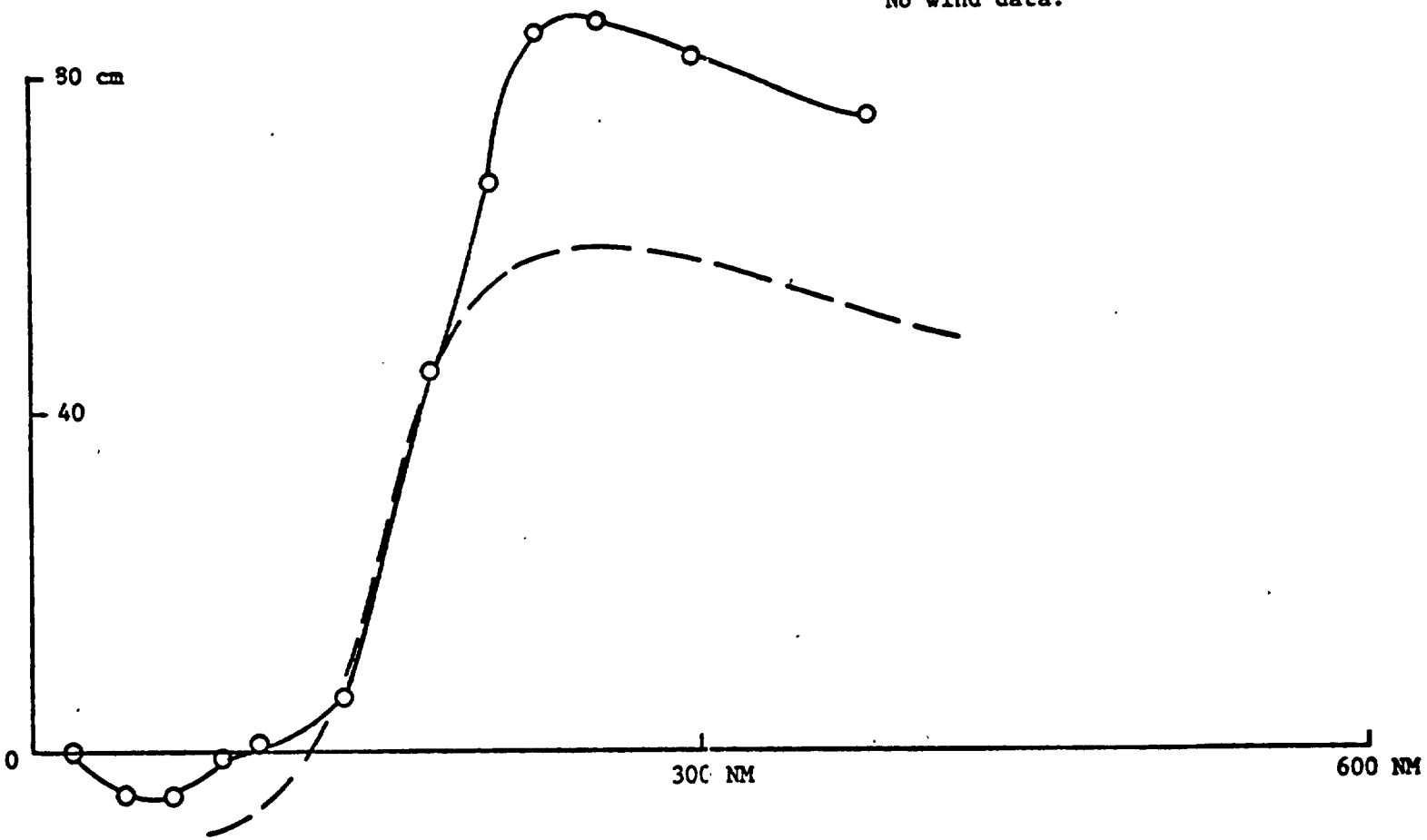

Fig. 3.4 Surface profile based on hydrographic data. Dashed line Keondzhyan Model.

November 30 to December 5, 1932

No wind data.

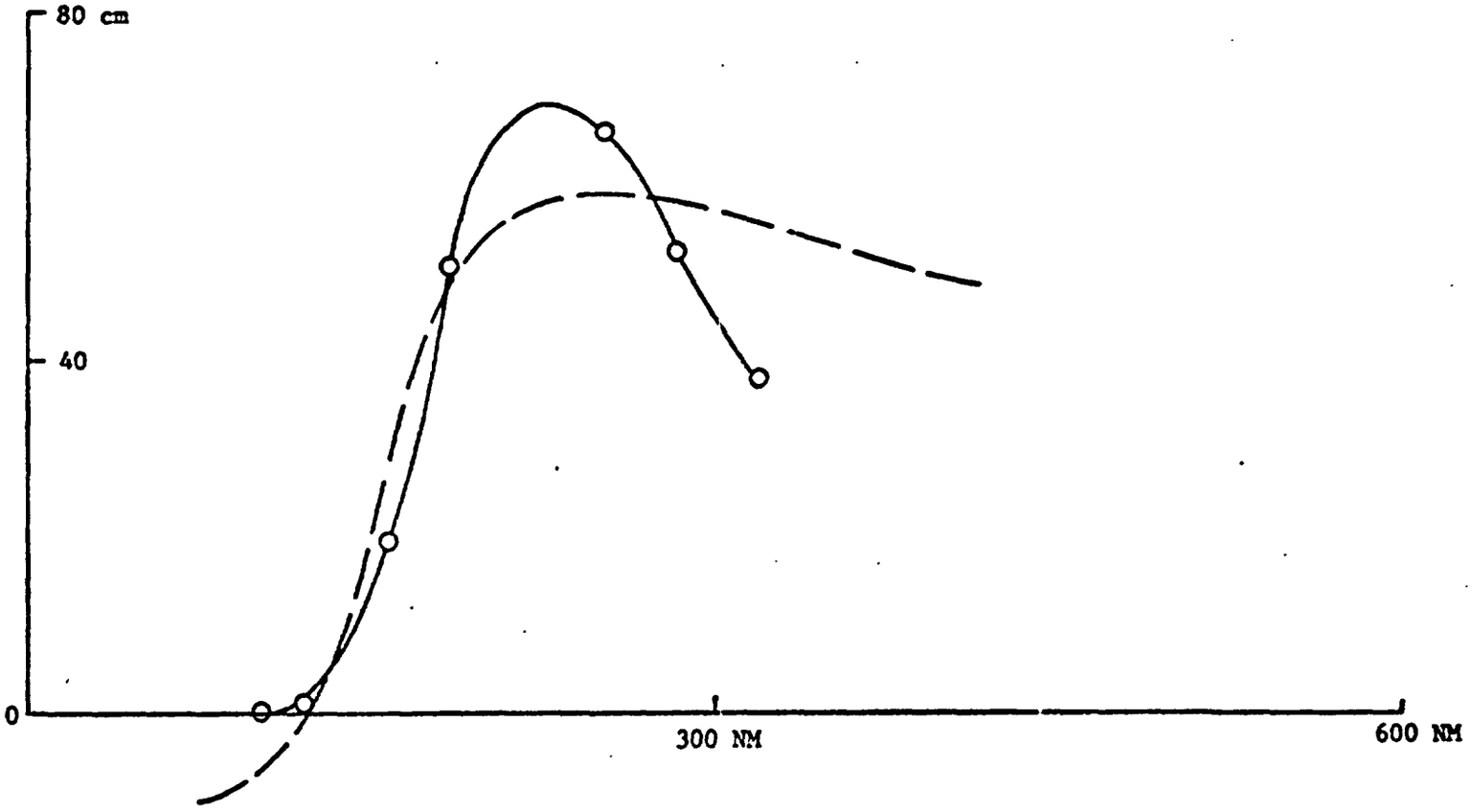

Fig. 3.5 Surface profile based on hydrographic data. Dashed line Keondzhyan Model.

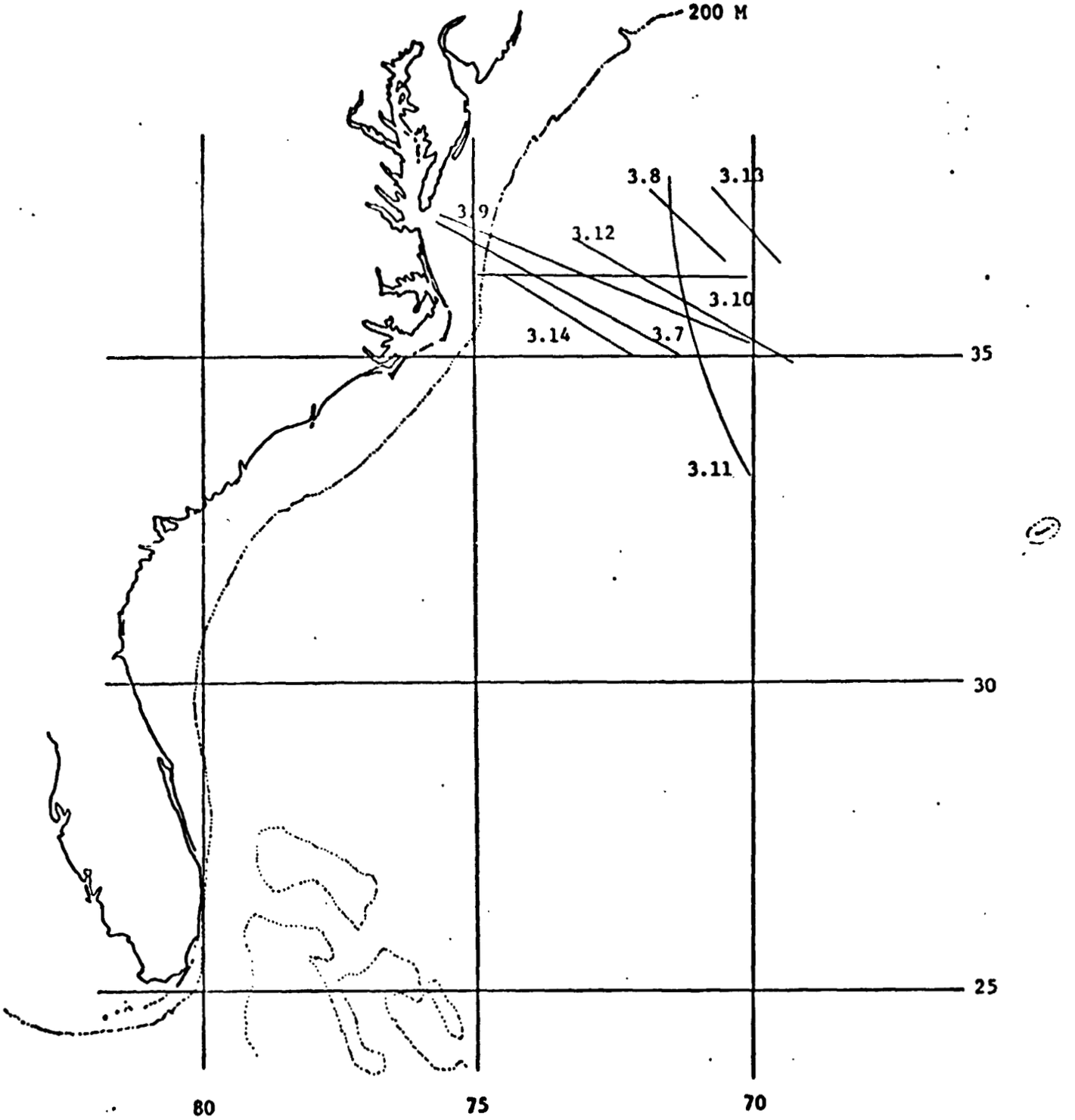

Fig. 3.6 Ship tracks for Figs. 3.7 to 3.14

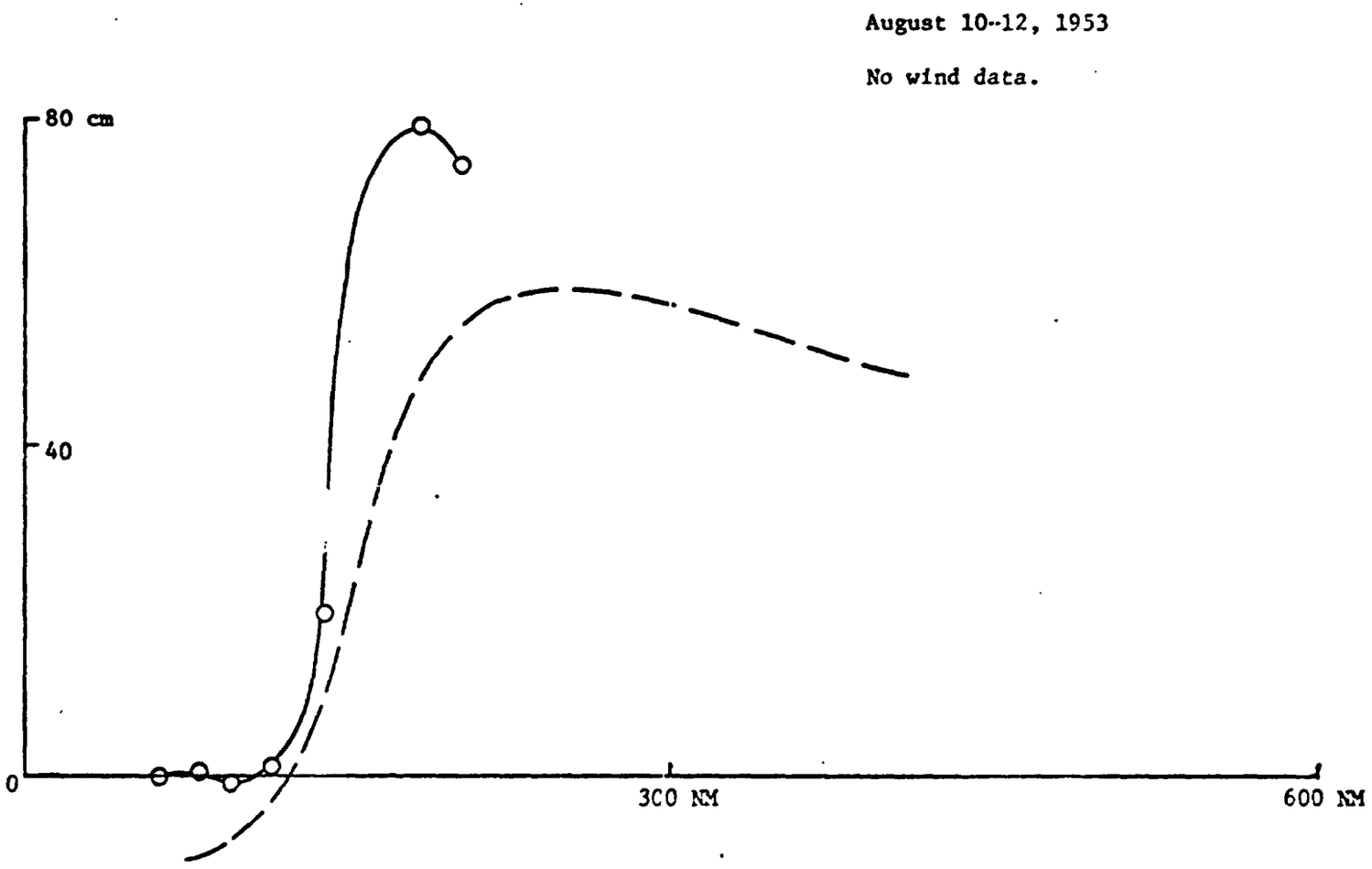

Fig. 3.7 Surface profile based on hydrographic data. Dashed line Keondzhyan Model.

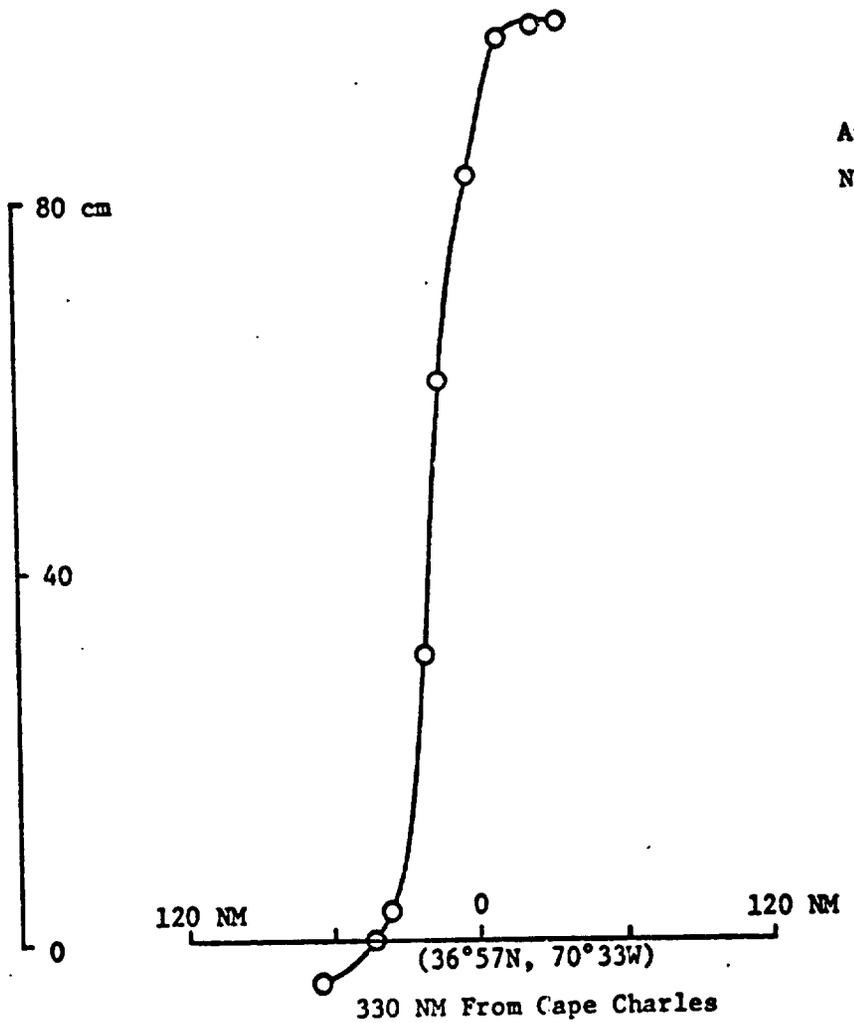

Fig. 3.8 Surface profile based on hydrographic data.

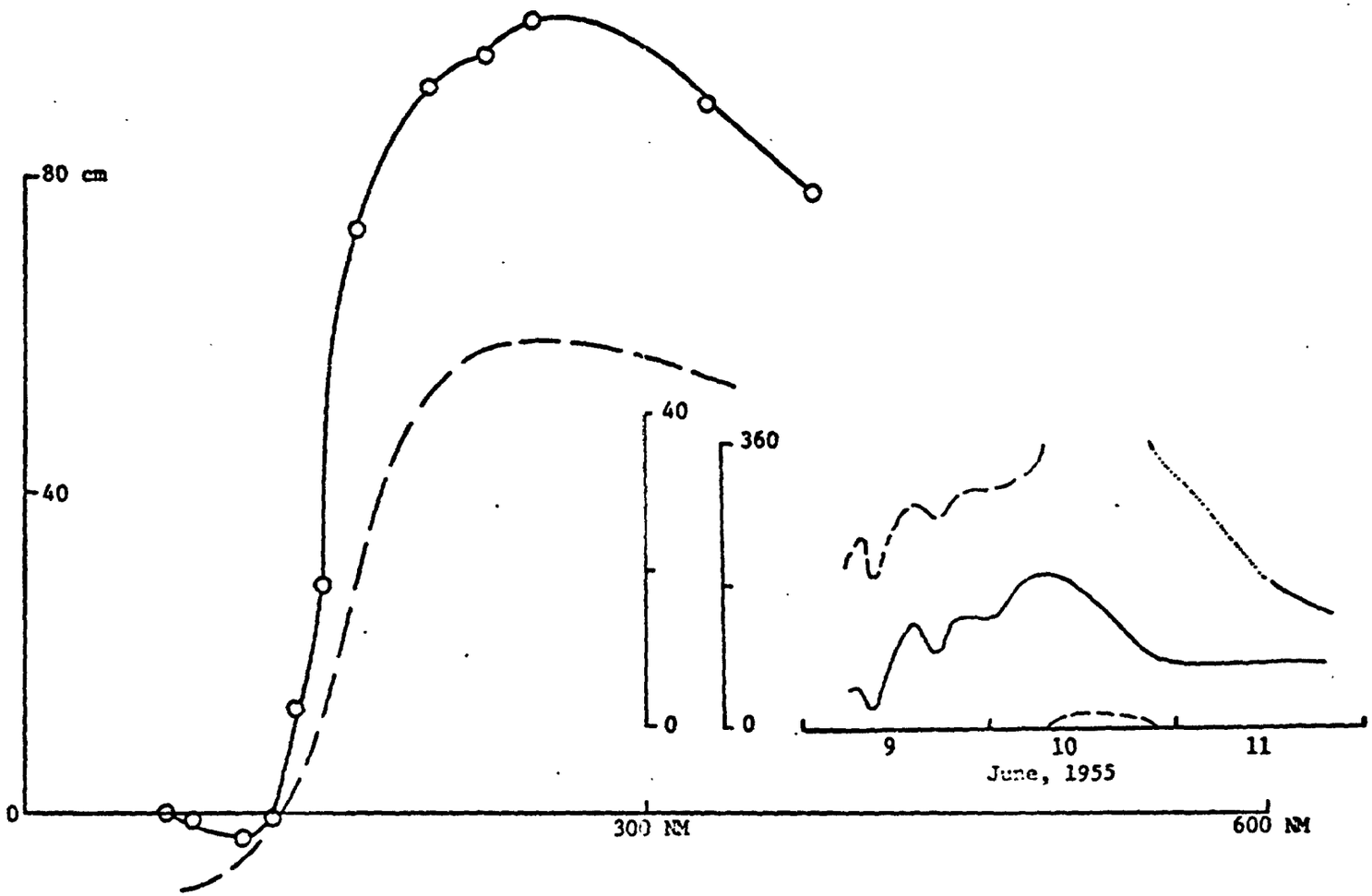

Fig. 3.9 Surface profile based on hydrographic data with wind data ---direction —— magnitude. Dashed line Keondzhyan Model.

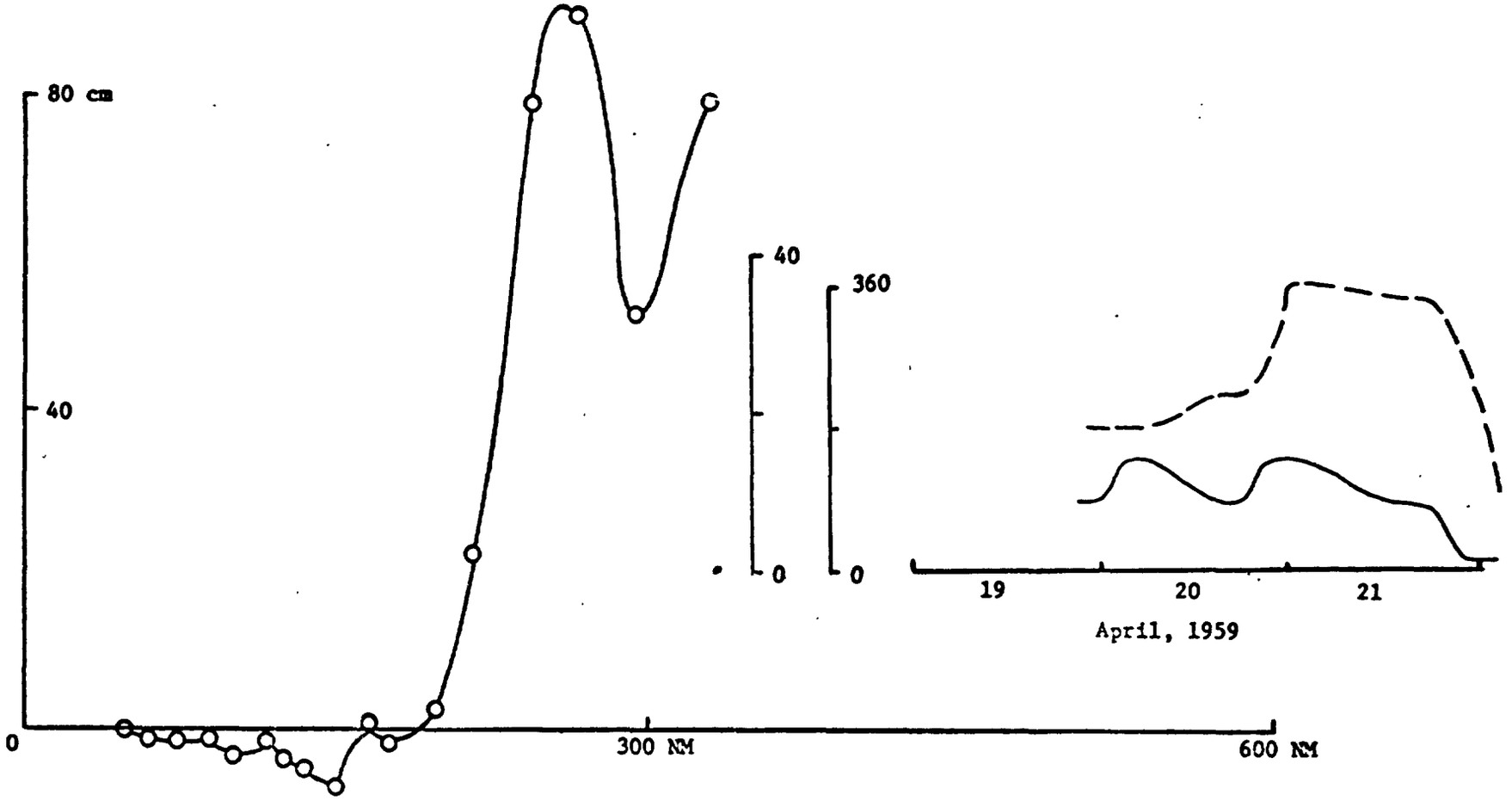

Fig. 3.10 Caption see Fig. 3.9

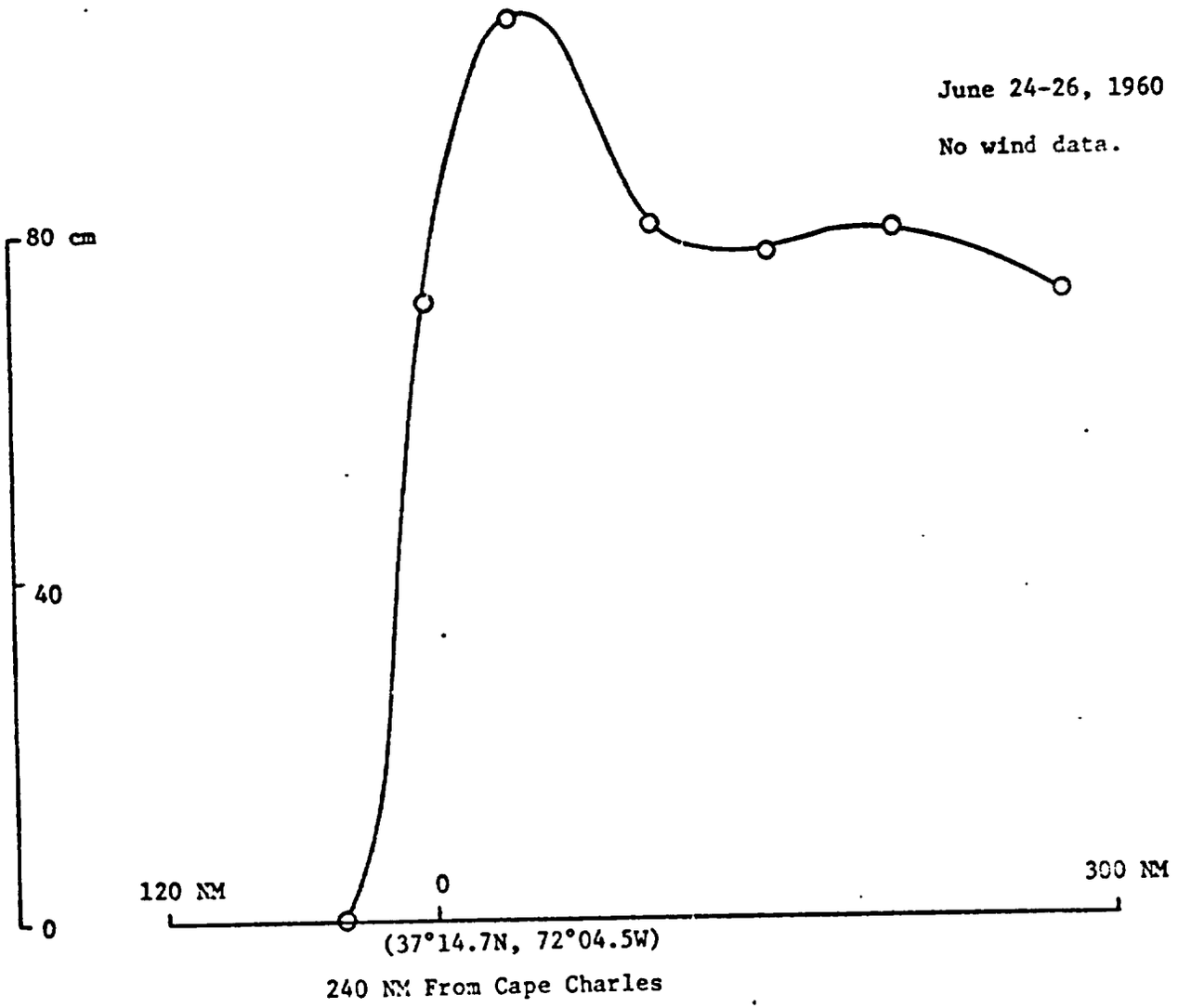

Fig. 3.11 Surface profile based on hydrographic data.

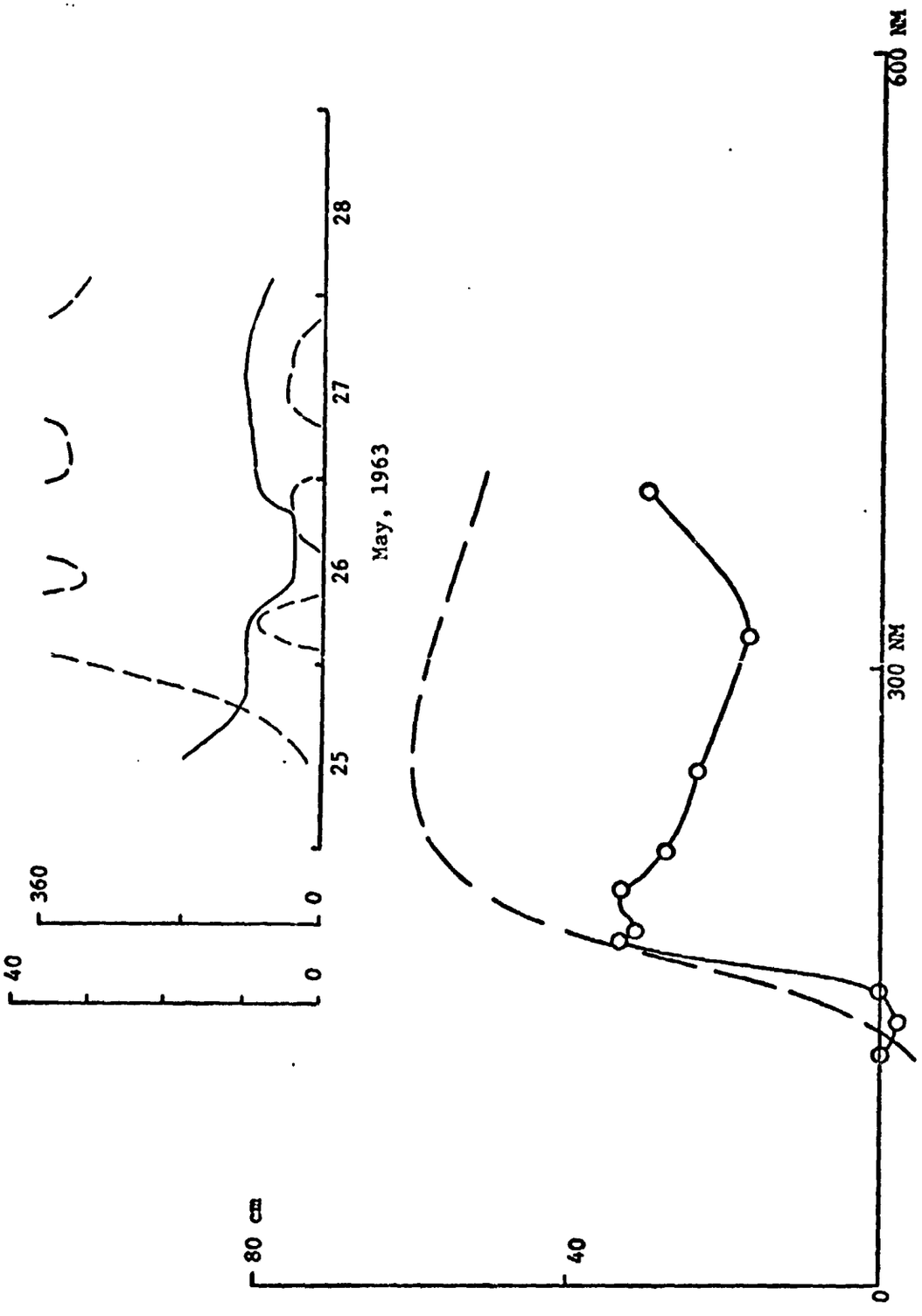

Fig. 3.12 Caption see Fig. 3.9

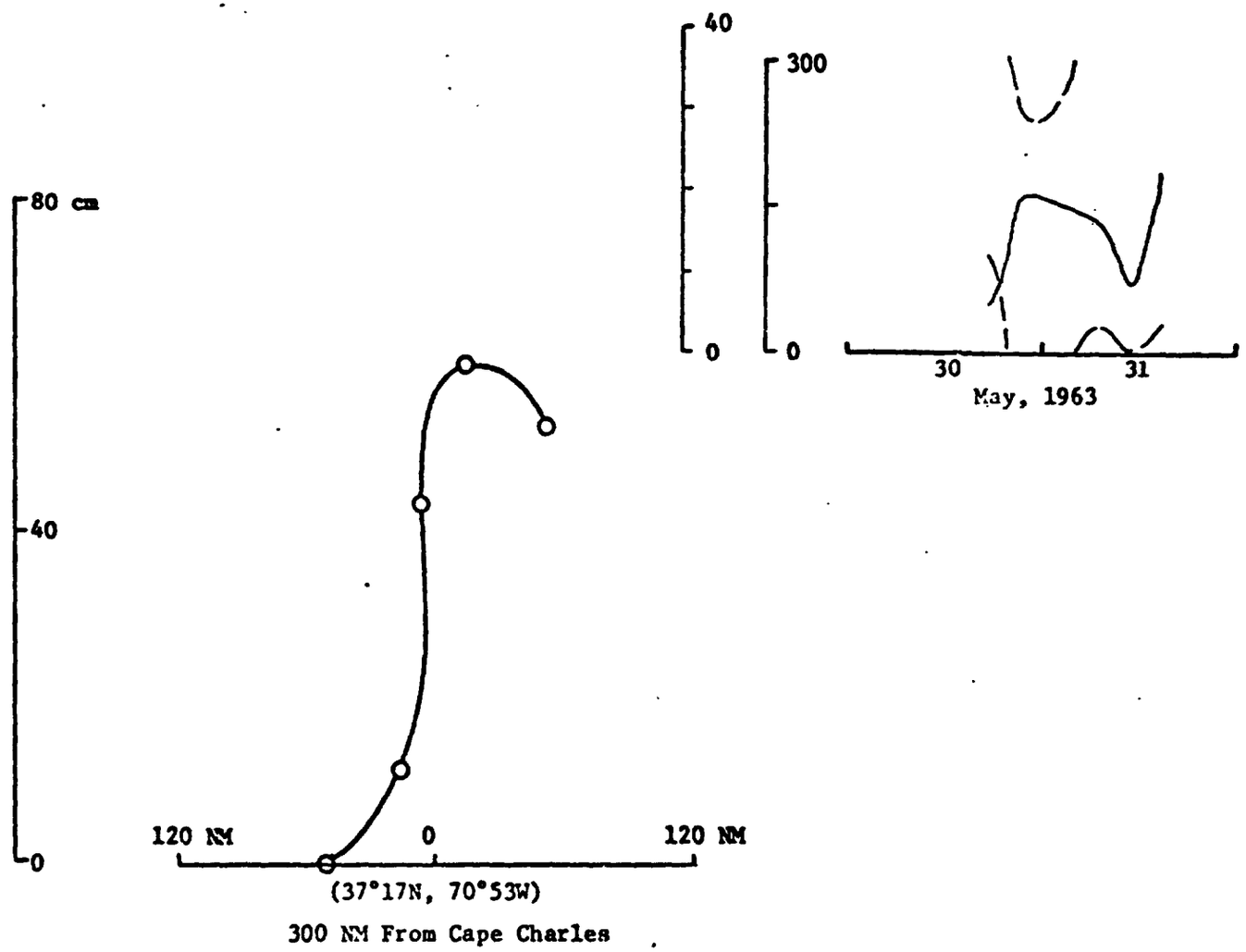

Fig. 3.13 Caption see Fig. 3.9

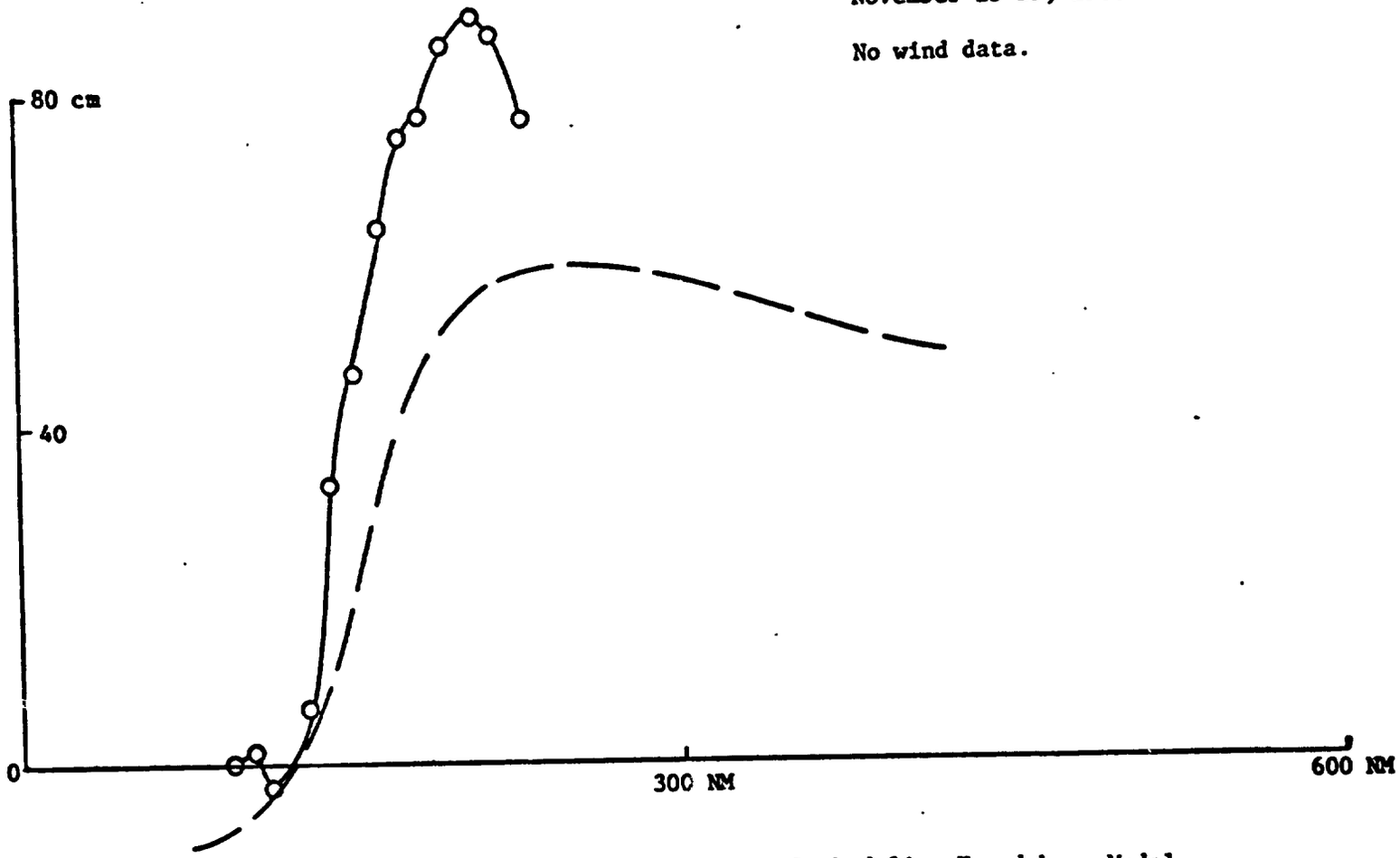

Fig. 3.14 Surface profile based on hydrographic data. Dashed line Keondzhyan Model.

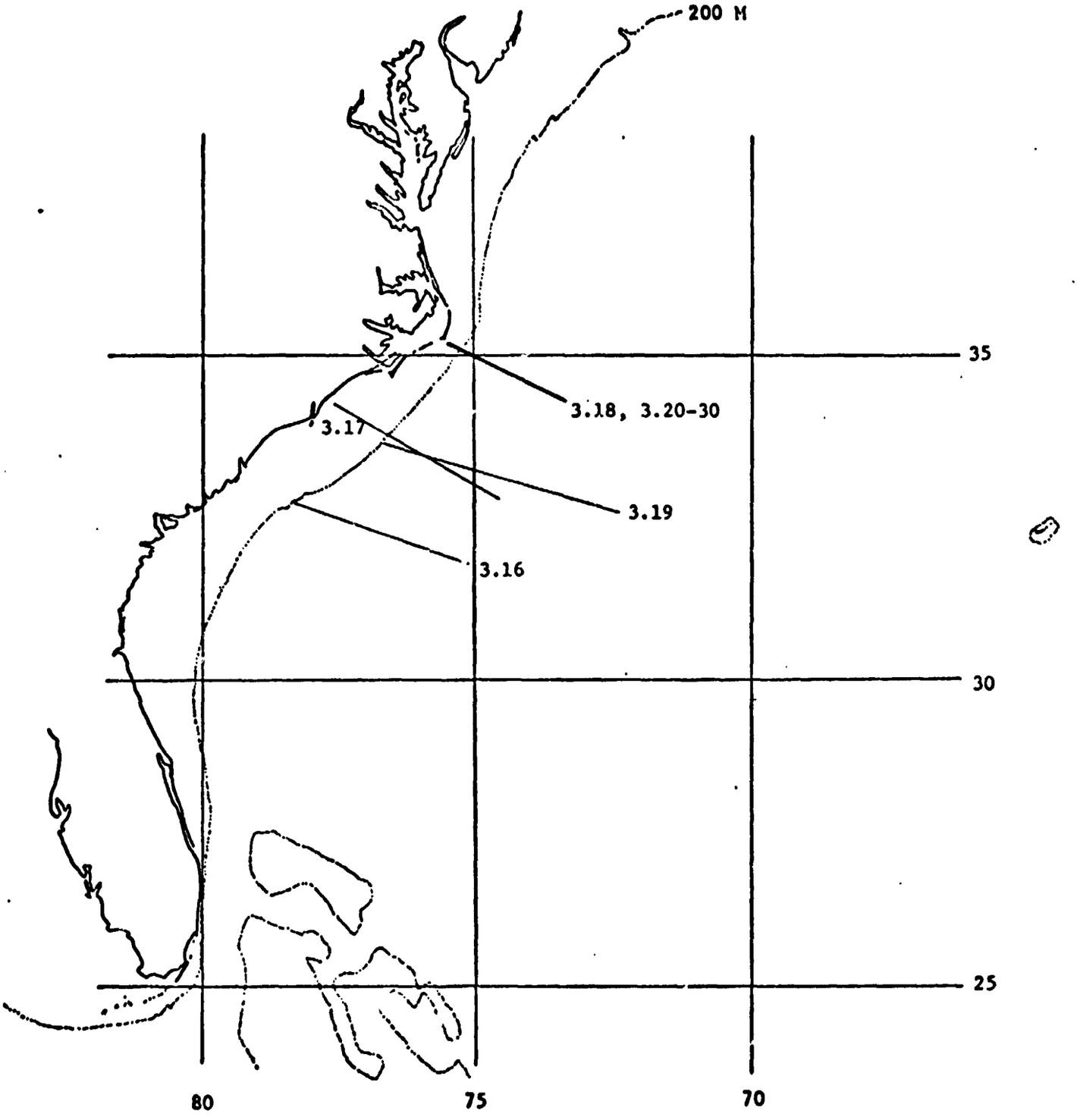

Fig. 3.15 Ship tracks for Figs. 3.16 to 3.30

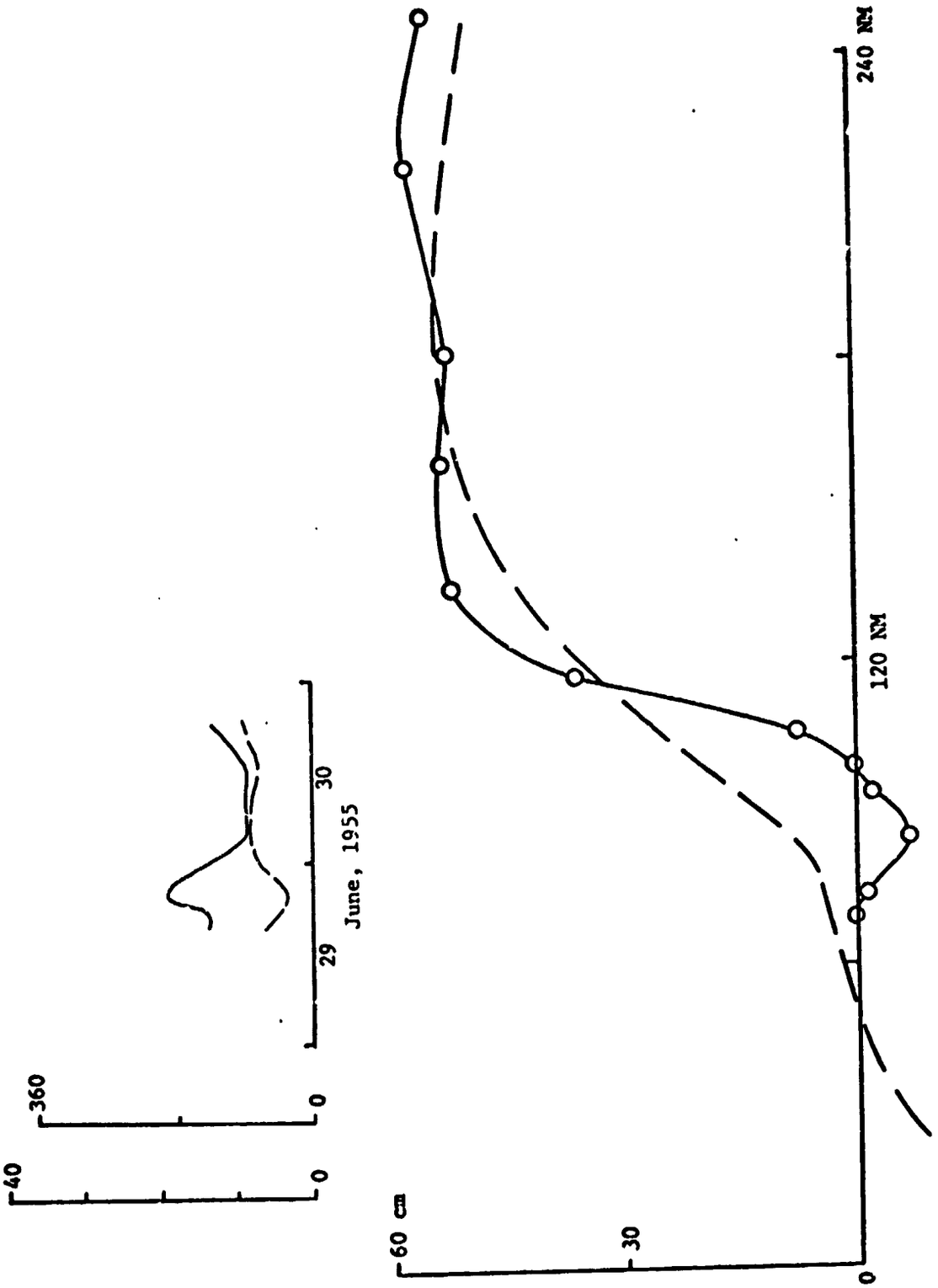

Fig. 3.16 Caption see Fig. 3.9

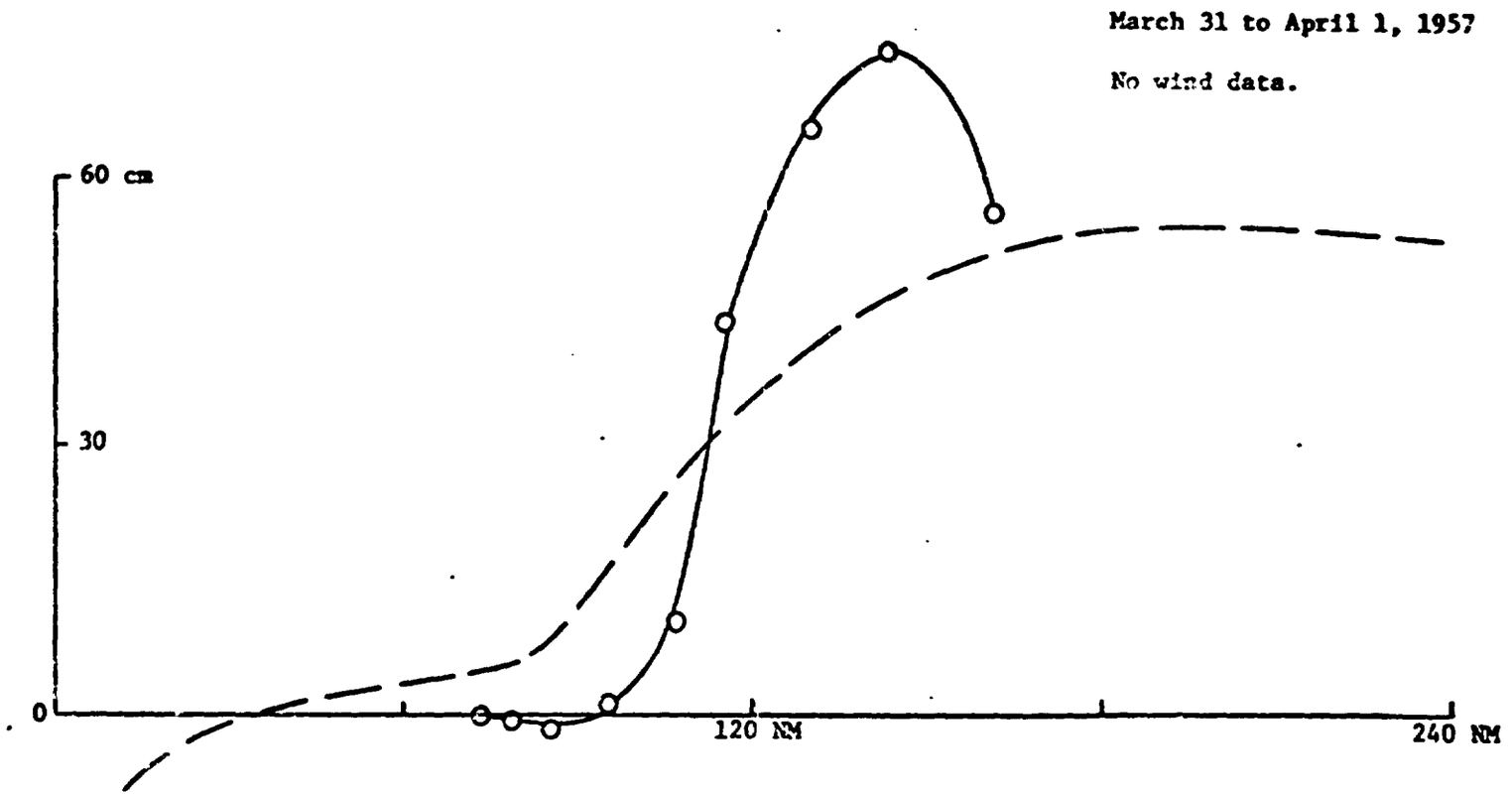

Fig. 3.17 Surface profile based on hydrographic data. Dashed line Keondzhyan Model.

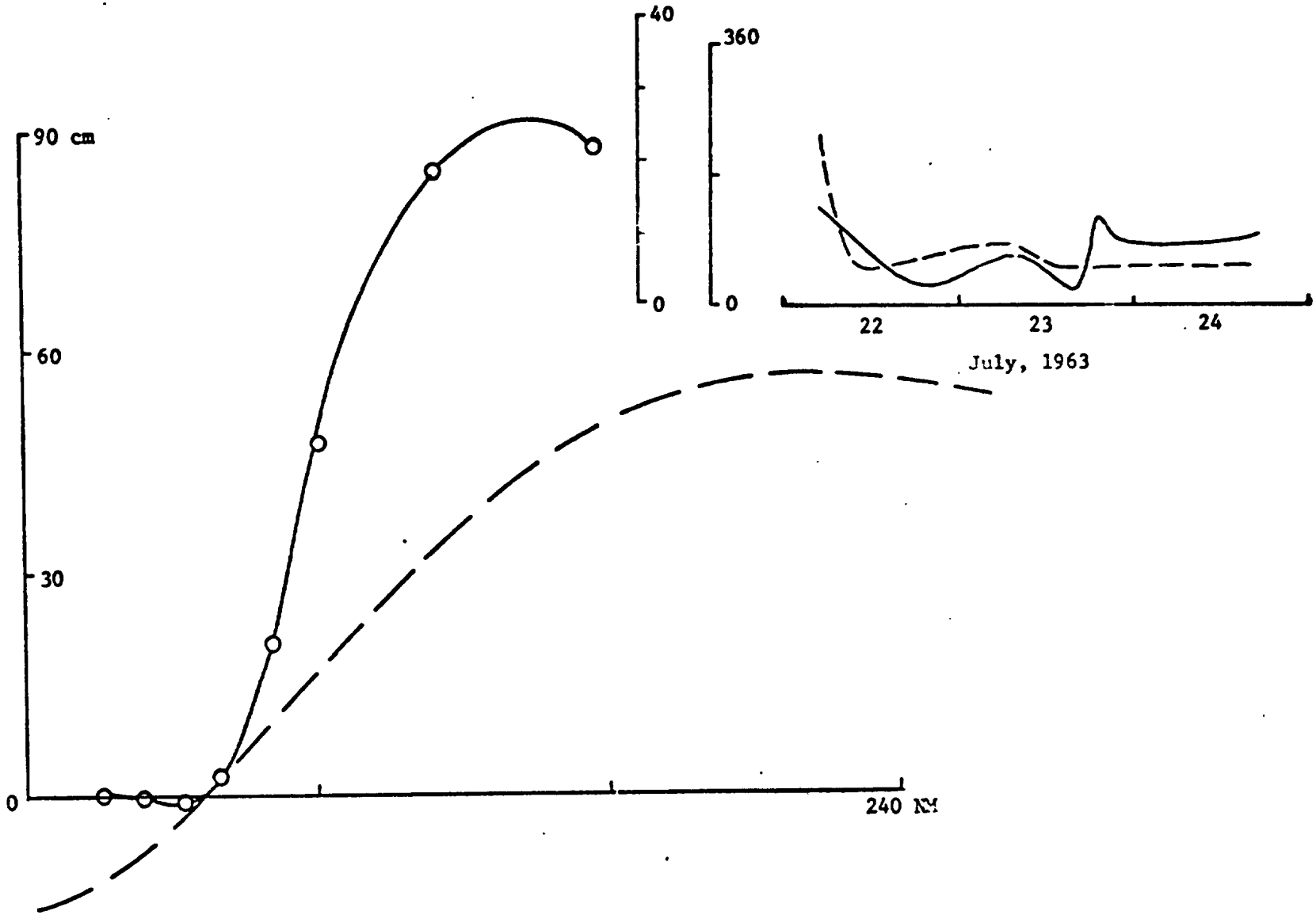

Fig. 3.18 Caption see Fig. 3.9

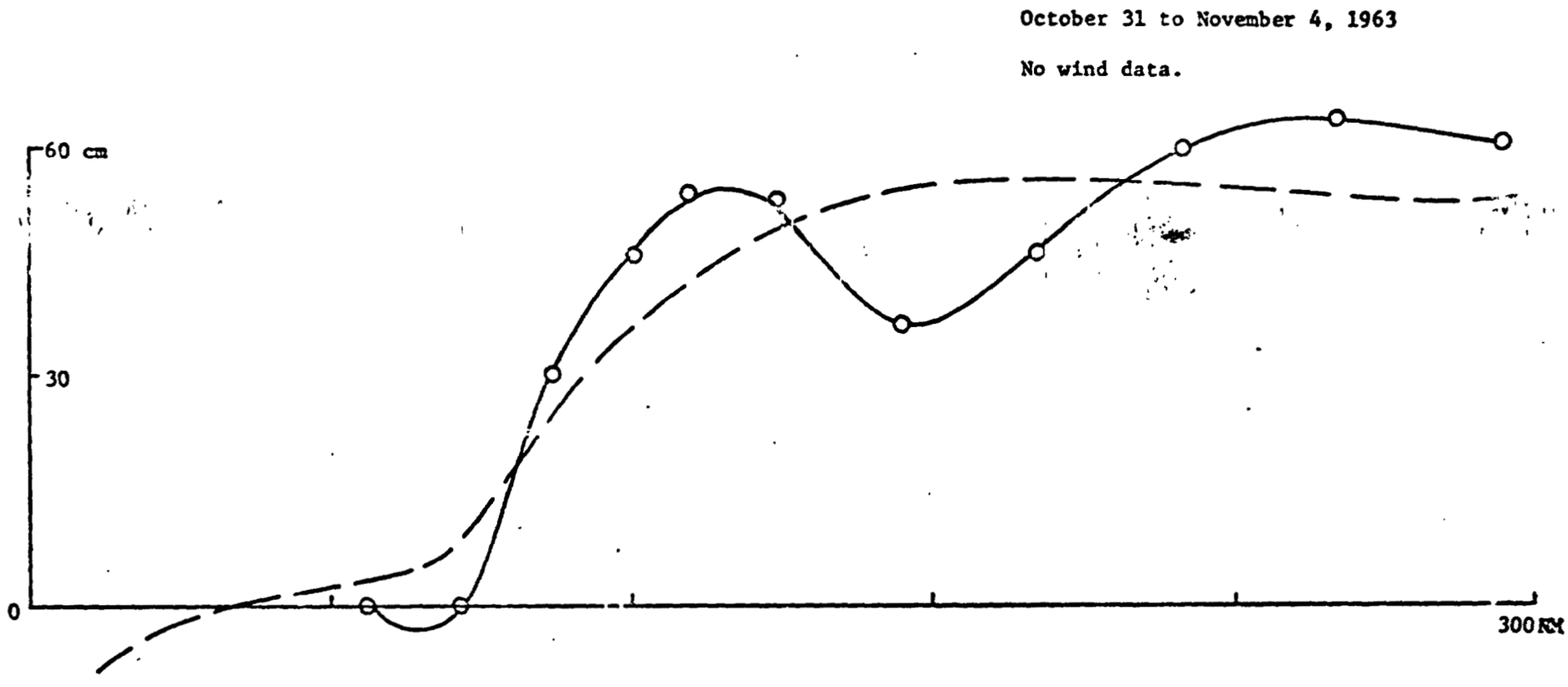

Fig. 3.19 Surface profile based on hydrographic data. Dashed line Keondzhyan Model.

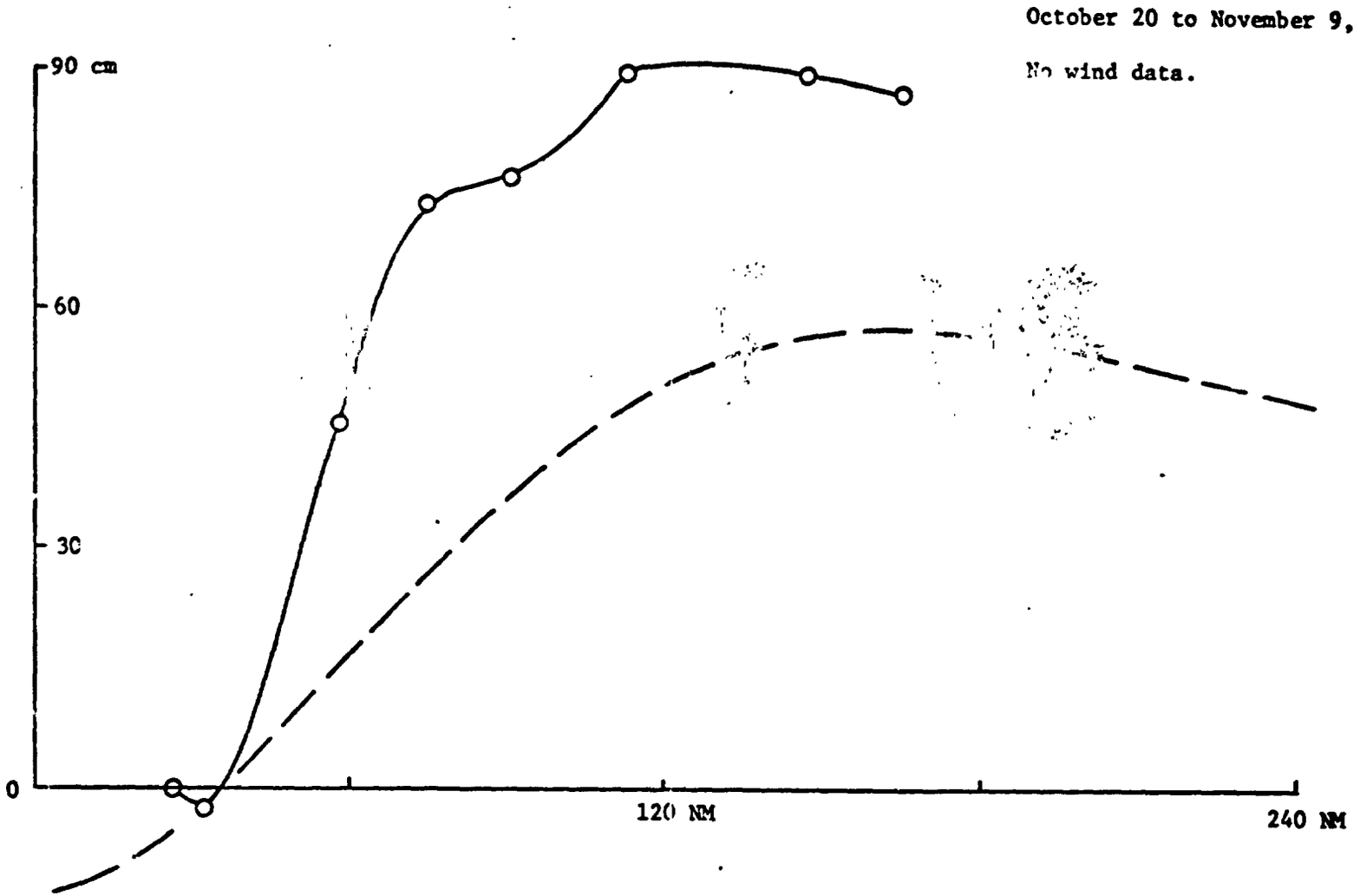

Fig. 3.20 Surface profile based on hydrographic data. Dashed line Keondzhyan Model.

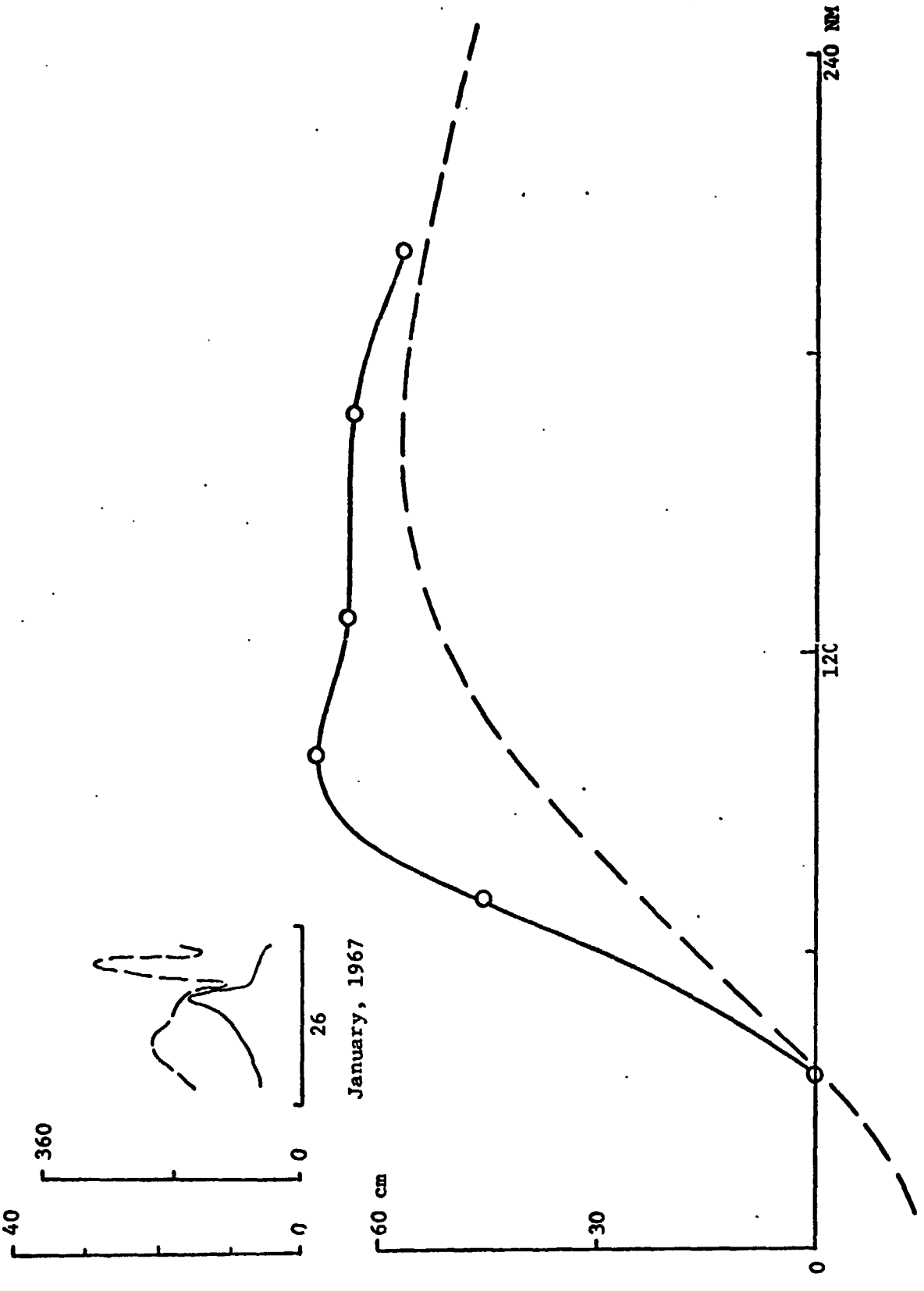

Fig. 3.21 Caption see Fig. 3.9

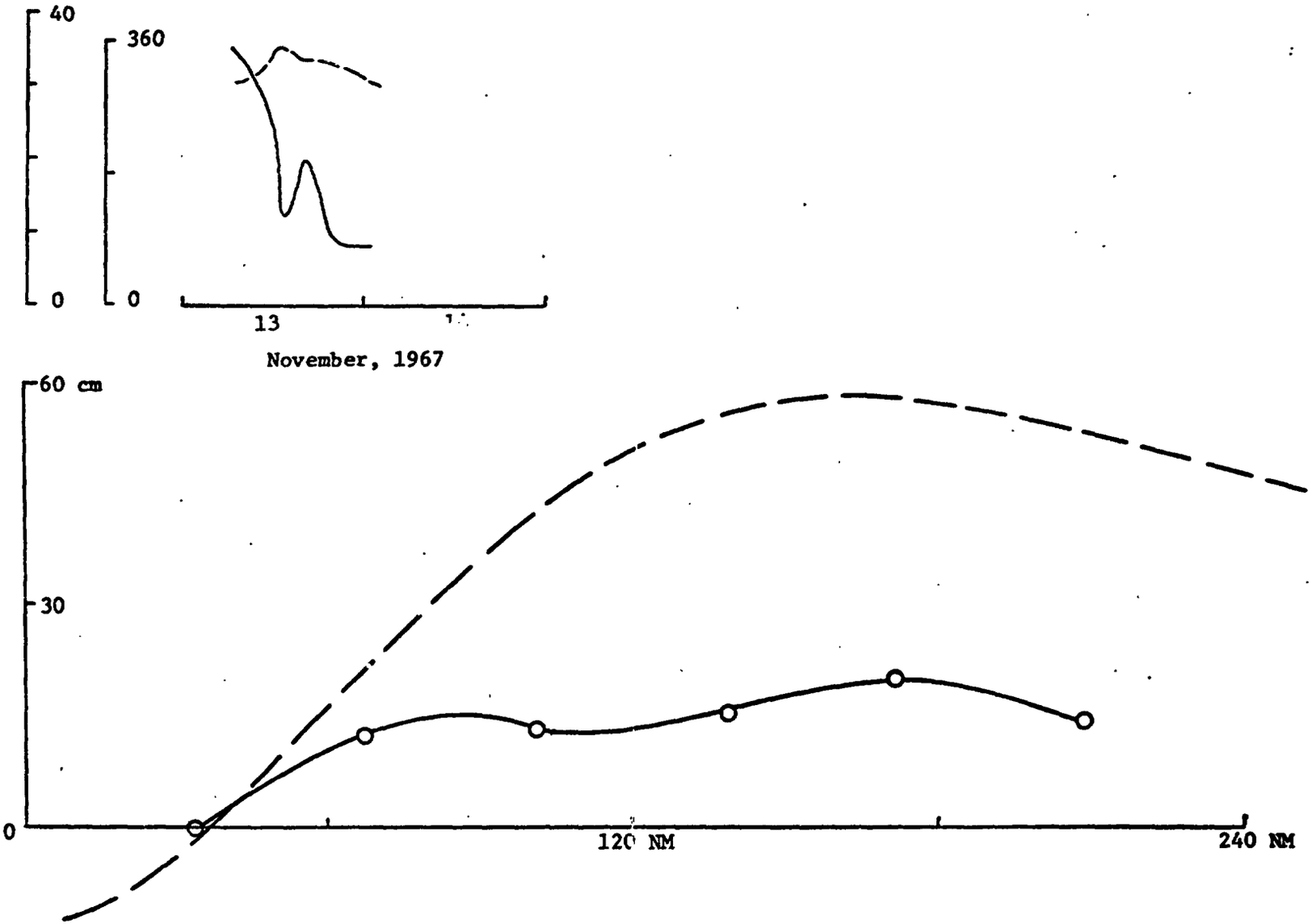

Fig. 3.22 Caption see Fig. 3.9

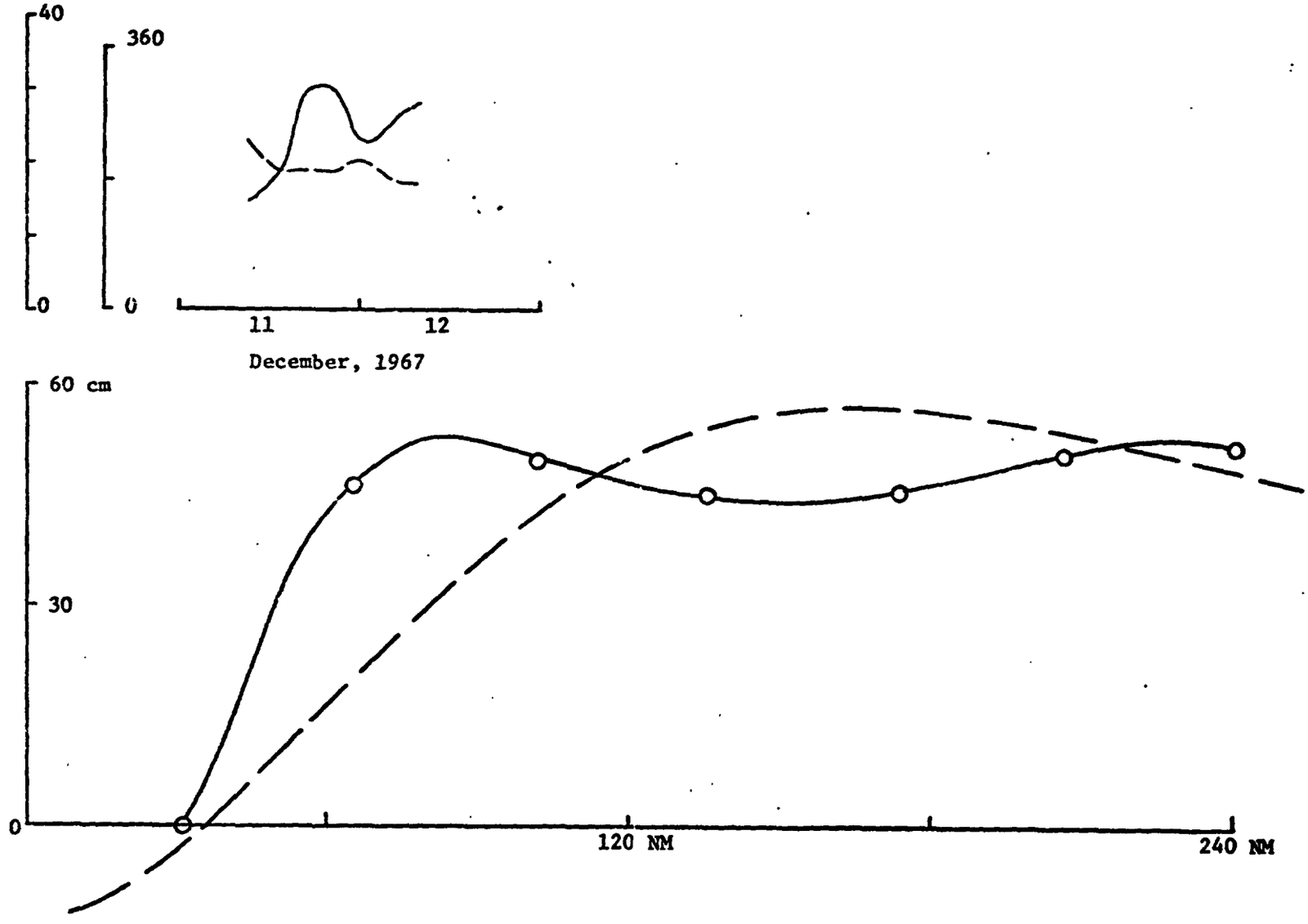

Fig. 3.23 Caption see Fig. 3.9

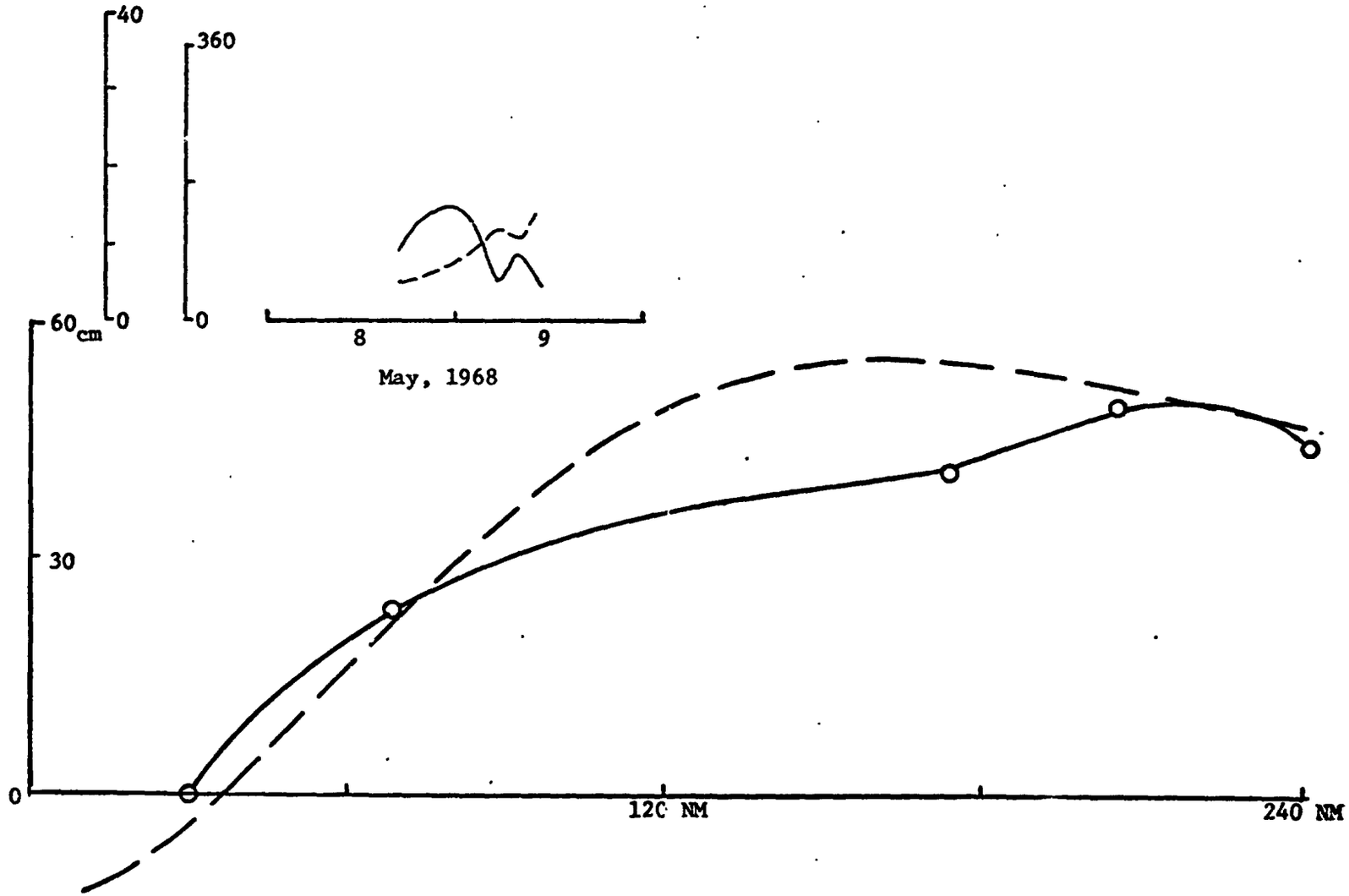

Fig. 3.24 Caption see Fig. 3.9

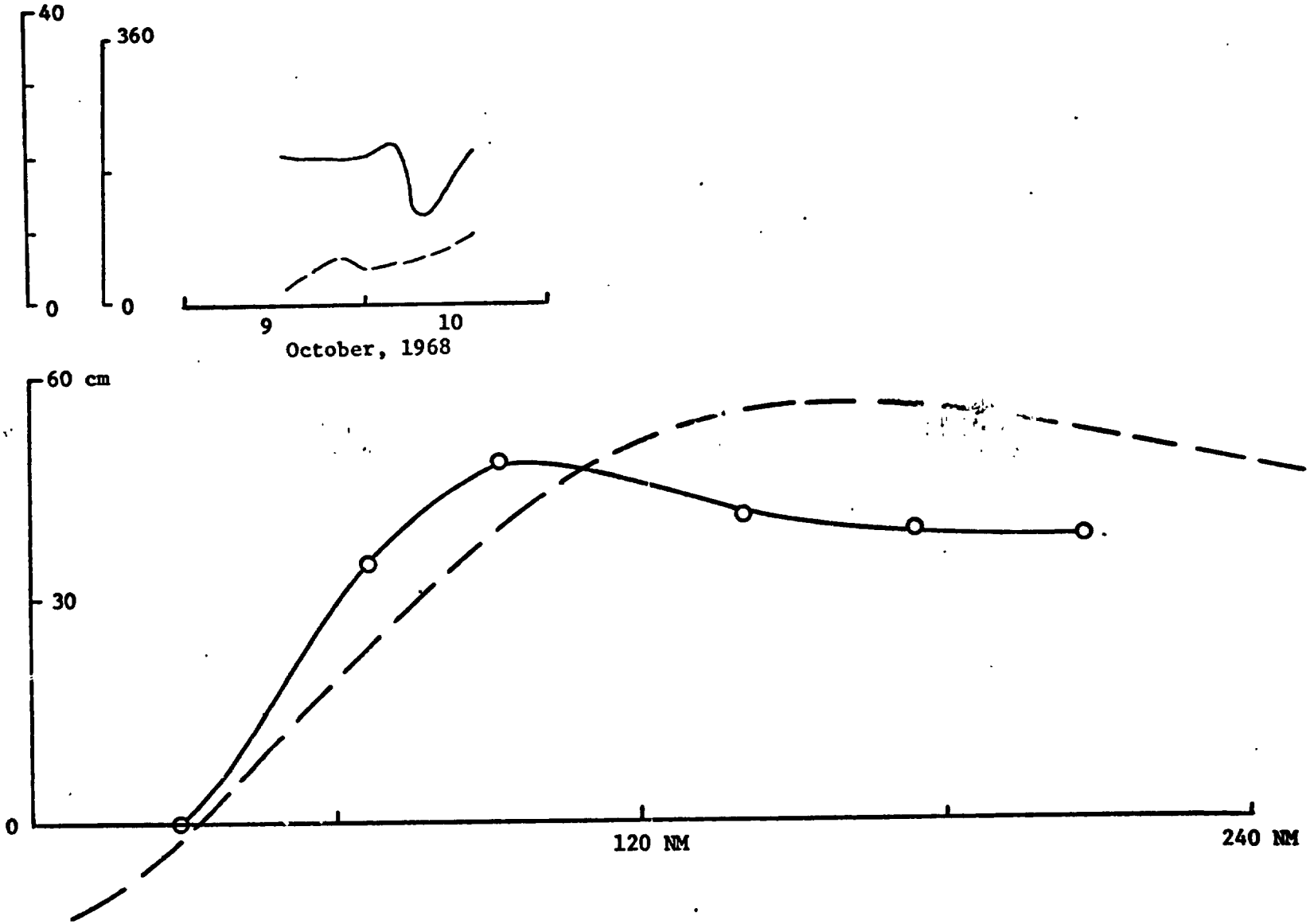

Fig. 3.25 Caption see Fig.3.9

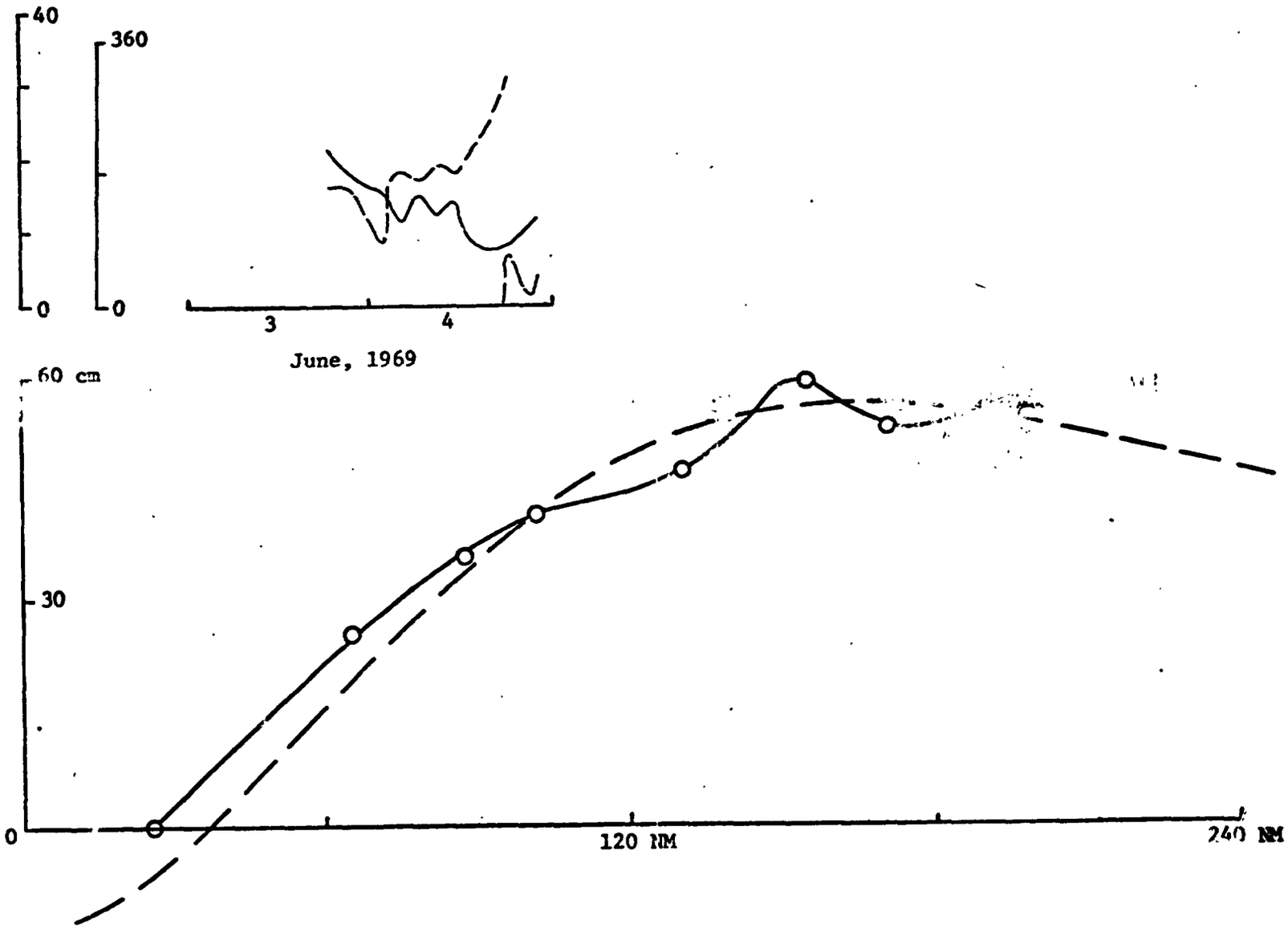

Fig. 3.26 Caption see Fig. 3.9

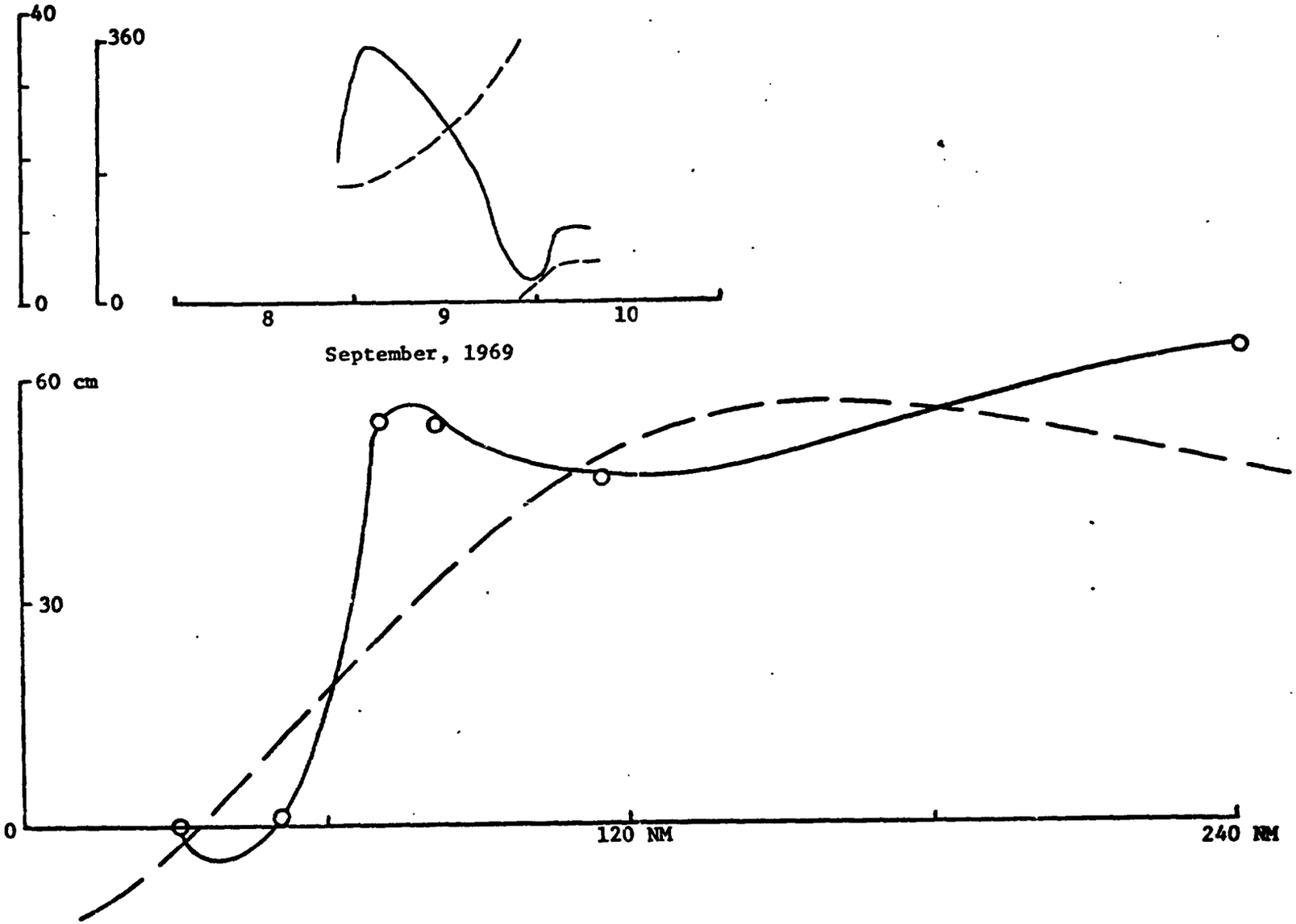

Fig. 3.27 Caption see Fig. 3.9

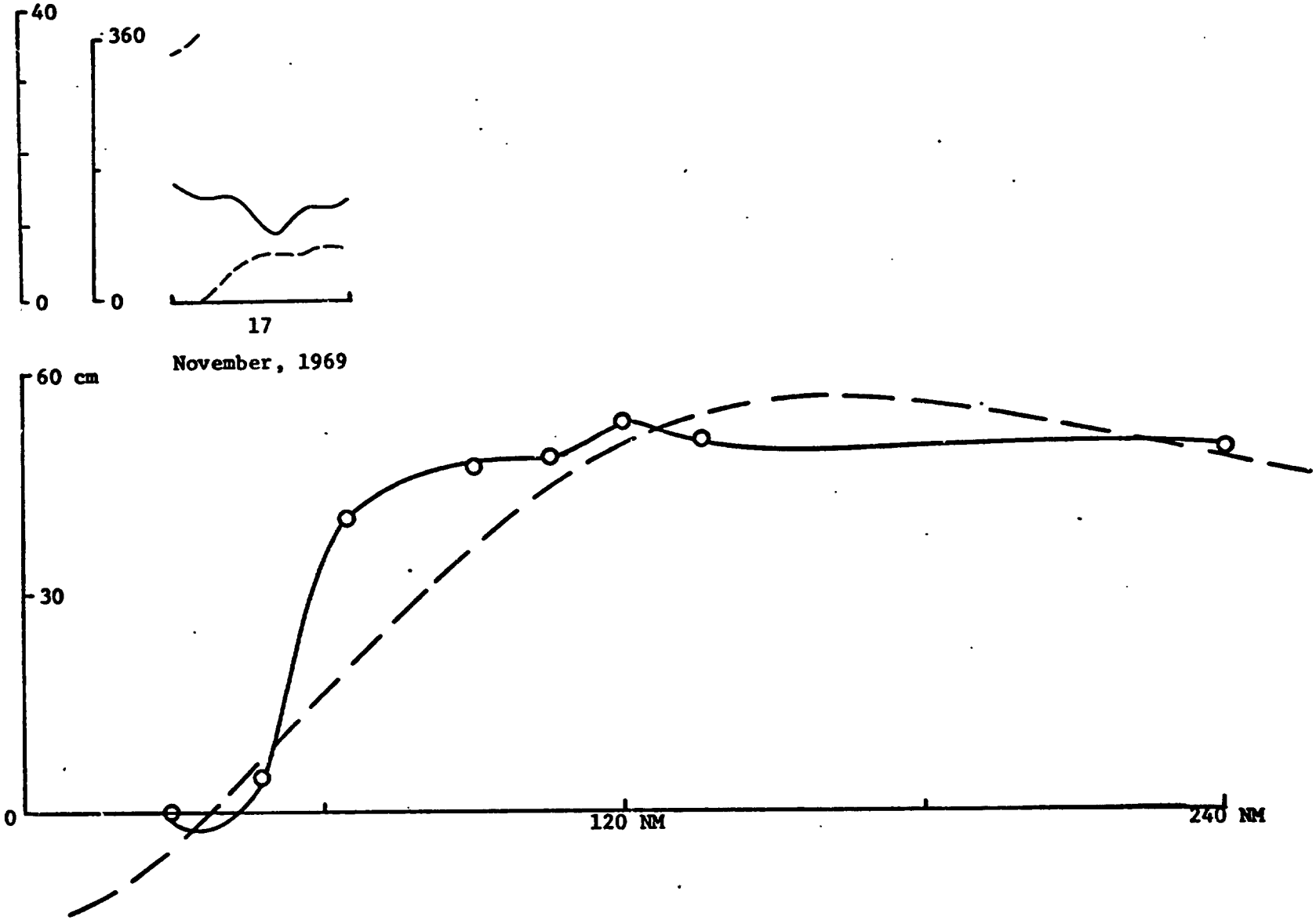

Fig. 3.28 Caption see Fig. 3.9

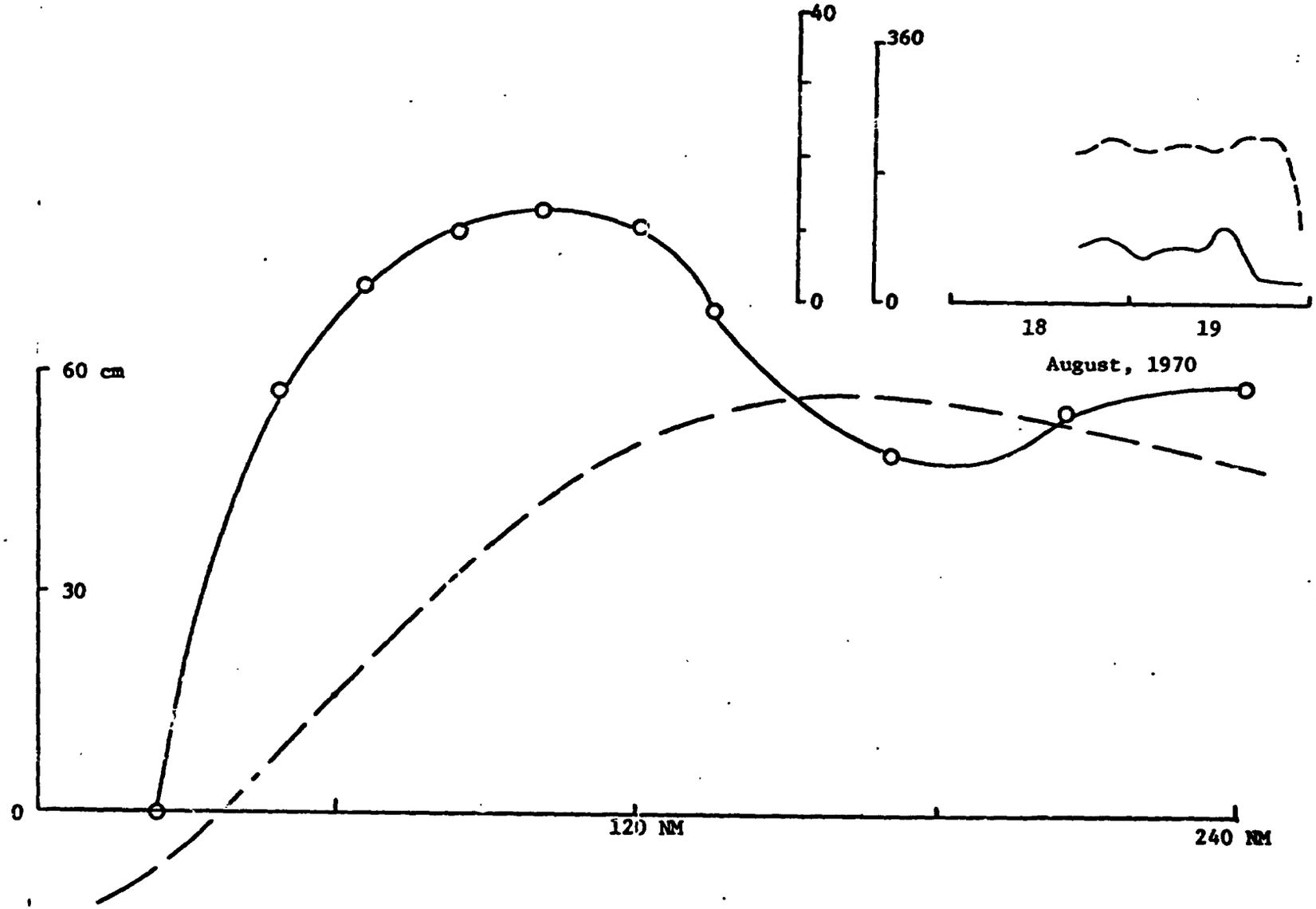

Fig. 3.29 Caption see Fig. 3.9

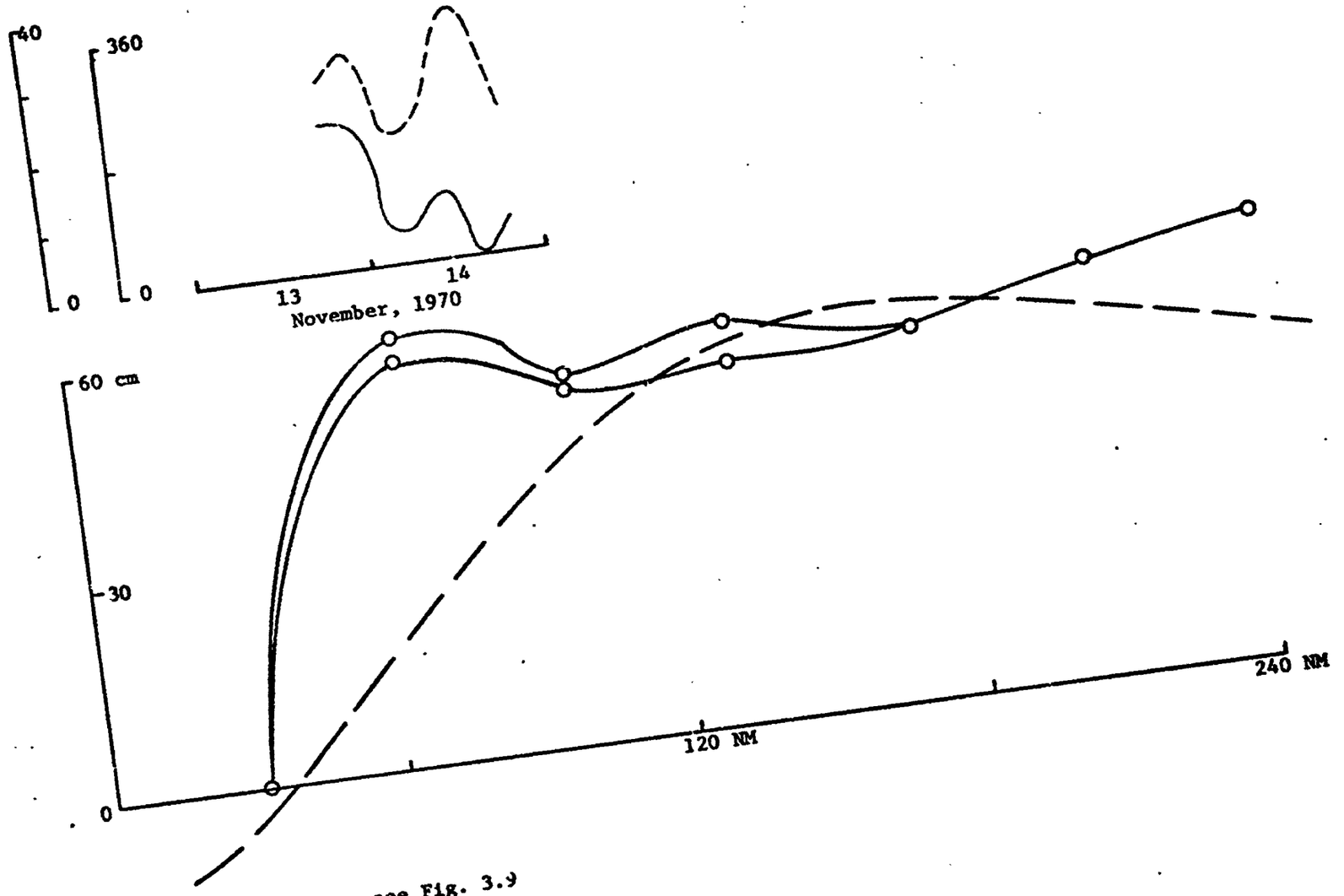

Fig. 3.30 Caption see Fig. 3.9

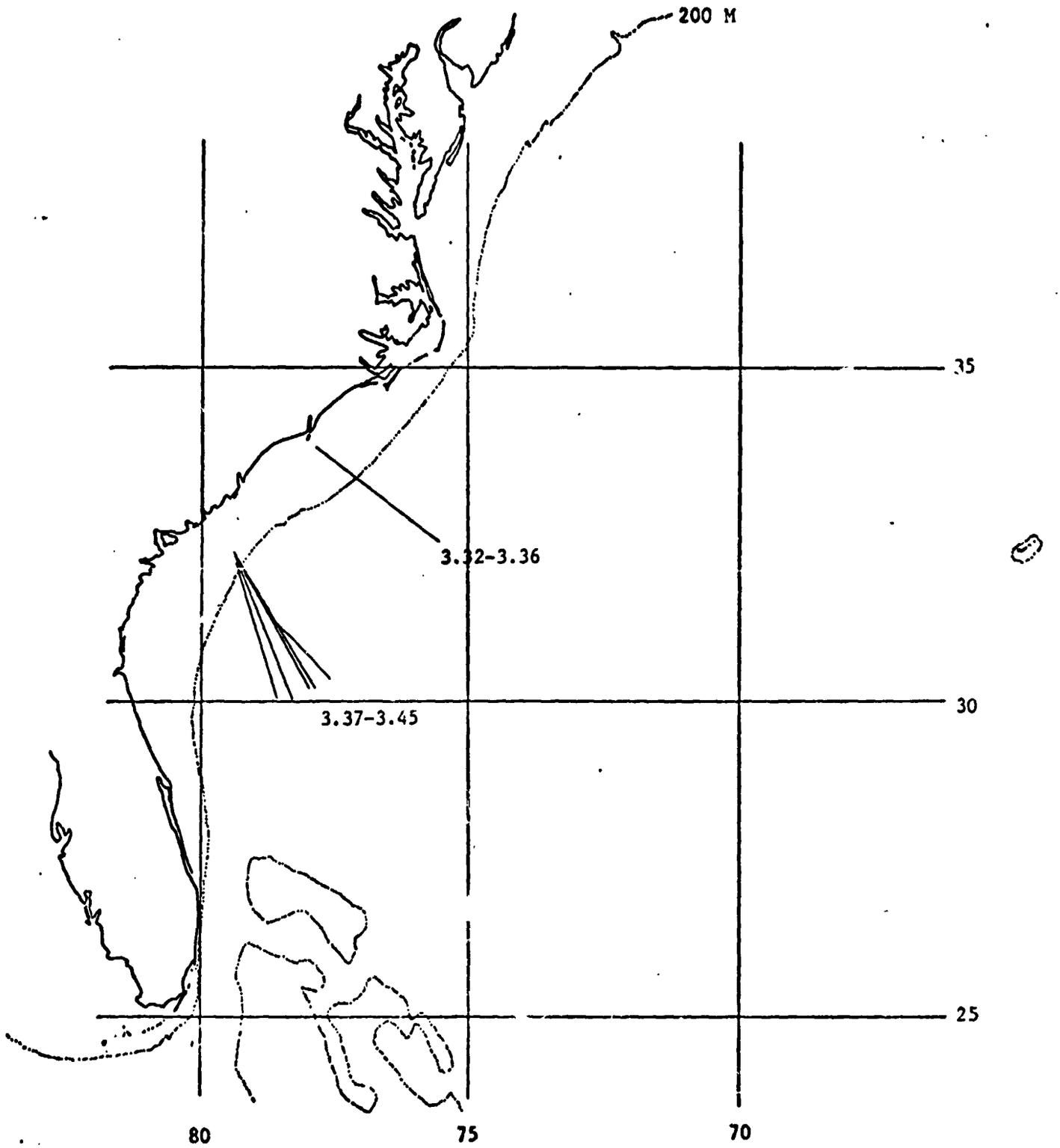

Figure 3.31 Ship tracks for Figs. 3.32 to 3.45

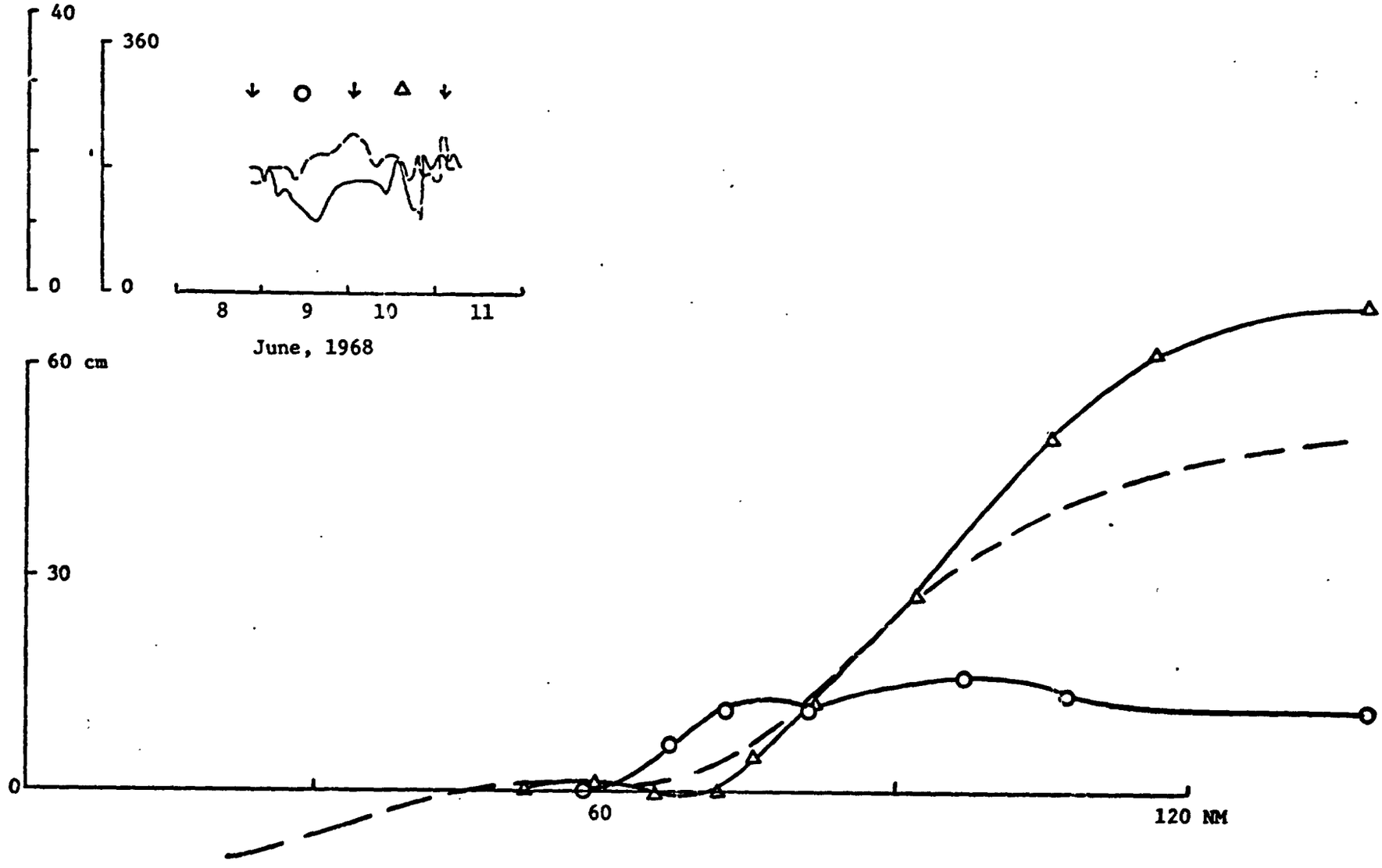

Fig. 3.32 Caption see Fig. 3.9

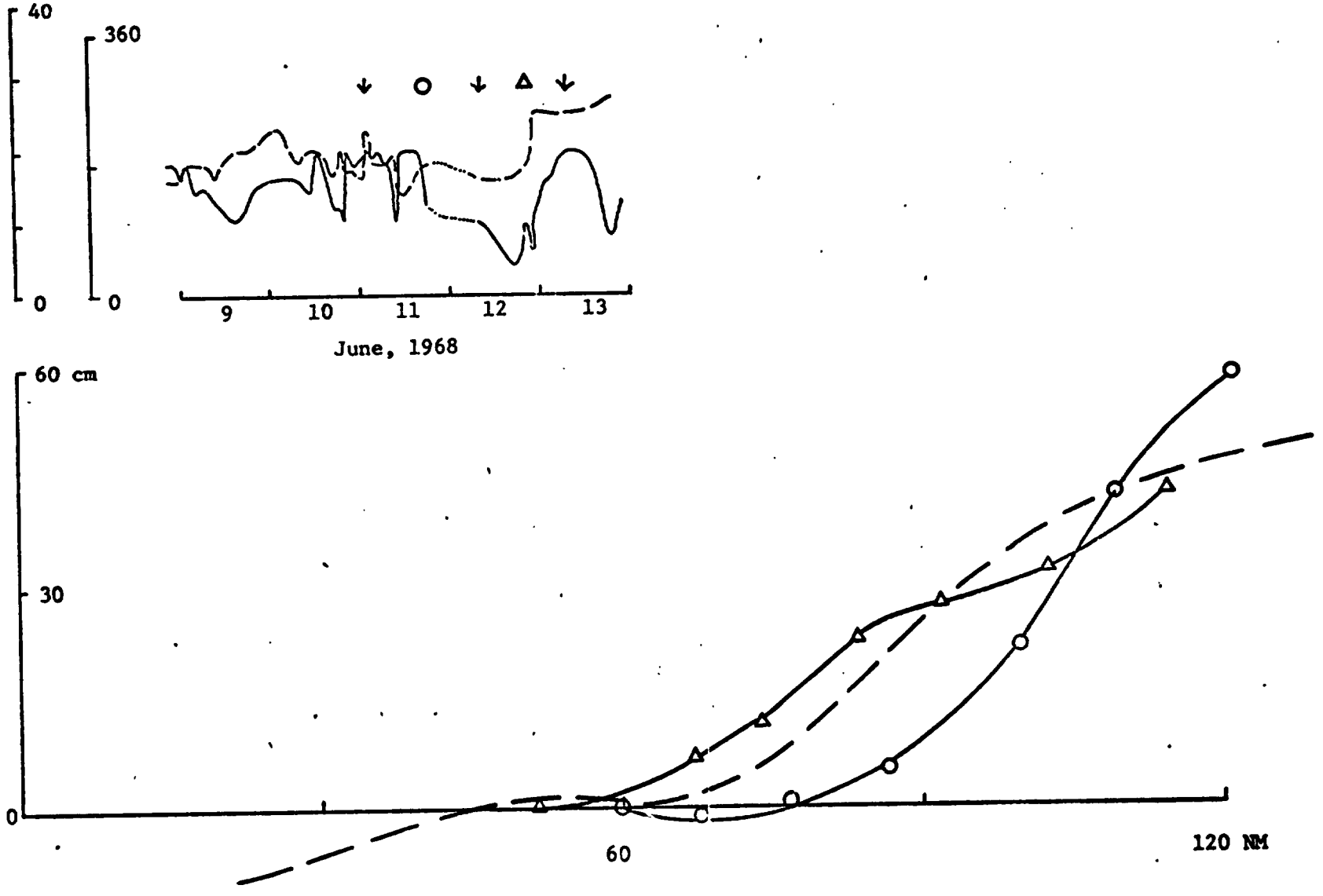

Fig. 3.33 Caption see Fig. 3.9

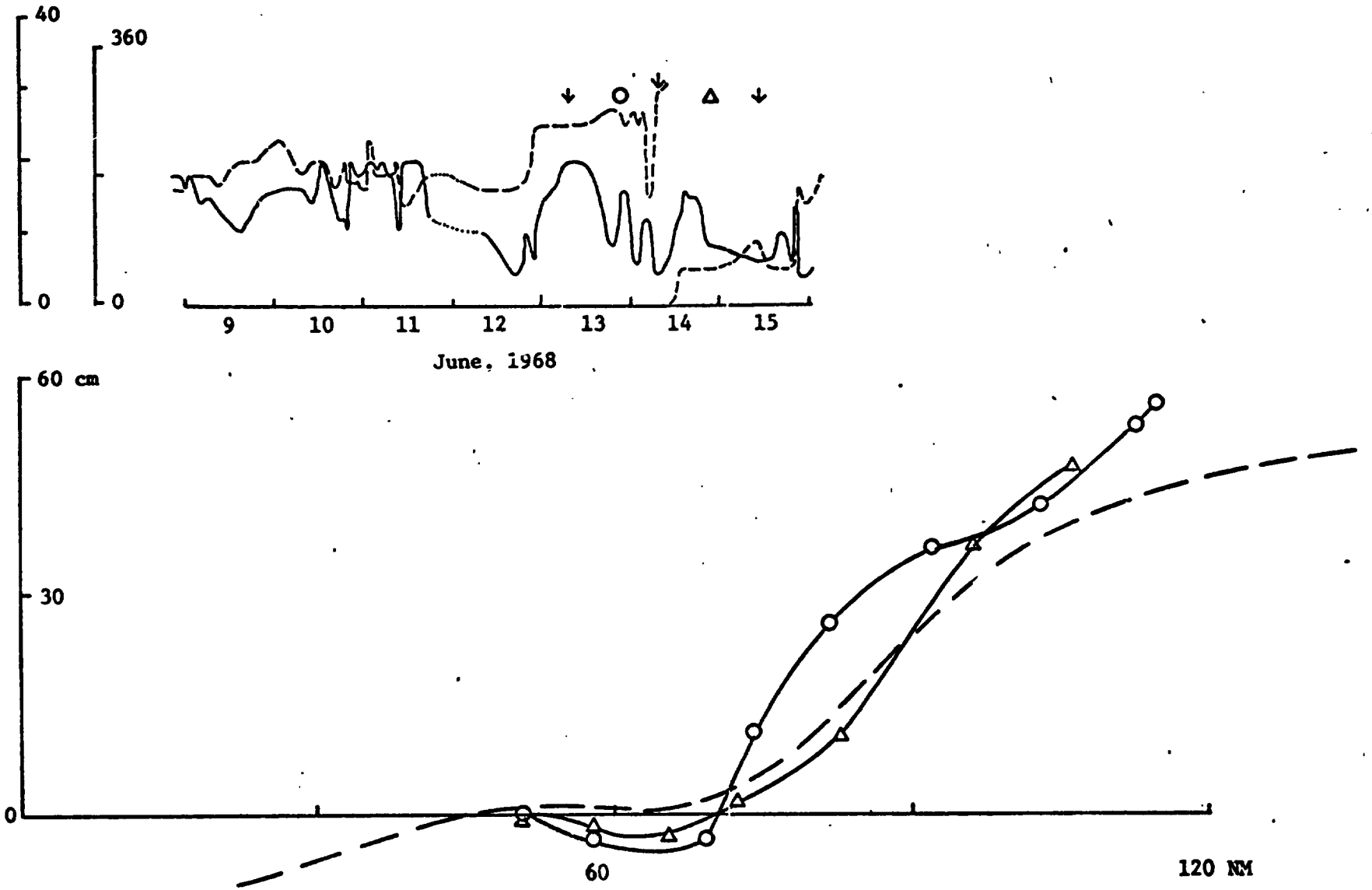

Fig. 3.34 Caption see Fig. 3.9

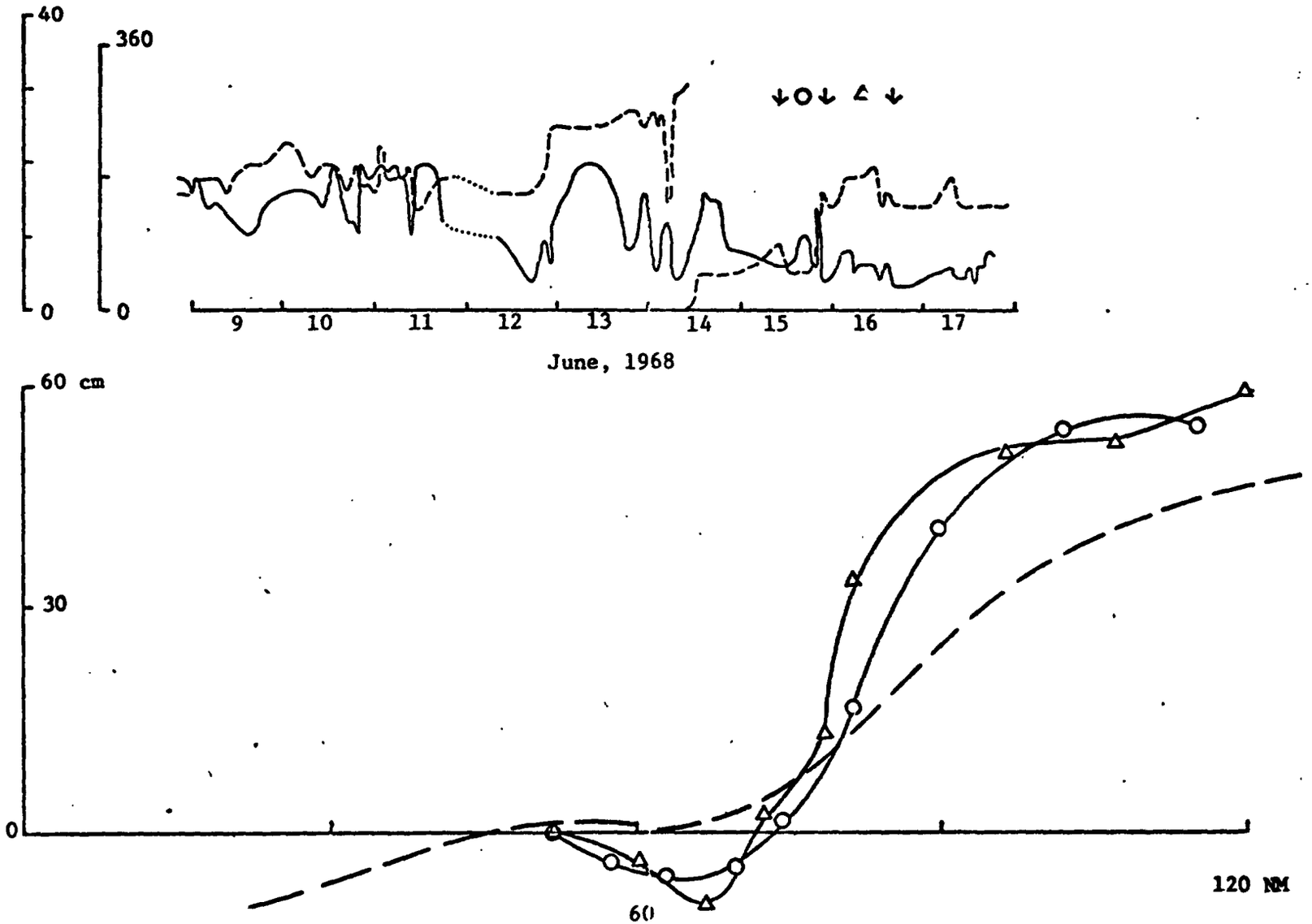

Fig. 3.35 Caption see Fig. 3.9

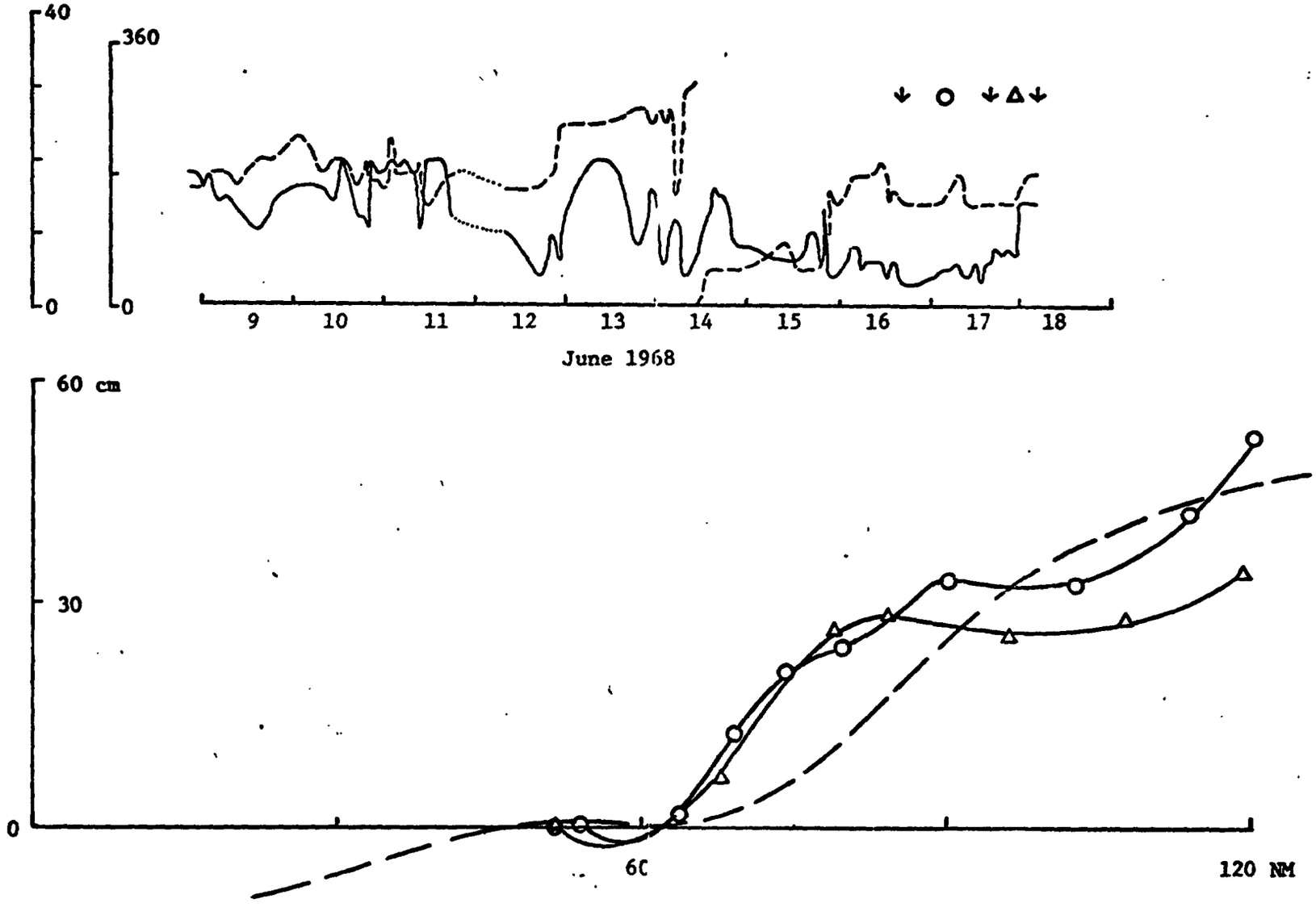

Fig. 3.36 Caption see Fig. 3.9

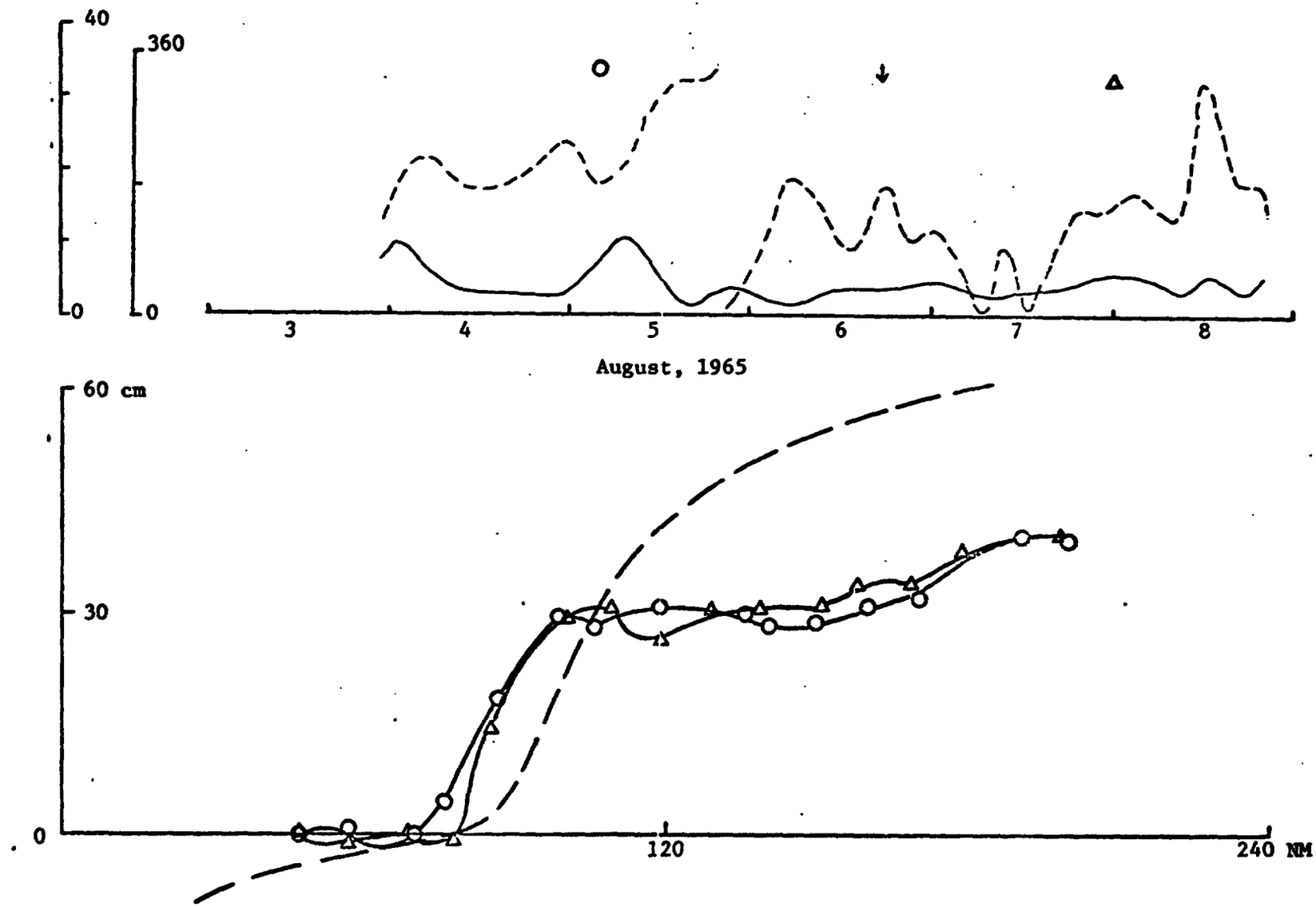

Fig. 3.37 Caption see Fig. 3.9

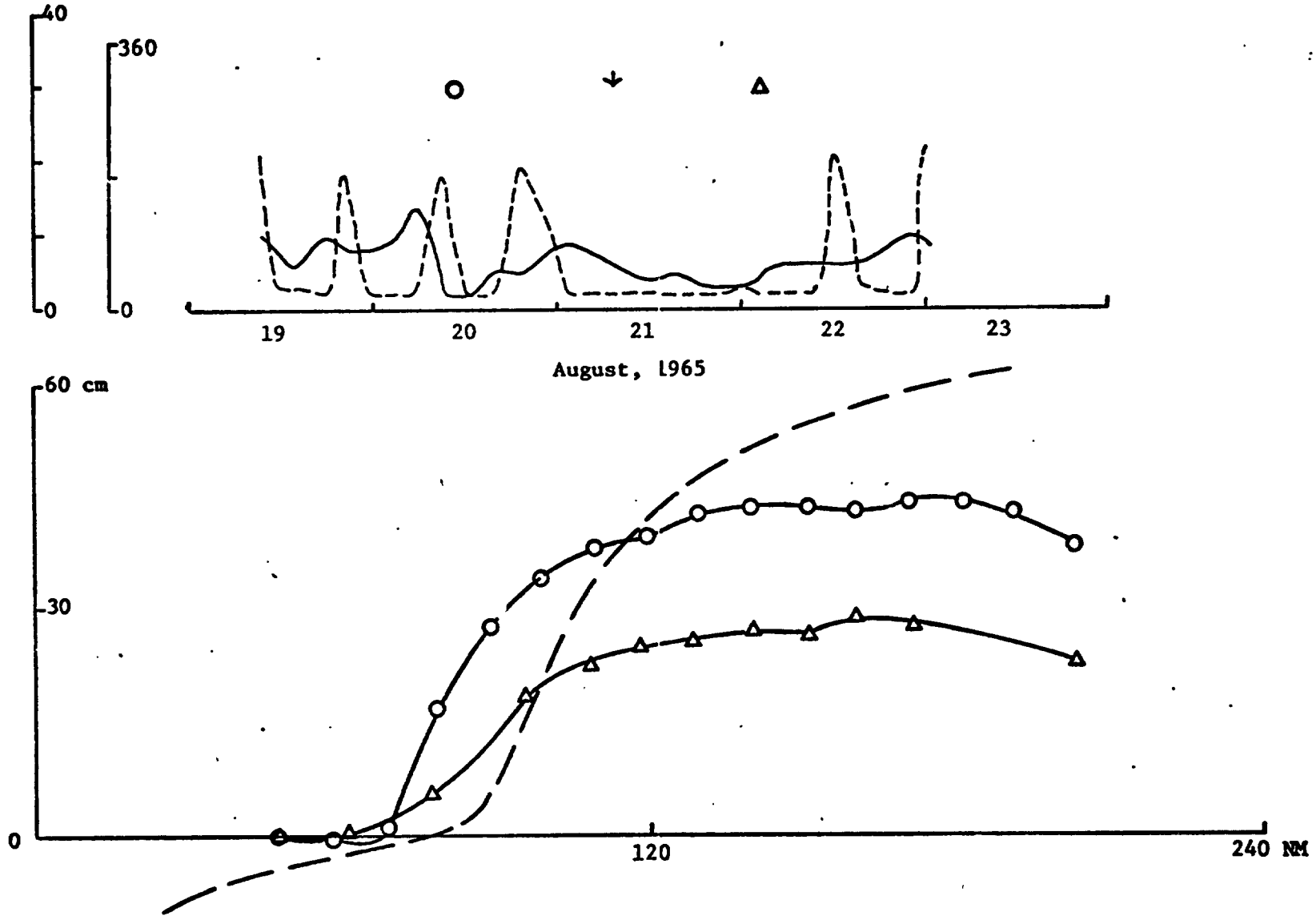

Fig. 3.38 Caption see Fig. 3.9

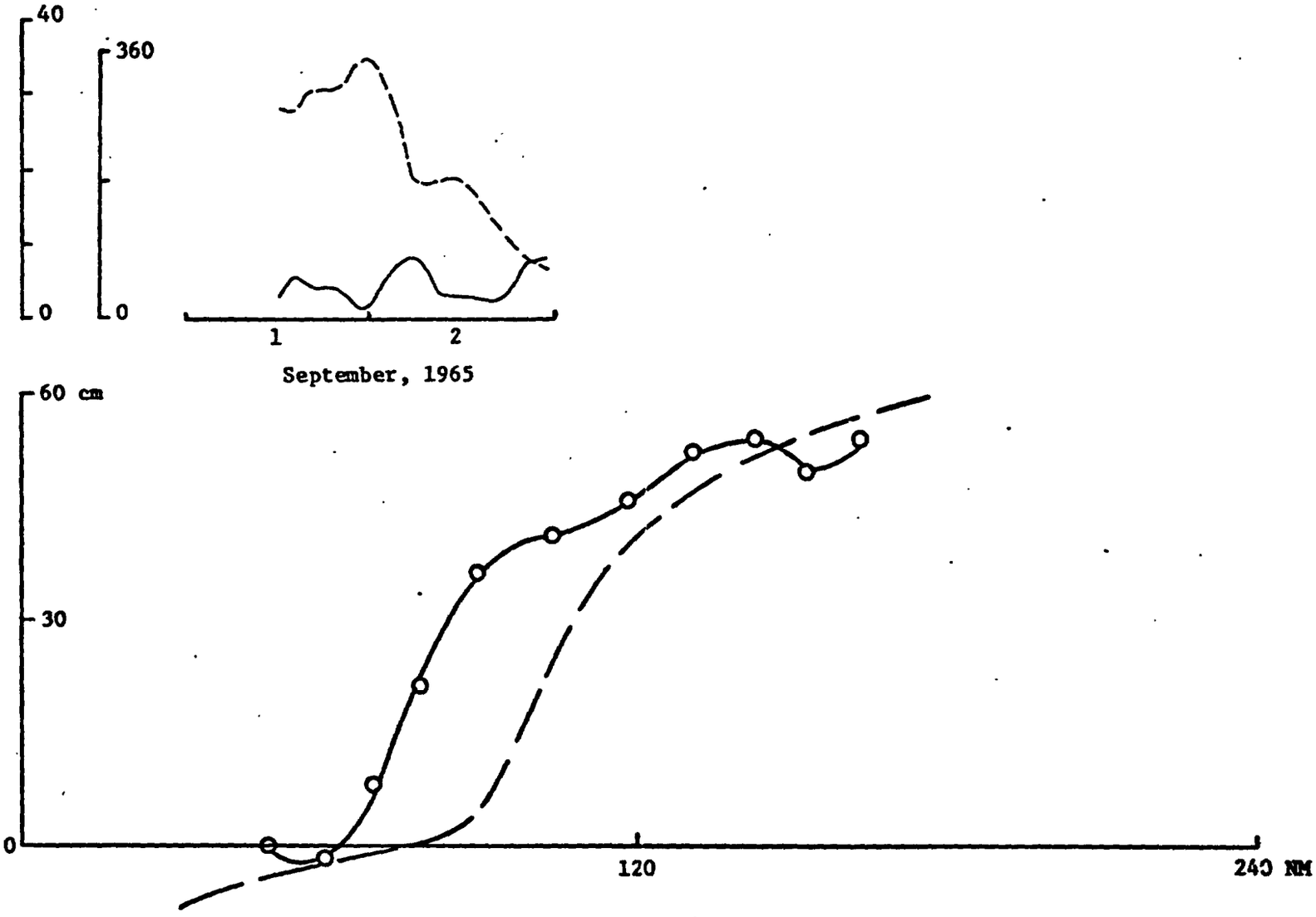

Fig. 3.39 Caption see Fig. 3.9

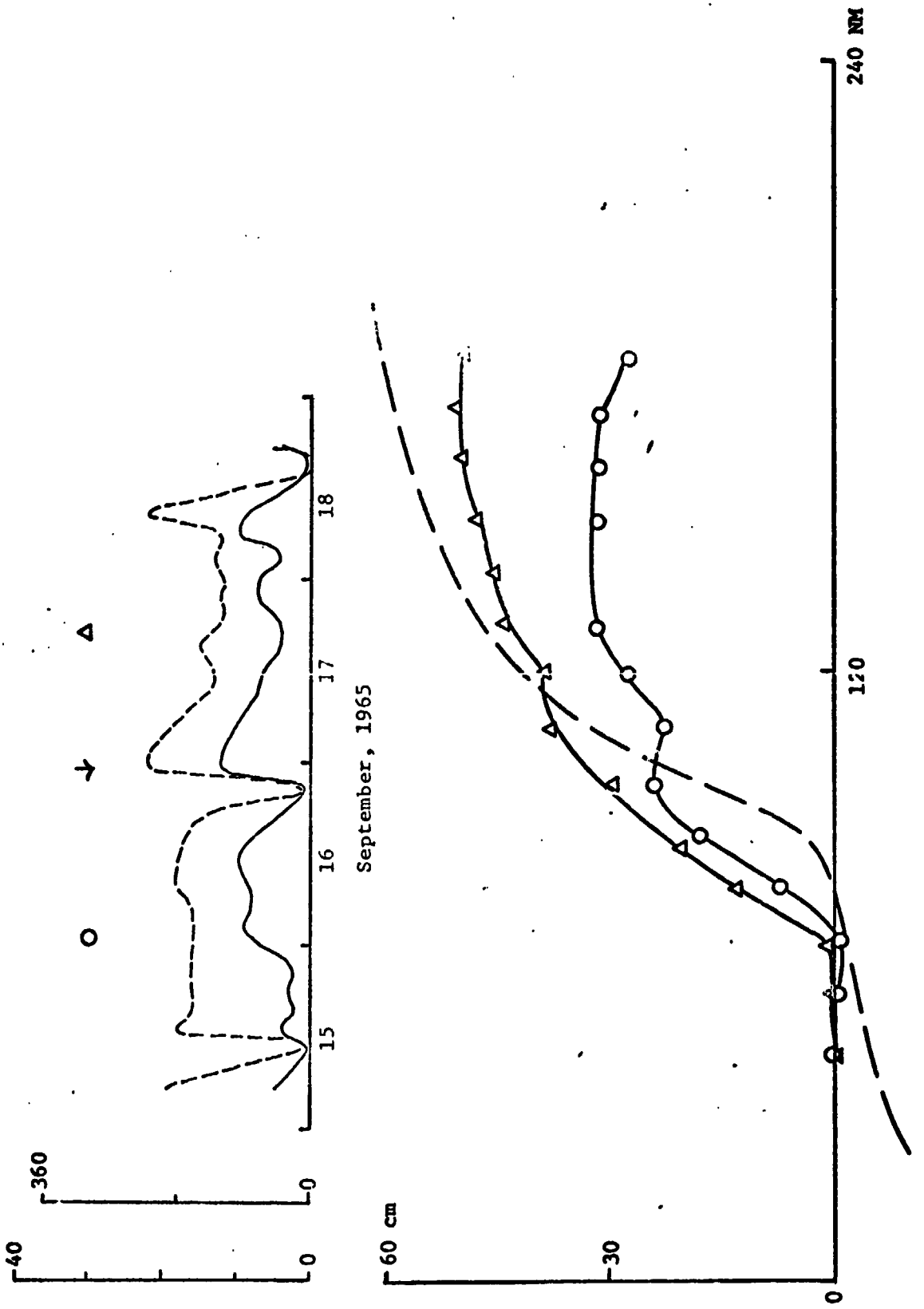

Fig. 3.40 Caption see Fig. 3.9

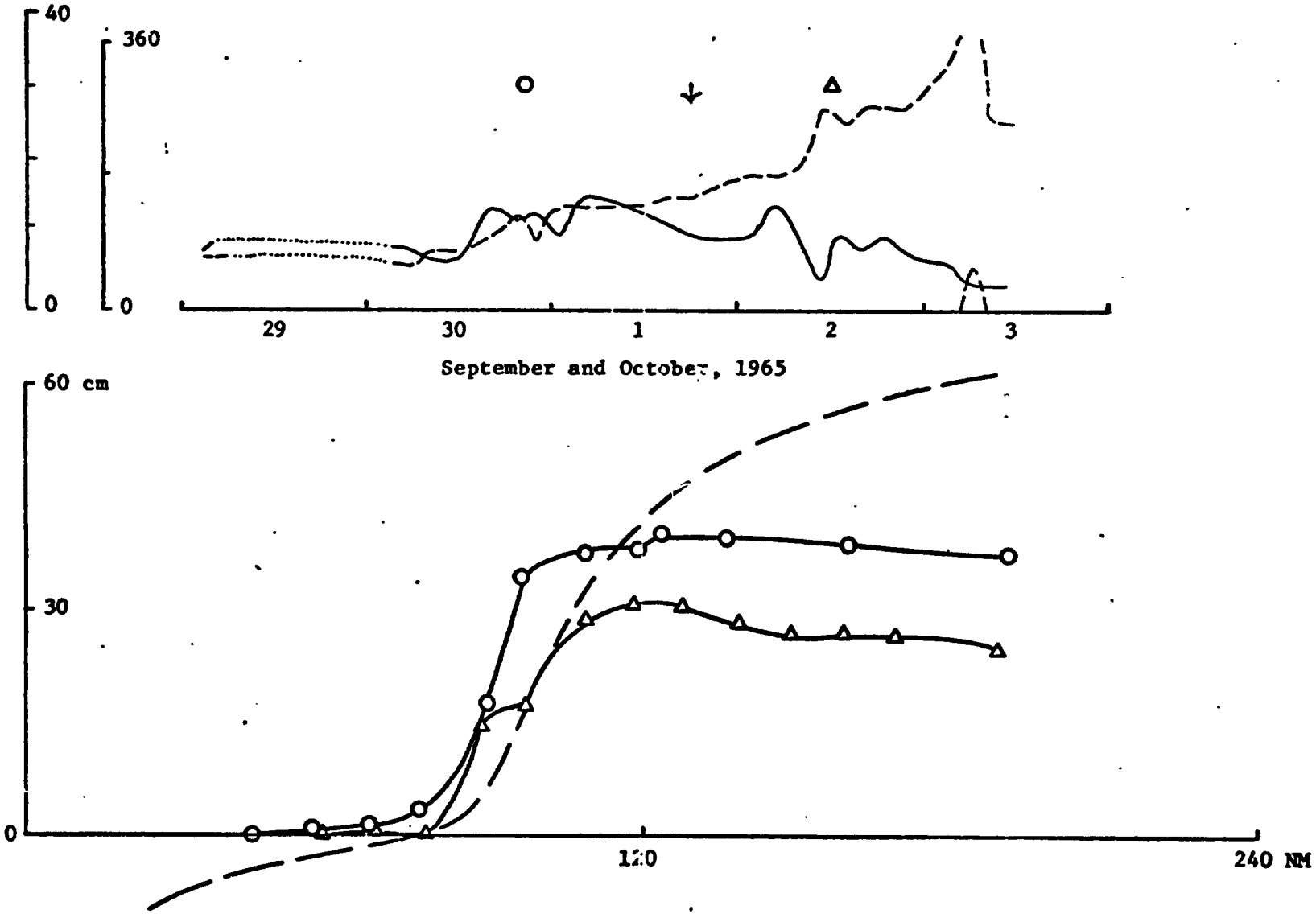

Fig. 3.41 Caption see Fig. 3.9

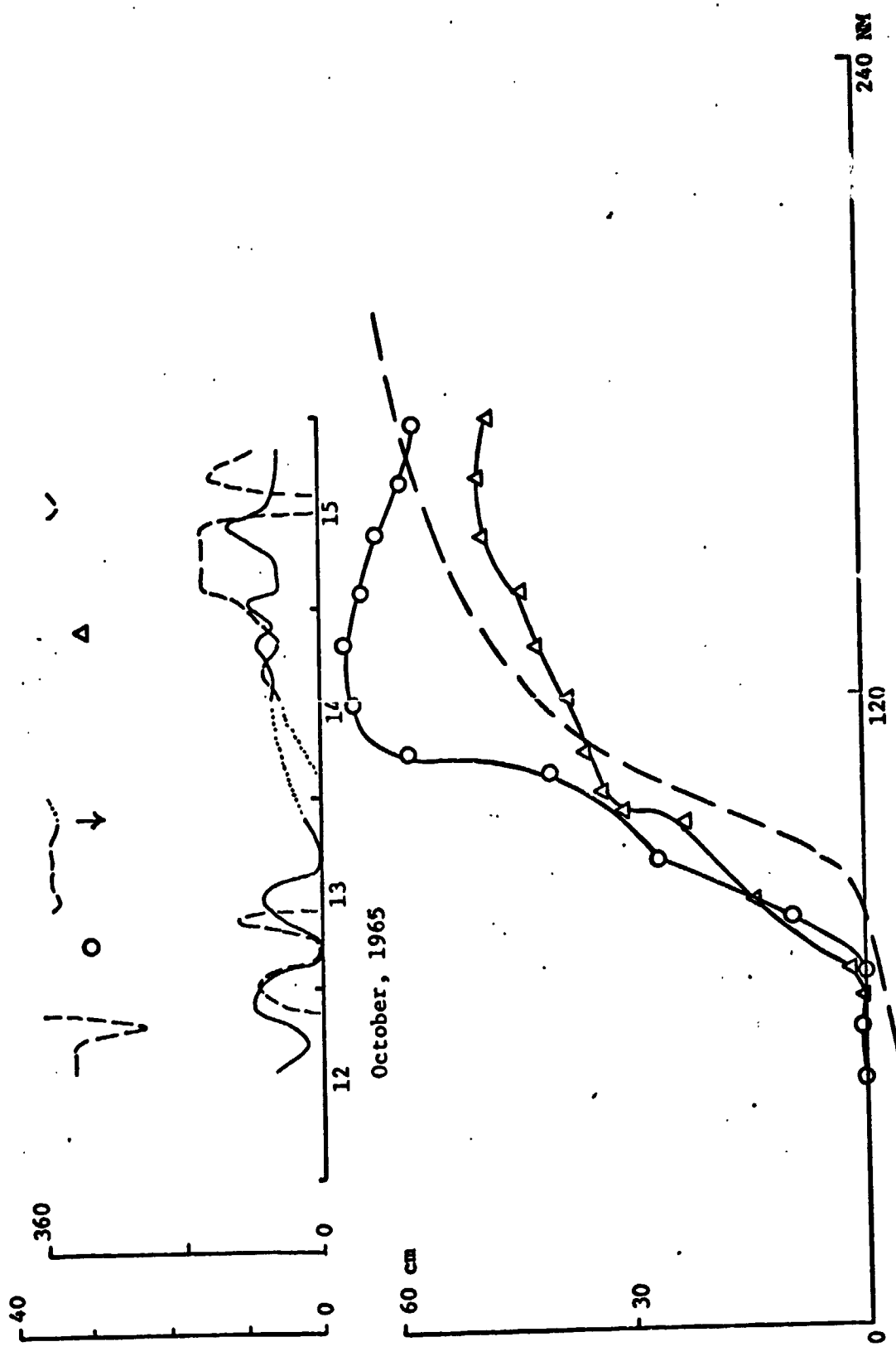

Fig. 3.42 Caption see Fig. 3.9

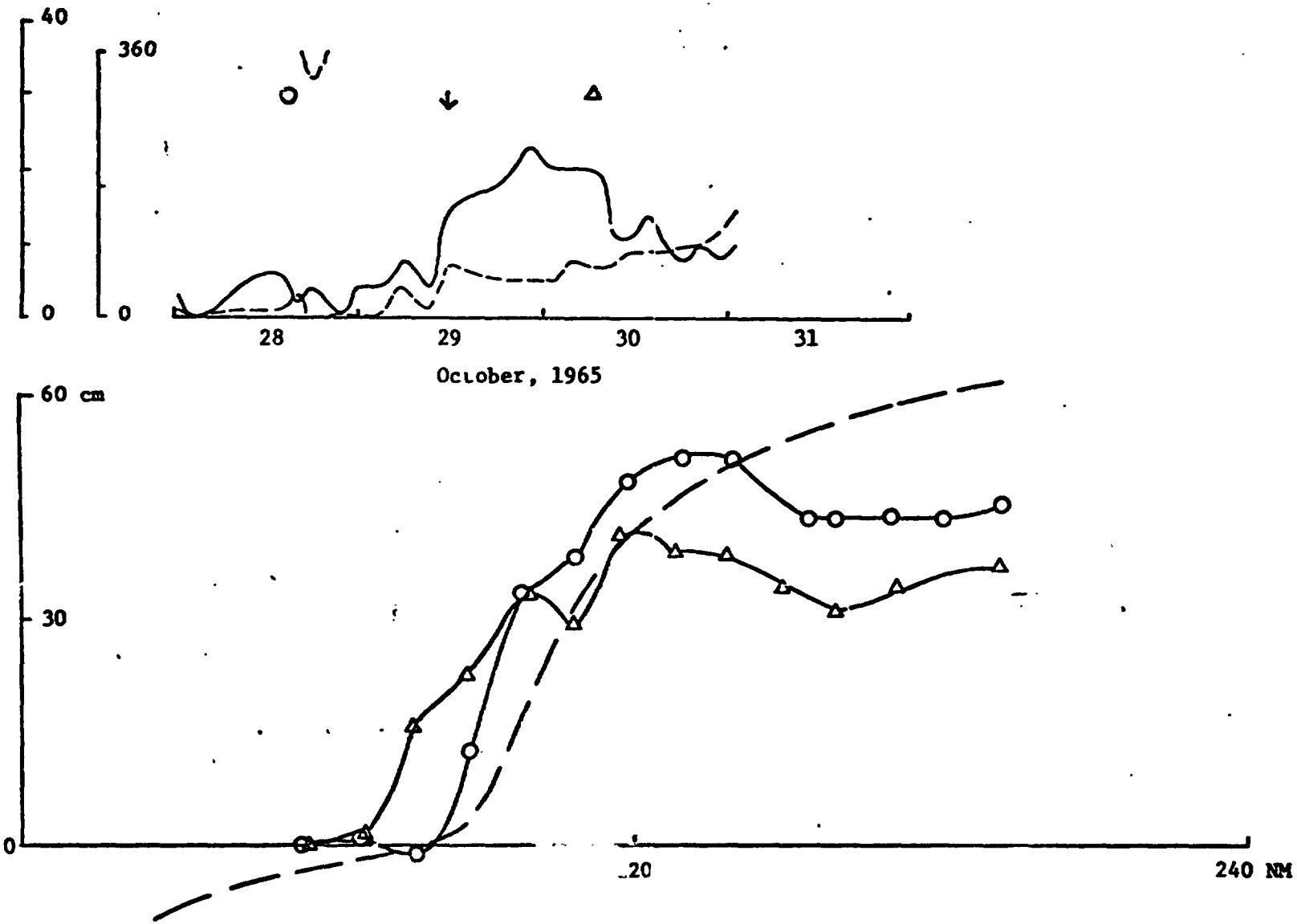

Fig. 3.43 Caption see Fig. 3.9

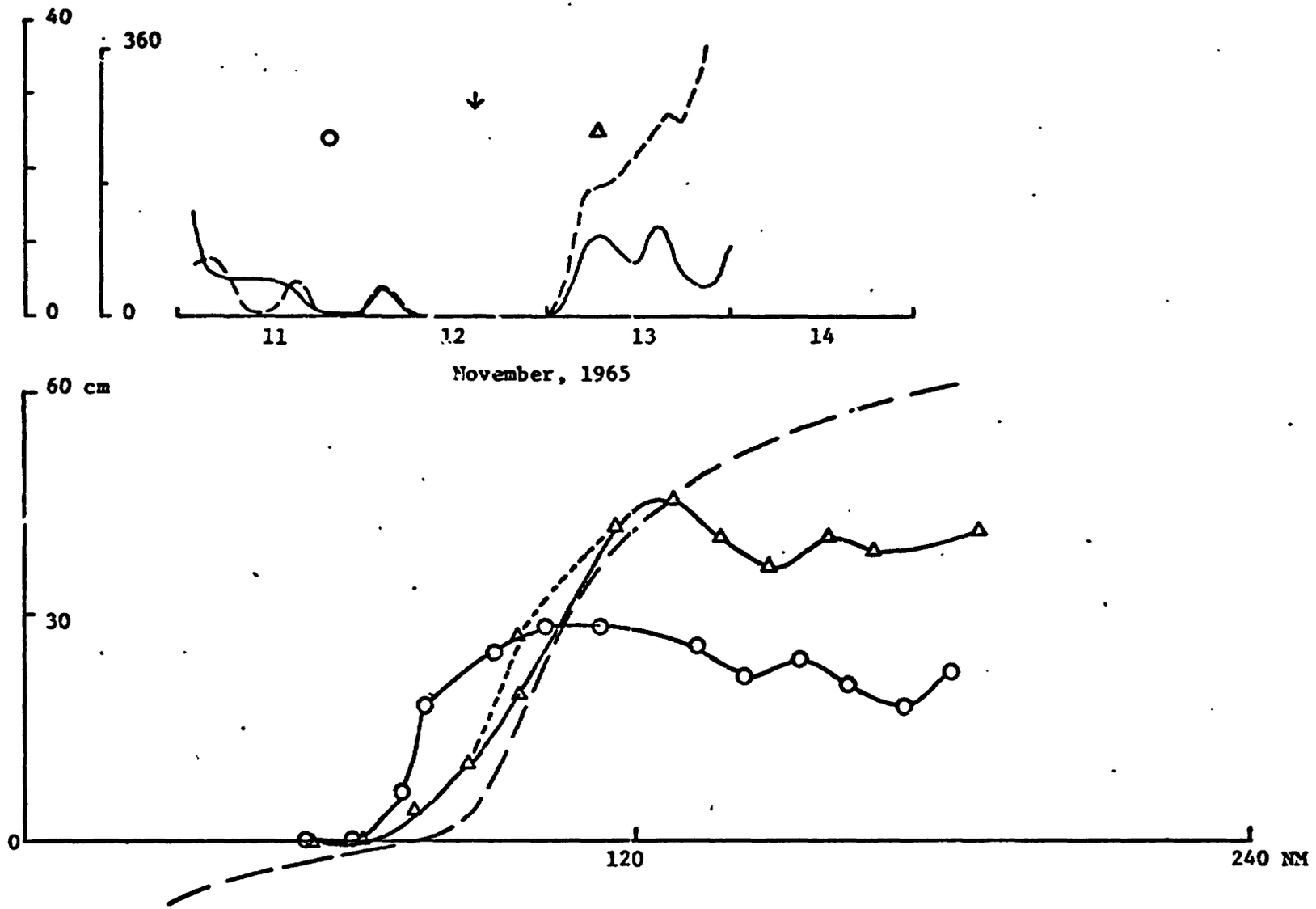

Fig. 3.44 Caption see Fig. 3.9

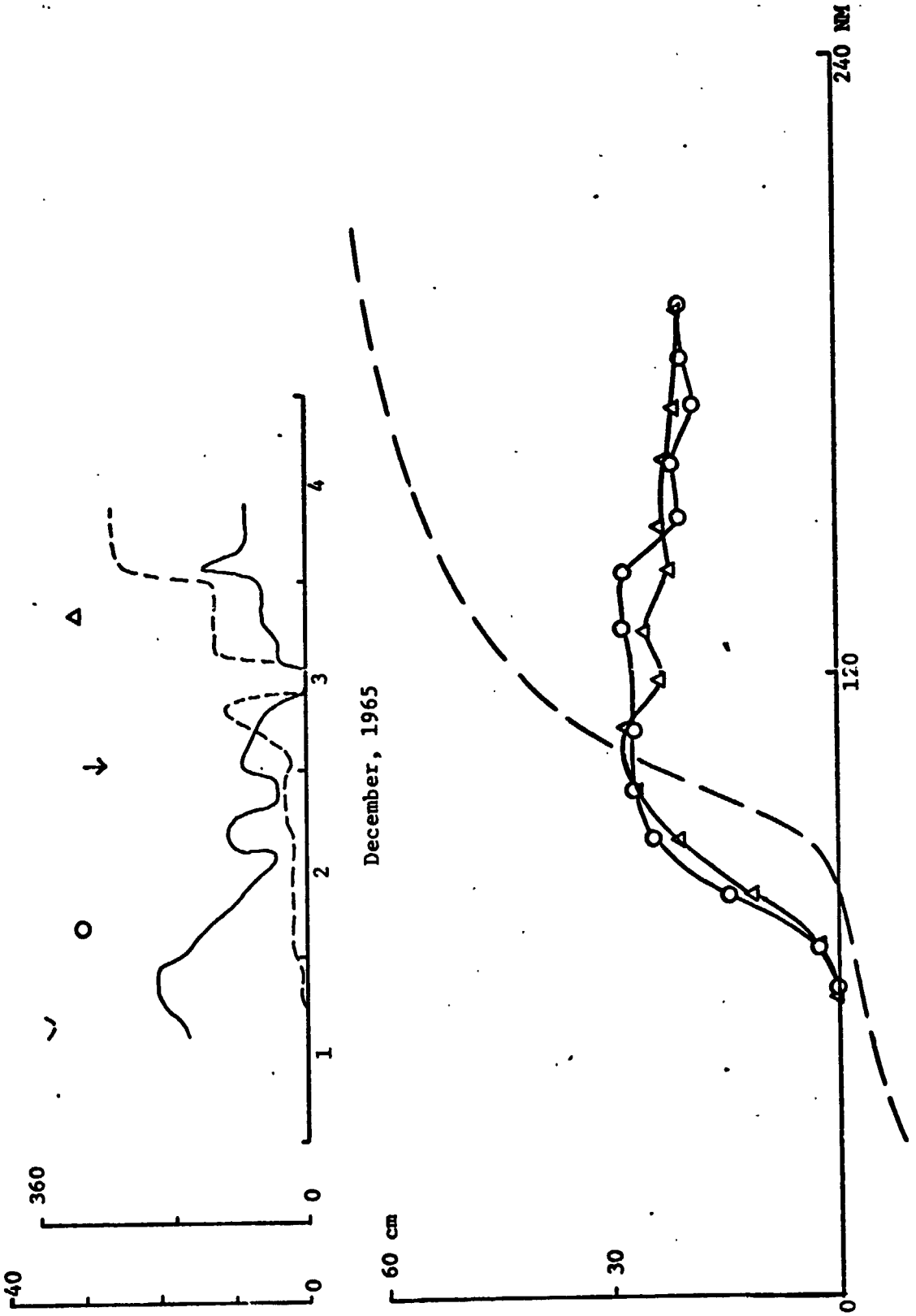

Fig. 3.45 Caption see Fig. 3.9

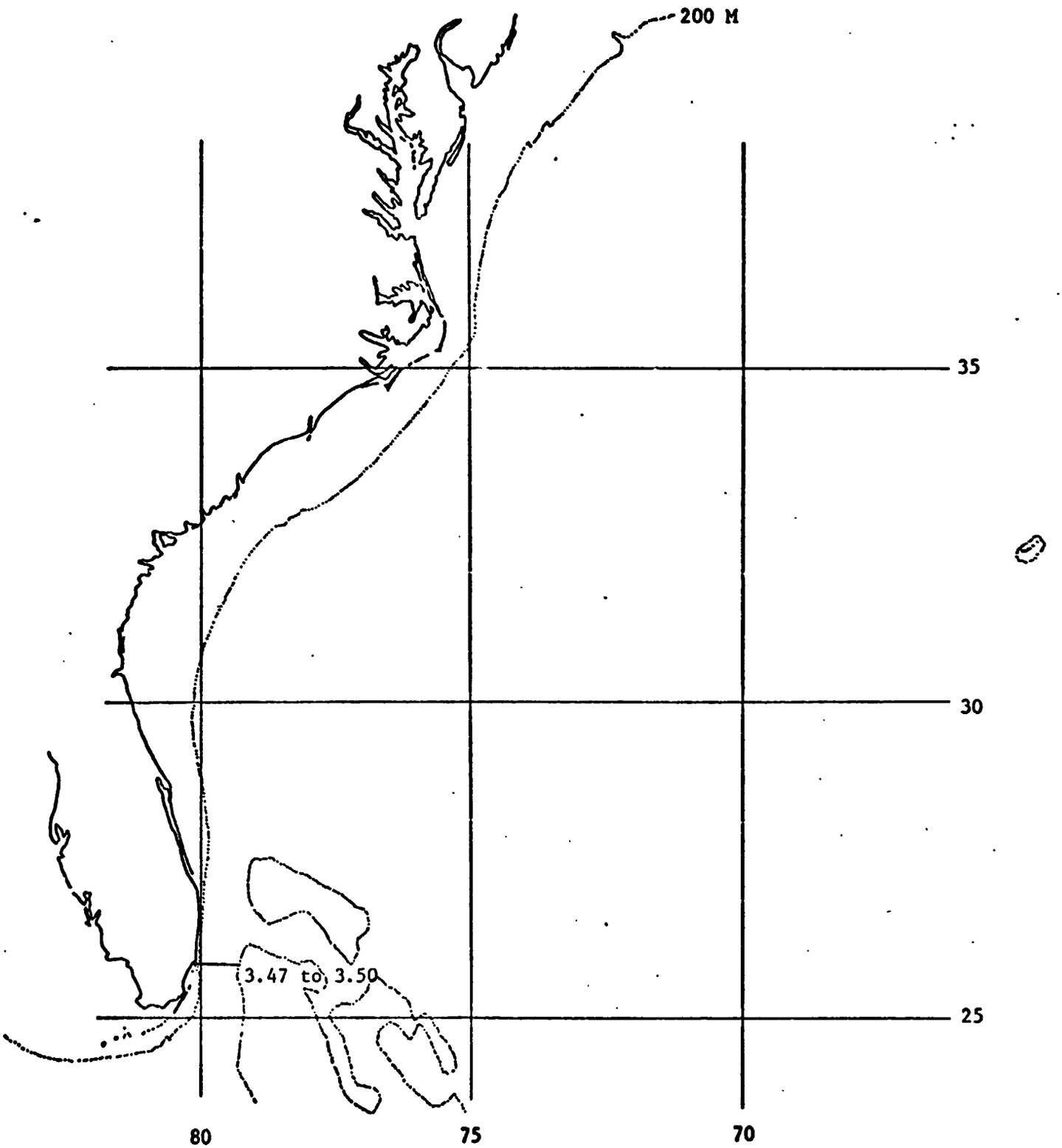

Fig. 3.46 Ship tracks for Figs. 3.47 to 3.50

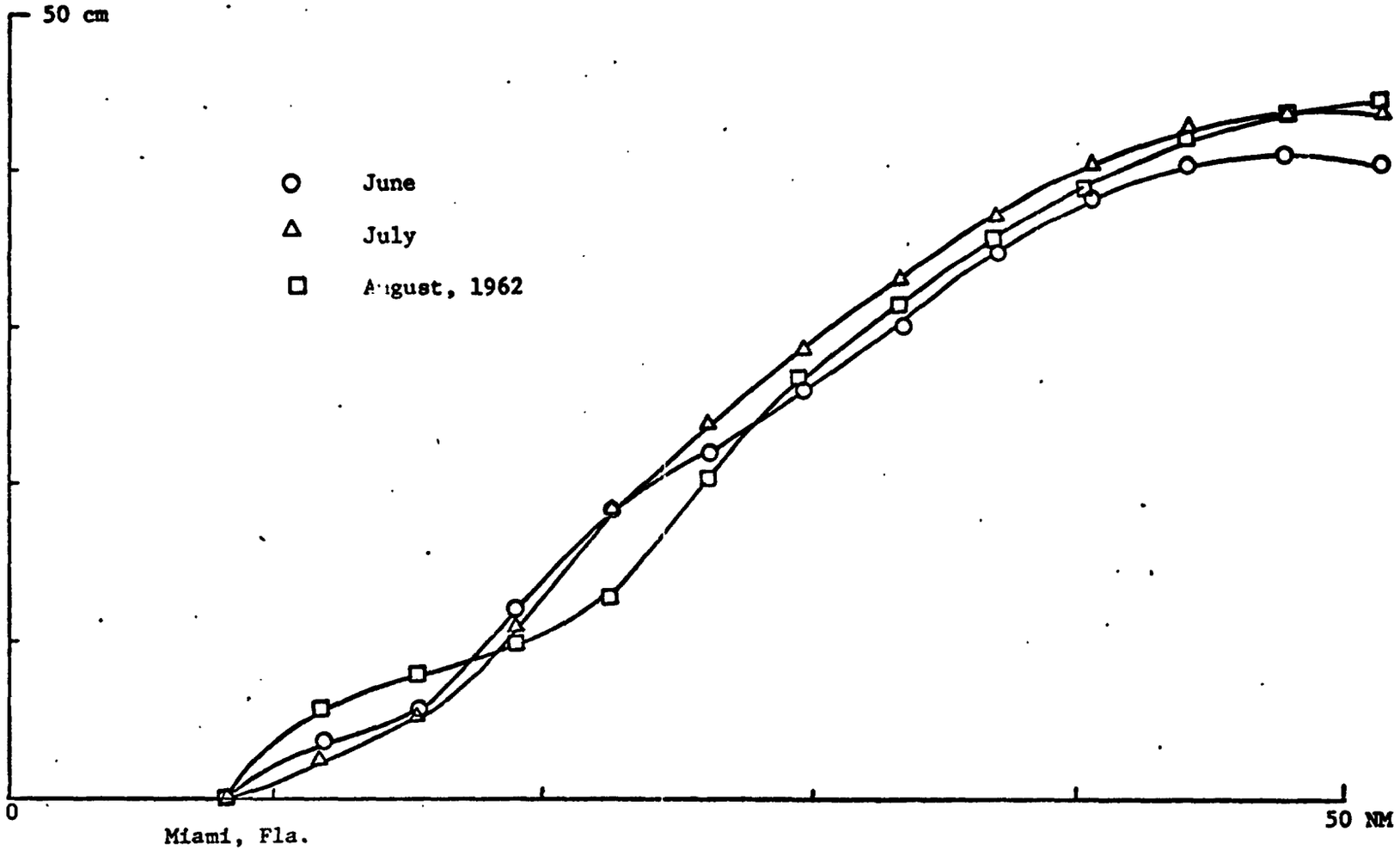

Fig. 3.47 Surface profile based on mass transport measurements.

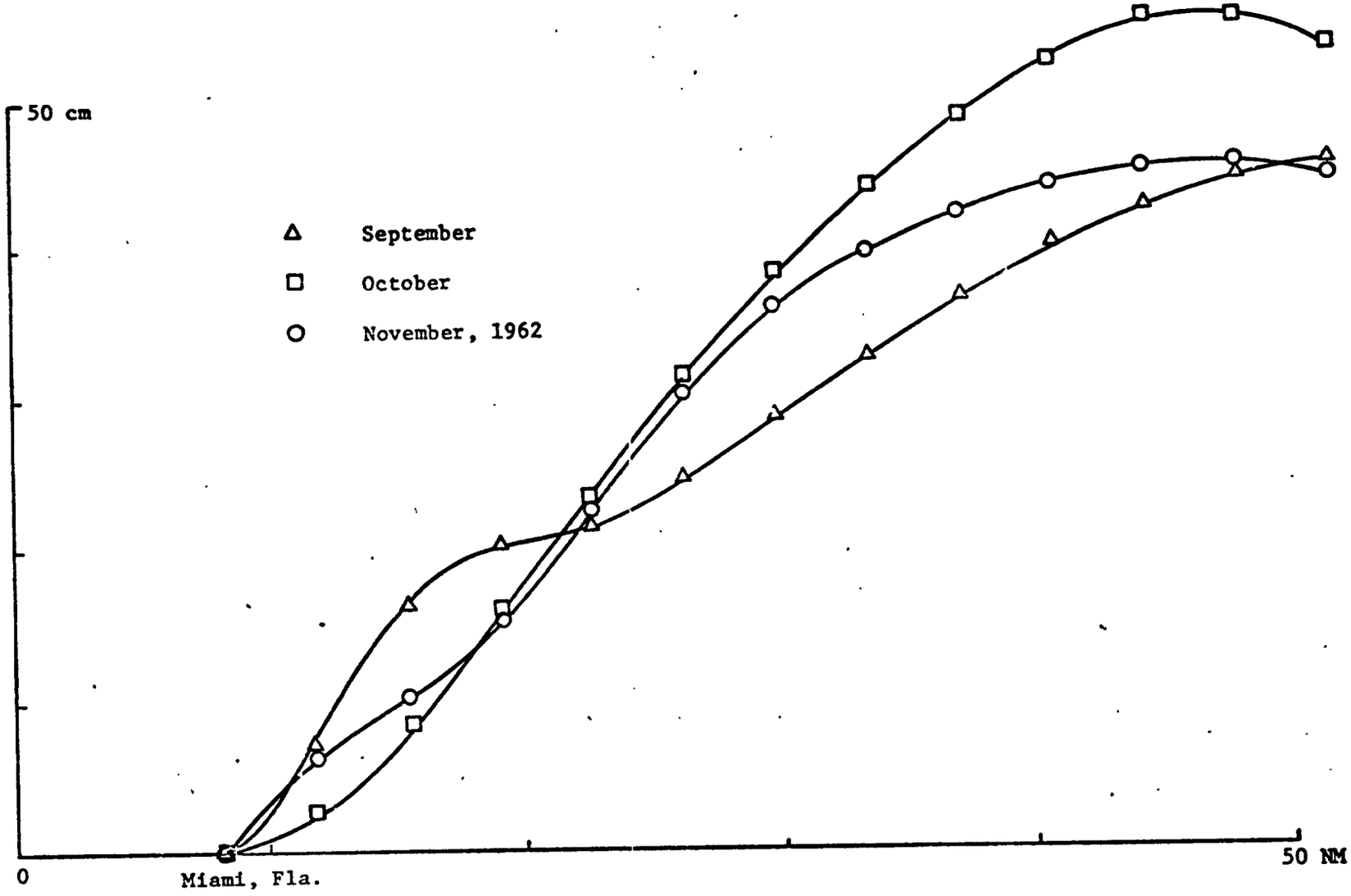

Fig. 3.48 Surface profile based on mass transport measurements.

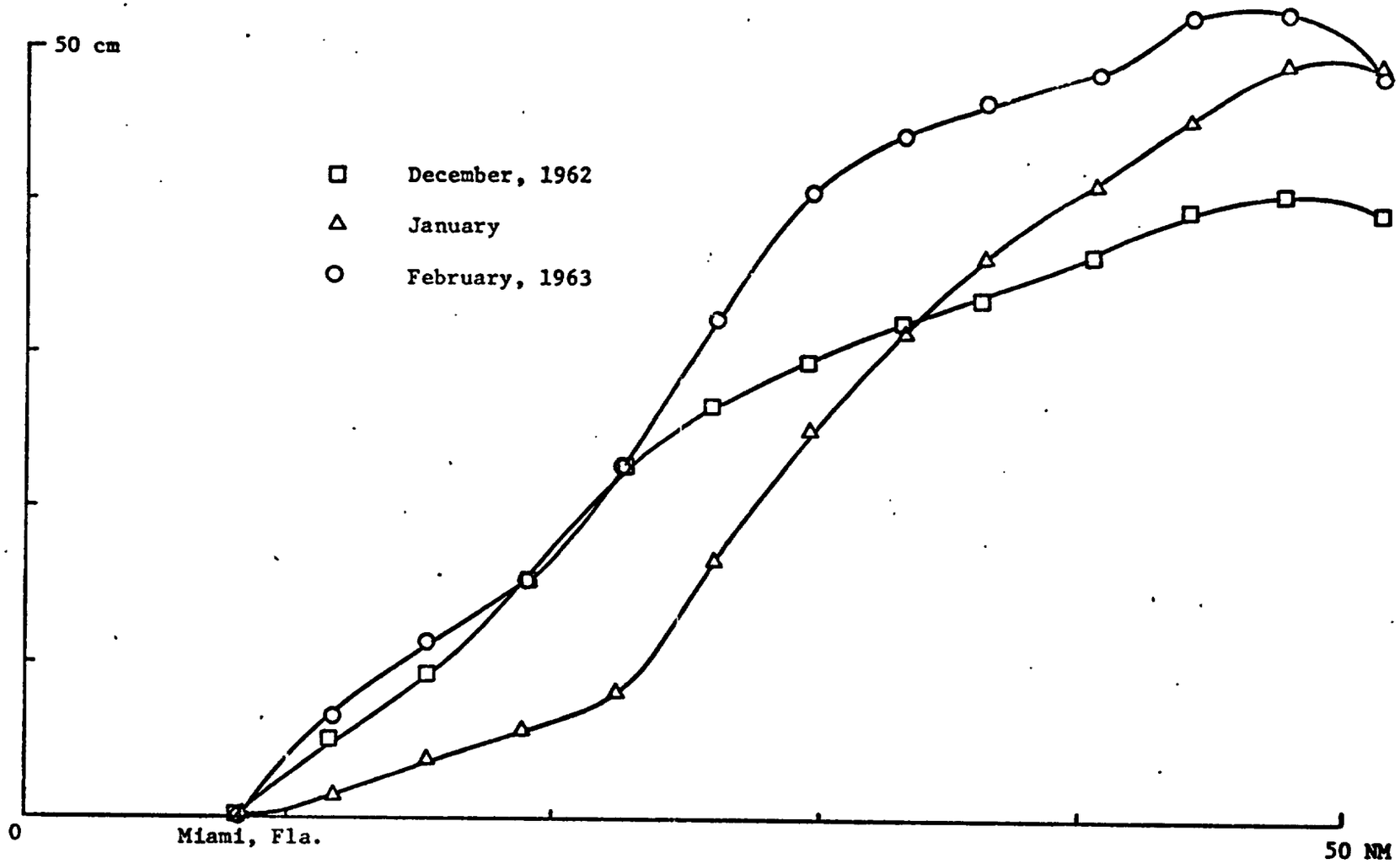

Figure 3.49 Surface profile based on mass transport measurements.

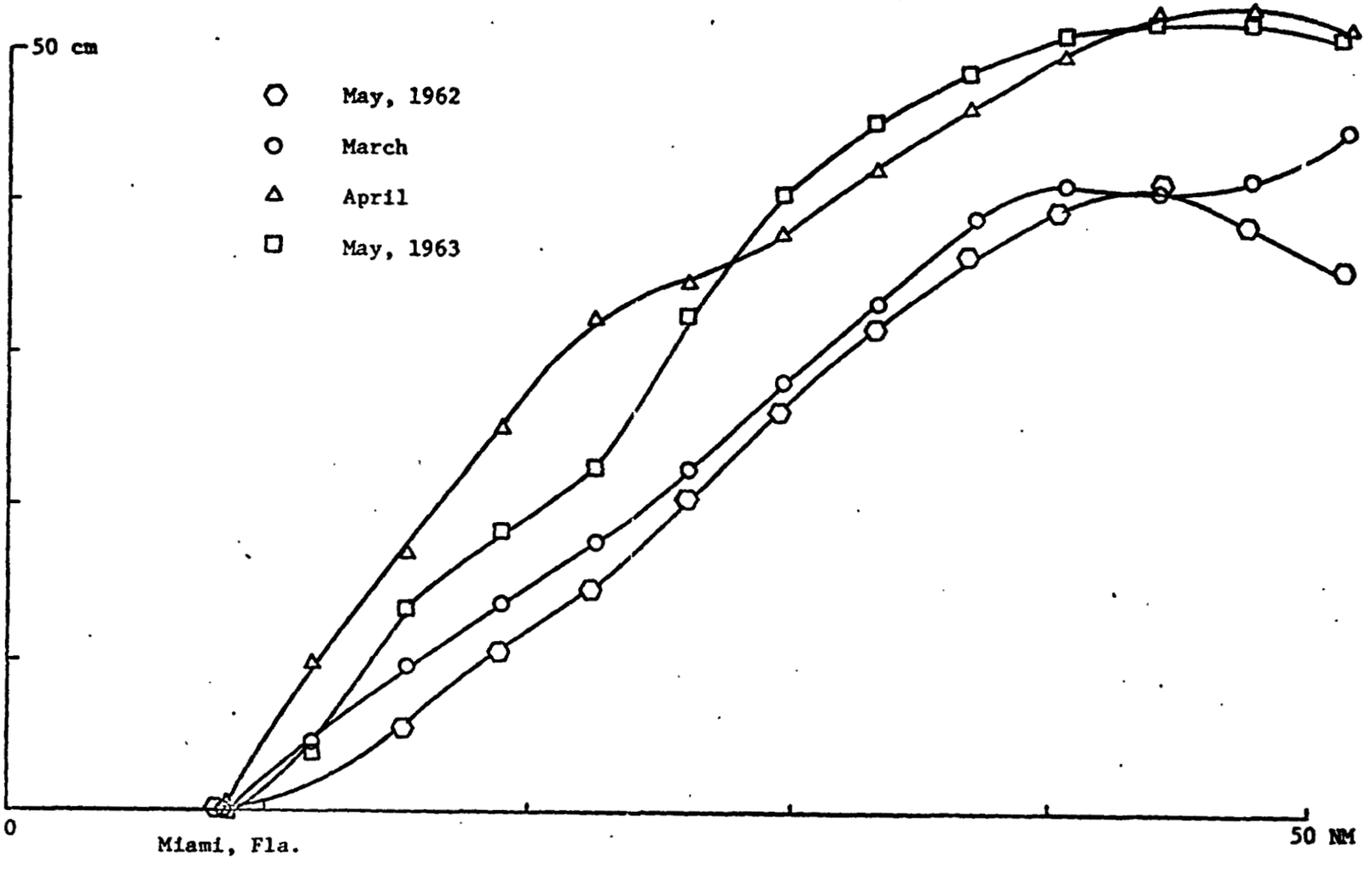

Fig. 3.50 Surface profile based on mass transport measurements.

4. GEOIDAL UNDULATIONS

4.1 BACKGROUND

We are interested in obtaining surface elevation information from satellites, and any departures from a flat surface over oceans are interpreted as having been caused either by current systems or to a larger extent, by changes in the local gravitational acceleration. The continental margins are regions of rather dramatic departure of the value of real g from a latitudinally based constant. Reasons for this fact are several, the two foremost due to the changes in ocean bottom depth of the order of three to six kilometers over lateral distances of the order of tens of kilometers. Factors influencing departures of sea surface elevation from a level of constant z are then geostrophic and hydrostatic adjustment and local changes in the value of the gravitational acceleration coefficient.

As it occurs, the Gulf Stream between Florida and Cape Hatteras generally follows the continental shelf contour. Thus a region of significant changes in the local gravitational potential, as is the shelf margin south of Cape Hatteras, can also be a regime of intense sea surface adjustment due to an intense western boundary current. Because of these integrated complications, surface slope calculations cannot be based simply on hydrographic data as done in section 2 of this report, but must also be adjusted with geophysical gravity determinations. The satellite cannot differentiate between anomaly source, it simply sees the resultant.

Undulations in the geoid and deflections of the vertical can be caused by unknown disturbing masses which create gravity anomalies. If one were to have complete knowledge of the gravity anomalies, Δg, around the earth, then one could accurately know the other quantities worldwide. There has been a

35% coverage, on a 1° by 1° basis, for the entire surface of the Earth. This is a credit to investigators of the twentieth century but unfortunate to the determinations of geoidal undulations and deflections of the vertical. One could of course extrapolate from the existing gravity net to unsurveyed areas of the world but confidence in such an extension could not be too high. Furthermore, based on our 35%, 1° by 1° coverage, and with the knowledge that requirements for anomalies are in area means and point values we can see that 1° squares may only yield general, as distinct from local, predictions, at best. The case of point by point prediction is related to the determination of area means of all point anomalies within the area being surveyed. In effect then, a large number of points for an area mean or an actual point observation are necessitated when dealing with point predictions.

Statistical methods have been used to extend gravity data to the unsurveyed areas of the Earth. It is generally felt that if Δg is unknown over distances between 10^3 to 10^6 kilometers then various modifications of statistical methods will allow one to fill the gap with reasonably good confidence, given no real dramatic change in g across the interval that will not be accounted for in an extrapolation. Since, however, we know that gravity anomalies exist, we can presume that they are caused by topographic mass deficiencies in the oceans and excesses on the continents and by isostatic compensating surpluses and deficiencies. Were the Earth in hydrostatic equilibrium, the equipotential surfaces, including level, would be a flattened mathematical ellipsoid (Heiskanen, 1966). It is known from geophysical methods though, that the Earth is to appreciable measure in isostatic equilibrium (Heiskanen and Meinesz, 1958) so that topographic mass excesses and surpluses are compensated for by appropriate masses. Simple response of the geoid to topographic change would mean that a 5 kilometer high coastal

mountain range parallel to a 5 kilometer deep abyssal plain would result in a geoid undulation of the order of 800 meters. Such changes have not been observed either by land, sea or airbourne instruments, so there is no doubt that isostatic compensation does occur to obvious measure. It can be assuredly claimed herein that topographic and compensating masses account for not less than 85% of g.

4.2 THEORY AND CALCULATION

With U, the potential of the ellipsoid, W, the potential of the geoid, γ, the gravity on the ellipsoid, g, the gravity on the geoid and Δg, equal to g minus γ, the gravity anomaly then the condition that the potentials of the ellipsoid and geoid are equal is

$$U = W = Uv + V = \text{constant}, \tag{3.1}$$

where Uv is the potential of the geoid if there were no mass anomalies and V is the disturbing potential. Now, though the potentials of the geoid and ellipsoid are equivalent, the two equipotential surfaces will not necessarily coincide, in which case they will be separated by N, the geoidal undulation in units of length. With the assumption that the geoidal undulation N is much less than the ellipsoidal geocentric radius, it can be assumed that

$$N = \frac{V}{\gamma} \tag{3.2}$$

G. G. Stokes developed an expression for V (Heiskanen and Moritz, 1967) which when substituted into 3.2 results in the following expression for N

$$N = \frac{1}{4\pi\gamma} \int_0^{2\pi} \int_0^{\pi} \Delta g(\psi,\alpha)\, S(\psi) \sin\psi \, d\psi \, d\alpha \ , \tag{3.3}$$

where

$$S(\psi) = \csc\frac{\psi}{2} - 5\cos\psi - 6\sin\frac{\psi}{2} + 1 - 3\cos\psi\left[\ln\left(\sin\frac{\psi}{2} + \sin^2\frac{\psi}{2}\right)\right] , \qquad (3.4)$$

and ψ is the angular distance between the area where Δg is determined for to the point for which a value for N is being sought, and α is the azimuth from the point causing the effect to the affected point. As is obvious from 3.3, integration is carried out over the entire globe, so one needs to have a knowledge of the kernal Δg, worldwide, in order to perform the integration in 3.3 The local value of Δg is essentially the difference between the locally observed g, g_o, minus the international gravity formula (Heiskanen, 1928)

$$\gamma = 978.0490\ (1+0.005\ 2884\ \sin^2\varphi\ -\ 0.0000059\ \sin^2\ 2\varphi) \qquad (3.5)$$

after several corrections have been applied to the observed gravity readings. It should be noted that the major contributions to N, are functions of values of Δg within three or four hundred kilometers of the point in question. Also of note is the fact that 3.3 is valid under the assumption that all masses producing the equipotential surface are contained inside of the geoid.

The following is a description of marine gravity theory given by Banks (1972); and modified by the authors of this report:

> In most areas of the world, Bouguer anomalies are negative in mountainous regions and positive over the oceans. These anomalies are explainable on the assumption that, above a depth of compensation, the average rock density under mountains is less than the average rock density under land masses at sea level, while the average rock density under oceans is greater than that under land masses at sea level. Thus, the effect of topography would be counterbalanced by mass or

density differences, manifested as roots or antiroots at the base of the earth's crust. These ideas have led to the hypothesis of isostatic equilibrium (see e.g., Heiskanen and Vening Meinesz, 1958).

Although different concepts on the mechanics of isostatic equilibrium have been advanced, only two will be used in the calculation of isostatic anomalies herein. These are the Pratt-Hayford and the Airy-Heiskanen concepts of isostasy, which have been extensively used in gravimetric studies.

The Pratt-Hayford concept assumes that equilibrium is attained through uniform vertical columns of different densities, all extending downward to the same depth of compensation. Columns in mountainous areas are assumed to consist of lighter material than columns in the lower elevation plains or ocean basins. At the depth of compensation all masses are in hydrostatic equilibrium, that is, they are subjected to equal pressures from all directions, whether the masses are under mountains or oceans. Thus, two vertical columns of equal cross sectional area, extending from the surface of the earth to the depth of compensation, will exert the same weight at the base of the columns.

The pressure at the base of Column 1 equals that at the base of Column 2.

Then,

$$(\rho - \rho')g_1 (D + h) = \rho g_2 D \qquad (3.6)$$

where ρ is the density of Column 2, which has a surface elevation of sea level, $\rho - \rho'$ is the density of Column 1, which has a surface elevation other than sea level, g_1 is the average value of gravity over Column 1 and g_2 is the average value of gravity over Column 2. D is the depth of

compensation below sea level and h represents the elevation above sea level. ρ', the density increase or decrease of each column, is a function of the topographic elevation h, the density ρ, and the depth of compensation D.

The Pratt-Hayford concept also assumes that each column is an independently compensated unit, that is, columns do not include compensations for topography in adjacent columns (see e.g., Heiskanen and Vening Meinesz, 1958).

Equation 3.6 shows that at the depth of compensation, pressures at the base of all columns are identical, and thus the weights of the total columns are the same. This is true assuming that average gravity is the same over both columns which introduces a small error, as gravity decreases with elevation.

Then

$$\frac{\rho + \rho'}{\rho} = \frac{D}{D+h} \tag{3.7}$$

which reduces to:

$$1 + \frac{\rho'}{\rho} = 1 - \frac{h}{D} + \frac{h^2}{D^2} \cdots \tag{3.8}$$

and, by neglecting higher order terms

$$\frac{\rho'}{\rho} = -\frac{h}{D} \tag{3.9}$$

gives

$$\rho' = -\frac{h}{D}\rho \quad . \tag{3.10}$$

Isostatic equilibrium can be expressed mathematically as equality of pressure at the depth of compensation or as equality of mass in overlying columns. Equation 3.10 does not satisfy either equality of pressure or of mass, but approximates the equality of pressure more closely. This is due

to the fact that only a small change of gravity is neglected for the different heights of the columns. According to Heiskanen and Vening Meinesz (1958) "the common opinion today is that isostatic compensation seldom occurs according to the Pratt-Hayford assumption."

The Airy-Heiskanen isostatic concept assumes that a lighter crust floats on a heavier mantle, much as an iceberg floats in water. An inadequacy in this comparison is that the root of an iceberg extends downward from sea level, while the root of a land mass extends downward from an average depth of the crust (depth of compensation), usually assumed to be 20, 30, 40, or 60 km below sea level.

In the Airy-Heiskanen system, materials that compensate for topographic variations are assumed to lie vertically beneath the topographic features. The density of the entire crust is assumed to be a uniform 2.67 gr/cm^3, and that of the underlying mantle 3.27 gr/cm^3, or 0.6 gr/cm^3 greater than that of the crust. The density of 2.67 gr/cm^3 for the earth's crust is an arithmetic mean of six estimates that were made between 1811 and 1882 (Harkness, 1891) this figure has been used by later investigators such as Hayford and Bowie (1912).

When calculating isostatic anomalies according to the Airy-Heiskanen system, the thickness of the crust for a sea level elevation (land area), T, must be assumed. As thicknesses of the crust are not exactly known, isostatic anomalies are often computed using various values of T. Analyses of anomalies based on these different values of T can provide indications of the probable thickness of the crust.

For isostatic anomalies at sea level stations, two corrections are applied. The first is the topographic correction, which removes the effect of all masses above sea level. This correction is also used to replace

ocean water by material having a density equal to the mean surface density of the solid earth. There are various methods for obtaining topographic corrections, based on reading elevations from topographic maps for certain zonal areas (see e.g., Gutenberg, 1959). Although the topographic corrections can be made for the entire earth, it is sufficient in some regions to correct for topography at distances out to 166.7 km of the station.

The second correction is made for the effect of the compensating mass, which is presumed to be directly beneath each topographic feature and below the assumed depth of compensation. Calculation of this second correction is lengthy; published tables and maps (Hayford and Bowie, 1912; Heiskanen, 1938; and Karki, Kivioja, and Heiskanen, 1961).

The Bouguer anomaly for stations at sea level includes only a correction for the effect of the surrounding topography. The topographic correction used in the isostatic anomaly calculation is also the Bouguer topographic correction. These topographic corrections are always added to the observed sea level gravity observation. This is due to the fact that the mountains above the station and the density deficiency of the water below the station both have the effect of reducing the observed gravity measurement from what would have been measured at sea level with no water or topography present.

The Bouguer reduction is sometimes viewed as a type of isostatic reduction corresponding to an infinitely thick crust (Heiskanen and Vening Meinesz, 1958).

Positive or negative isostatic anomalies are interpreted to mean that hydrostatic equilibrium does not exist at the assumed depth of compensation,

or that the method of obtaining the anomalies needs some modification (Coulomb and Jobert, 1963).

Isostatic theories propose that at some depth below sea level the pressure on equal areas is the same everywhere. The horizontal dimensions required for a region to be in equilibrium are not defined nor generally agreed upon. Some investigators believe that cross sections of the order of 10,000 km^2 may be large enough to be compensated (Bowie, 1917); other studies indicate that an area the size of the Hawaiian Islands (16,638 km^2) is too small to be in complete equilibrium (Niskanen, 1945). Some people envision that an area must be as large as the United States before equilibrium can be achieved (Bowie, 1924). Tsuboi (1940) has calculated that equilibrium requires an area with the horizontal dimension about three times the depth of compensation. This estimate is generally accepted as reasonably correct. Due to the strength of the earth's crust, it is believed that complete equilibrium is extremely unlikely for any topographic feature (Heiskanen and Vening Meinesz, 1958).

The depth of compensation or the proper thickness of the crust must also be assumed when calculating isostatic anomalies. Much as Bouguer anomalies can be considered to be as forms of isostatic anomalies when the depth of compensation is infinite (completely rigid materials of great thickness), so free-air anomalies can be considered as forms of isostatic anomalies when the depth of compensation is at sea level (zero crustal thickness, with topographic masses having zero rigidity). A geologically more realistic picture, in view of the high but not infinite rigidity of crustal rocks, is that there is a depth of compensation at some real depth beneath the surface. The depth at which compensation

occurs is assumed. In the Airy-Heiskanen concept, the assumed depths are 20, 30, 40 and 60 km; in the Pratt-Hayford concept, the assumed depth is 113.7 km.

A particular density structure for the crust and mantle is also assumed for the various isostatic systems. Although the constant crustal density assumed in the Airy-Heiskanen theory may closely approximate the world average, specific areas of the world may deviate from this assumed value (see e.g., Walcott, 1967). This fact could affect the results obtained from an isostatic study.

In making Airy-Heiskanen isostatic reductions, the Mohorovicic discontinuity is assumed to be the boundary between the crust consisting of one uniform density and the mantle consisting of another uniform density. Seismologists find that two and possibly three discontinuities exist above the Mohorovicic discontinuity, and possibly some beneath the discontinuity. Calculated isostatic anomalies have shown, however, that nearly the same isostatic result can be obtained by assuming either one or even several discontinuities. Thus, before two or more discontinuities can be used in calculations, more reliable evidence is needed concerning the discontinuities (Heiskanen and Vening Meinesz, 1958).

So, one can correct gravity observed at sea by making four corrections (Grant and West, 1965). The first correction is the Free-Air correction, which takes into account the position of the gravimeter with respect to sea level. The correction is subtracted from g_o as a function of depth of measurement below sea level, and is given by the following equation

$$\Delta g_{fc} = 0.3086d. \qquad (3.11)$$

This correction, of itself at sea, has little meaning because of the fact of having to account for the thin plate of water above the ocean floor. The Bouguer Plate Correction must be applied herein. This correction deletes the effect of the upward pull of the water section and in a second application will restore the pull downward by the water section if the measuring device had been located at the ocean surface. This reduction is always positive in nature and is given as

$$\Delta g_{bc} = 0.0861d. \tag{3.12}$$

It should be mentioned that the combined corrections to g_o, as given by Δg_{bc} and Δg_{fc} are referred to as the free-air-at-sea correction.

A correction, $\Delta g_{b'c}$, based on the assumption that the ocean basins represent a mass deficiency not compensated isostatically, and is then always positive. This correction is called the Secondary Plate Correction and is given by the following relation

$$\Delta g_{b'c} = 0.0688h \tag{3.13}$$

where h is total ocean depth.

A fourth correction, Δg_i, called the Isostatic Correction can be applied and can be based on the aforementioned theories of Pratt-Hayford and Airy-Heiskanen.

Another correction is that due to the fact that measurements are being made from a moving vehicle and is called the Eotvos correction and must be removed from observations. It is

$$\Delta g_{ec} = \pm 0.14584\ v_{SV}, \tag{3.14}$$

where the plus sign denotes eastward ship movement, the negative sign denotes westward motion and v_{SV} denotes the ships velocity. This correction is based

on the fact of existence of the ficticious centrifugal force due to the Earth's rotation.

Knowing the constituents of the gravity corrections then, one derives a series of resultant anomalies, representing the free-air-anomaly-at-sea, Δg_f the Bouguer anomaly at sea, Δg_b and the isostatic anomaly at sea, Δg_i. The appropriate relations are as follows

$$\Delta g_f = g_o - \Delta g_{fc} + \Delta g_{bc} - \Delta g_{ec} - \gamma, \tag{3.15}$$

$$\Delta g_b = \Delta g_f + \Delta g_{b'c} \tag{3.16}$$

$$\text{and} \quad \Delta g_i = \Delta g_b + \Delta g_{ic} \tag{3.17}$$

From comparisons, it appears that the free-air anomalies, Δg_f, are generally like those which result from isostasy reduction considerations and are then, considering the greater simplicity of calculating g_f, used to calculate the Stokes function N in expression 3.3.

Worzel and Shurbet (1955) compiled a series of gravity observations made at 104 sea stations. Three of their seven transects (Figure 4.1) are appropriate to our Gulf Stream area of interest and the marine gravity data which has been used in an attempt to calculate the Stokes function is shown in Figures 4.2 through 4.5.

It has been mentioned previously that, as Garland (1965) said, the calculation of N at any point is dependent on a knowledge of Δg over the whole earth and there are barely sufficient observations in some regions to permit accurate calculations anywhere. To avoid this problem, then, Vening Meinesz (Heiskanen and Meinesz, 1958) demonstrated that where gravity anomaly gradients are "smooth," then the azimuth of the near field vertical deflection is measurably co-incident

with the direction of the gravity anomaly gradient. If one draws a circle of radius 30 kilometers (e.g., Heiskanen and Meinesz, 1958) around the point in question and computes average free-air gravity anomaly gradients across the meridional and zonal diameters of the circle then, one can use the Meinesz development to imply an approximated Stokes function. This procedure was followed in the development of the curves depicted in Figure 4.6 through 4.8 and was based on the Worzel and Shurbet data.

The results, as shown in the curves indicate that in general the Stokes function increases in magnitude from Cape May to Cape Henry to Cape Hatteras with the total differential in the geoidal undulation being augmented from approximately one meter at Cape May to two and a half meters at Cape Henry to three meters at Cape Hatteras.

Since the order of magnitude of these undulations is at least as large and usually several times as large as sea level change due to Gulf Stream systems adjustment (cf. Sections 2 and 3 of this report) then the non-ocean current based causes must be subtracted from the total deviation in the geoid if one is to look at sea surface slopes related to ocean systems with any insight and confidence.

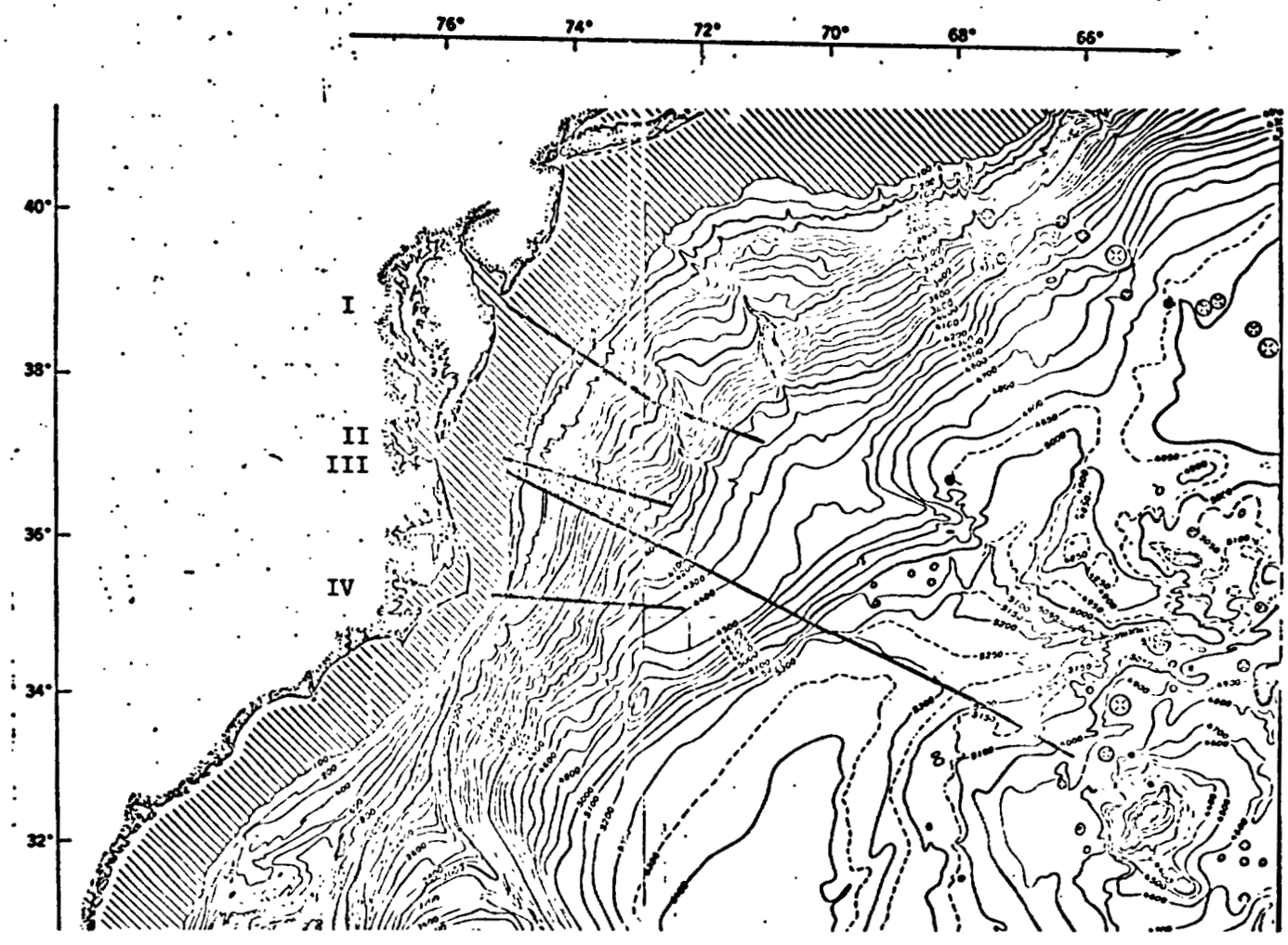

Figure 4.1 Curves I, II and IV are ship track lines along which marine gravity anomaly observations were made (Worzel and Shurbet, 1955). Curve III is an extrapolated but ficticious ship track line from Cape Henry to Bermuda (see text for details).

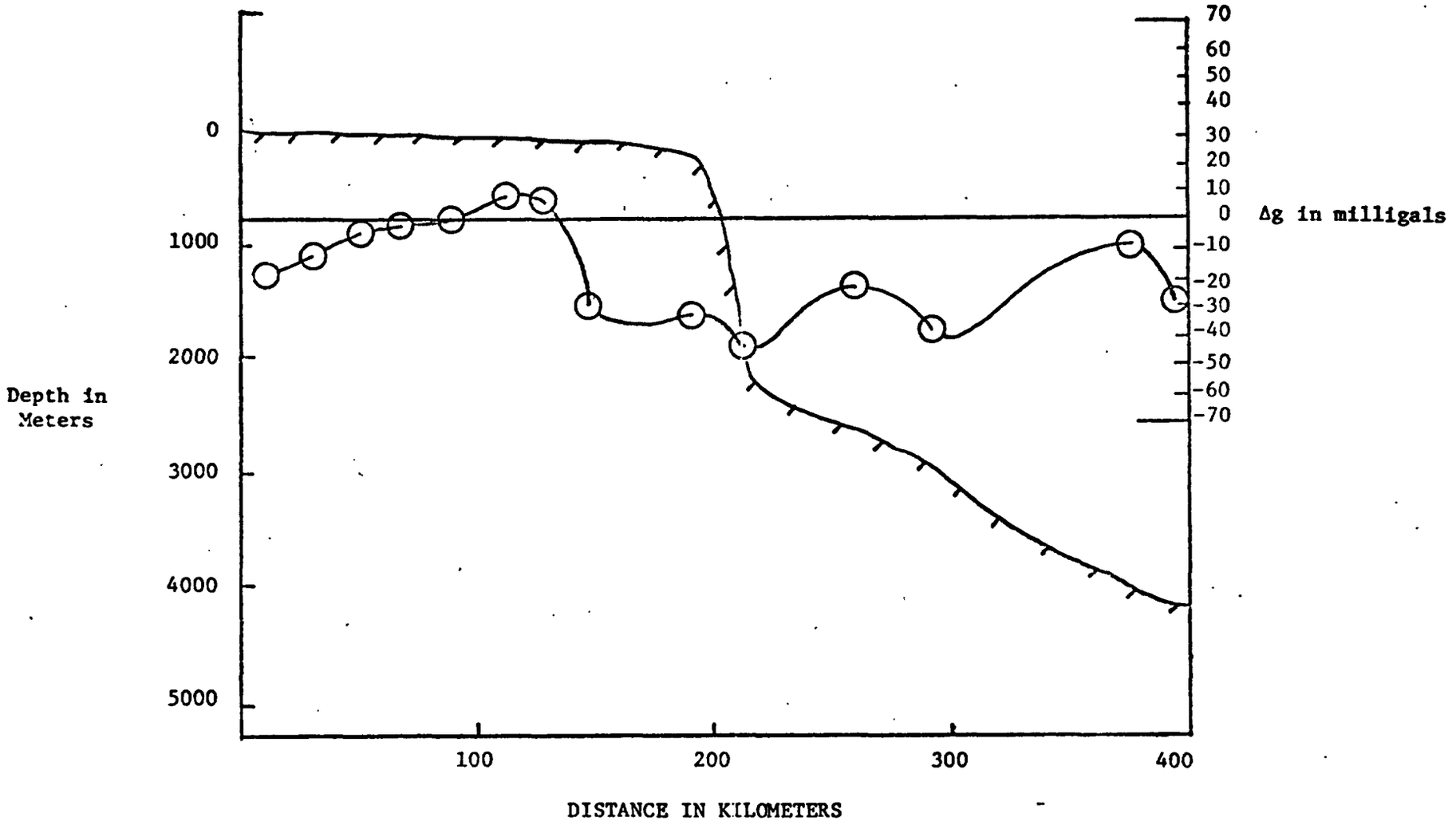

Figure 4.2 Bottom topography and marine gravity anomalies off of Cape May (Transect I, Fig. 4.1).

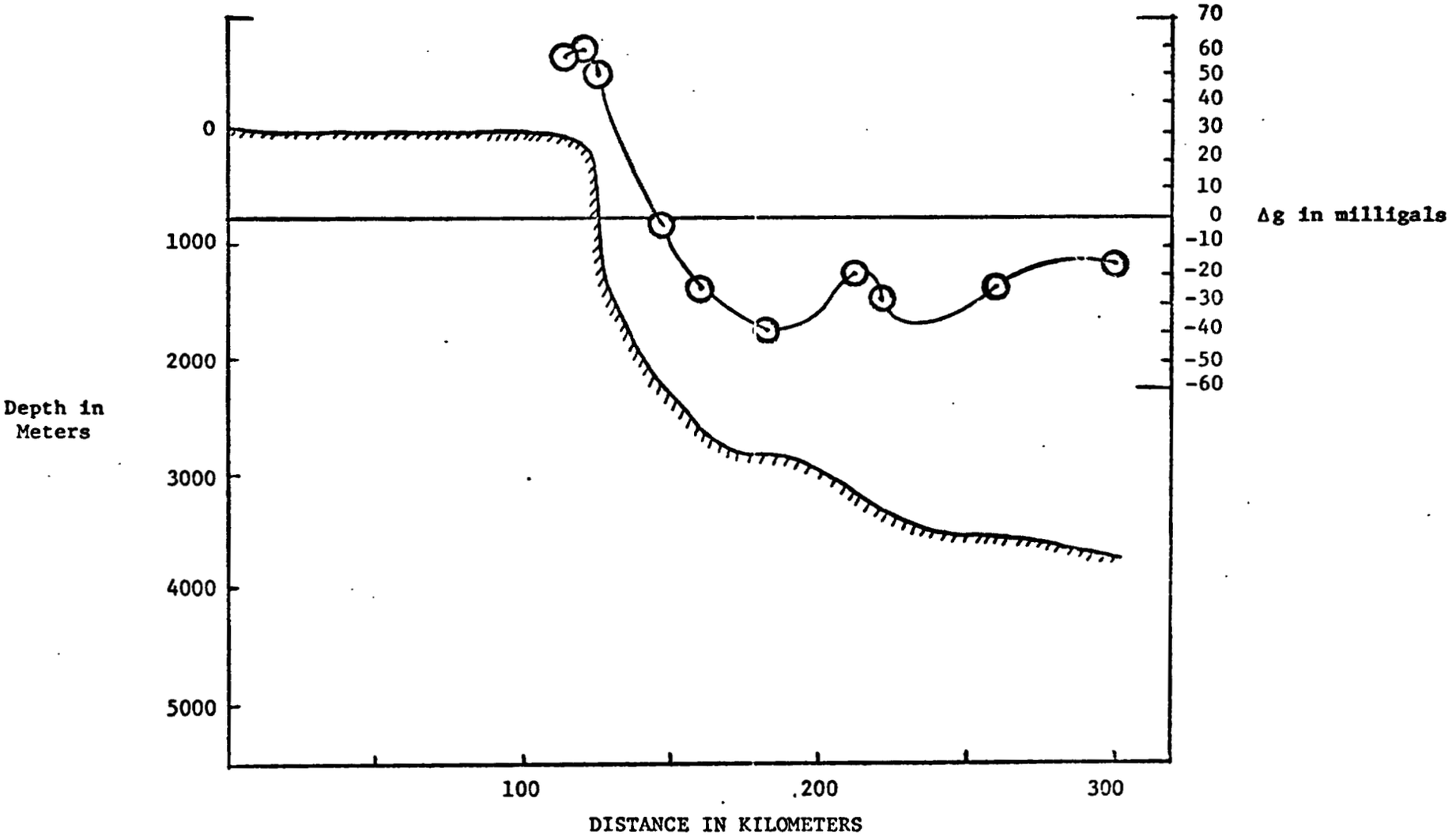

Figure 4.3 Bottom topography and marine gravity anomalies off of Cape Henry (Transect II, Fig. 4.1).

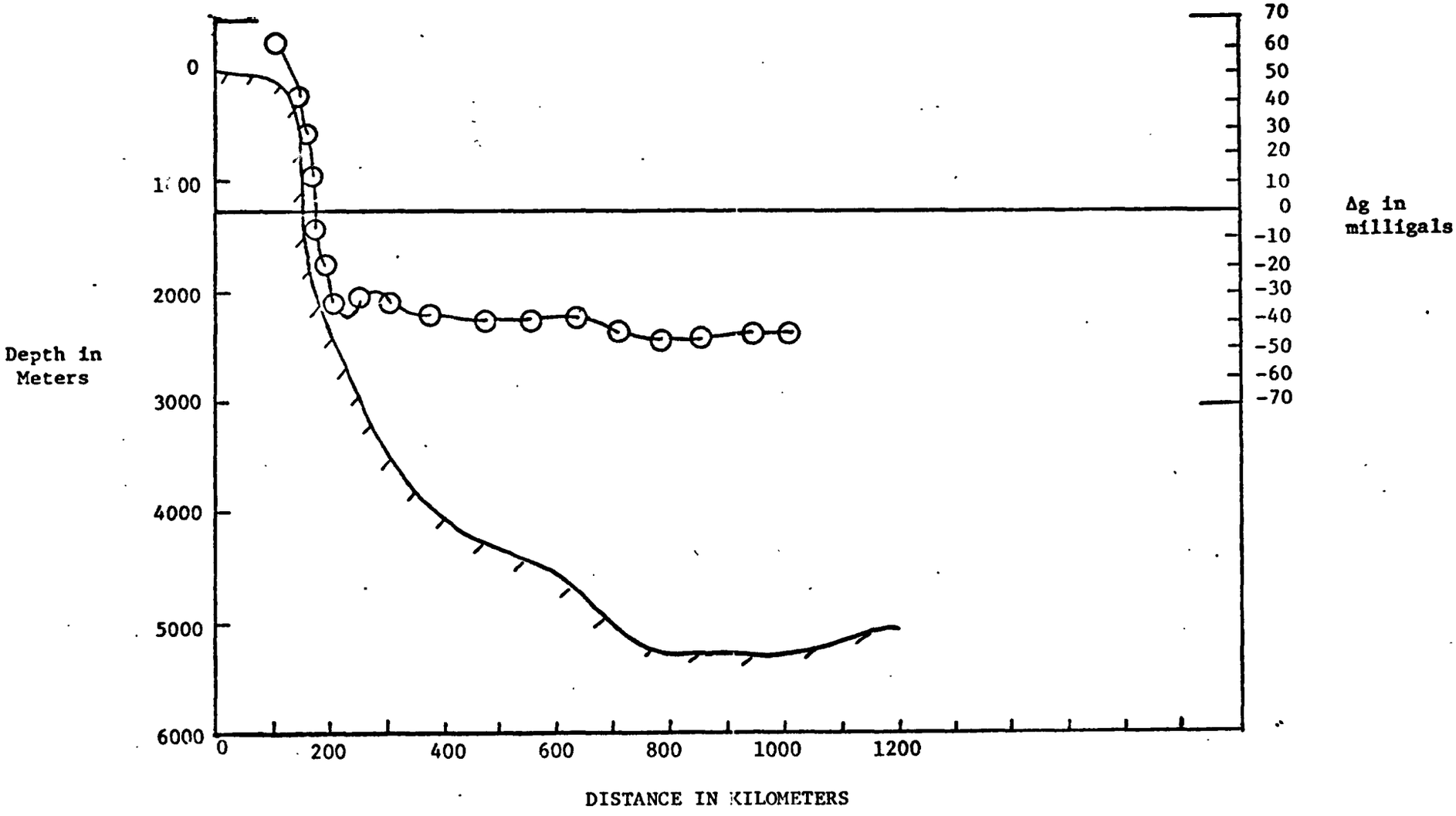

Figure 4.4 Bottom topography and marine gravity anomalies from Cape Henry to Bermuda (Transect III, Fig. 4.1).

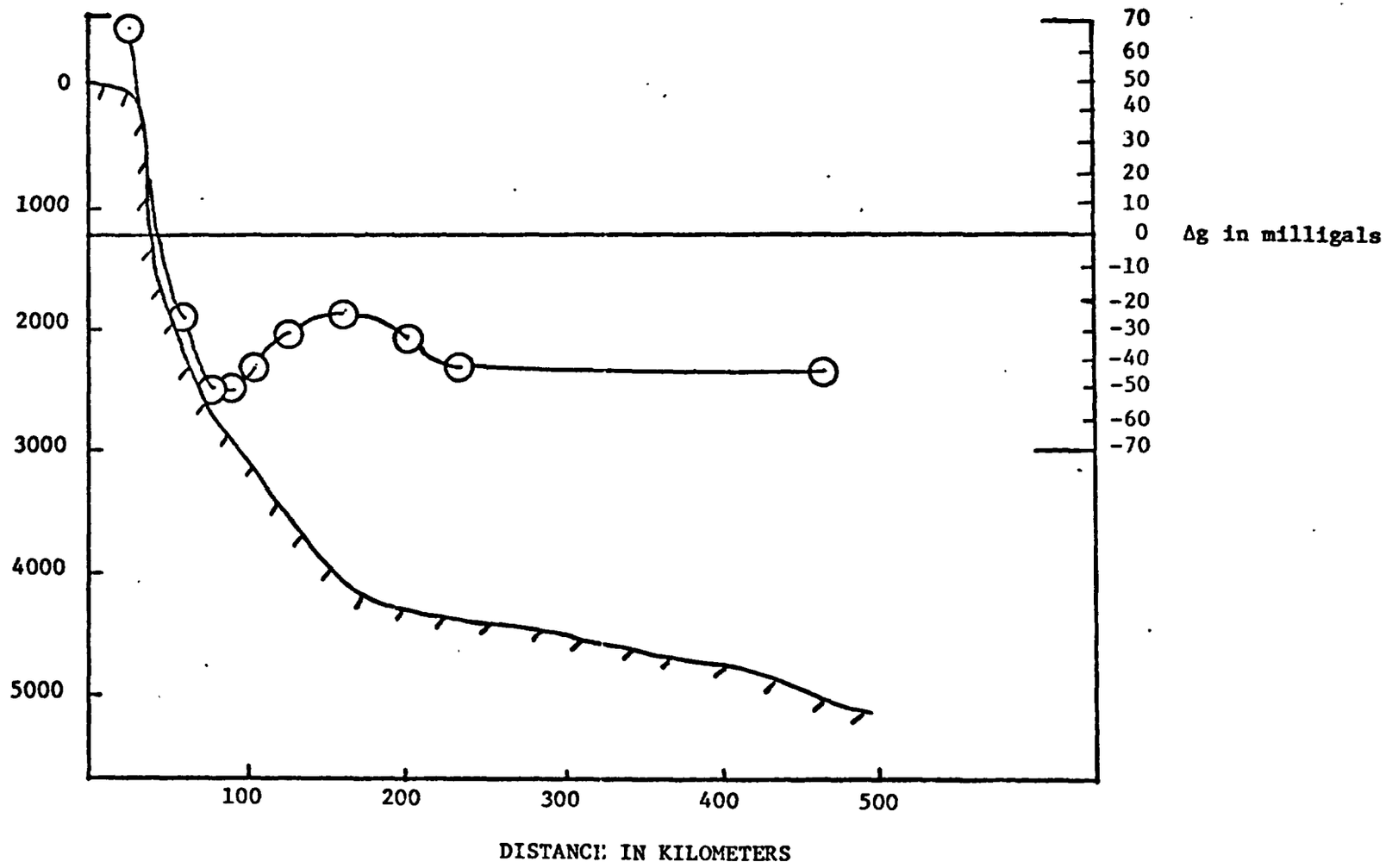

Figure 4.5 Bottom topography and marine gravity anomalies off of Cape Hatteras (Transect IV, Figure 4.1).

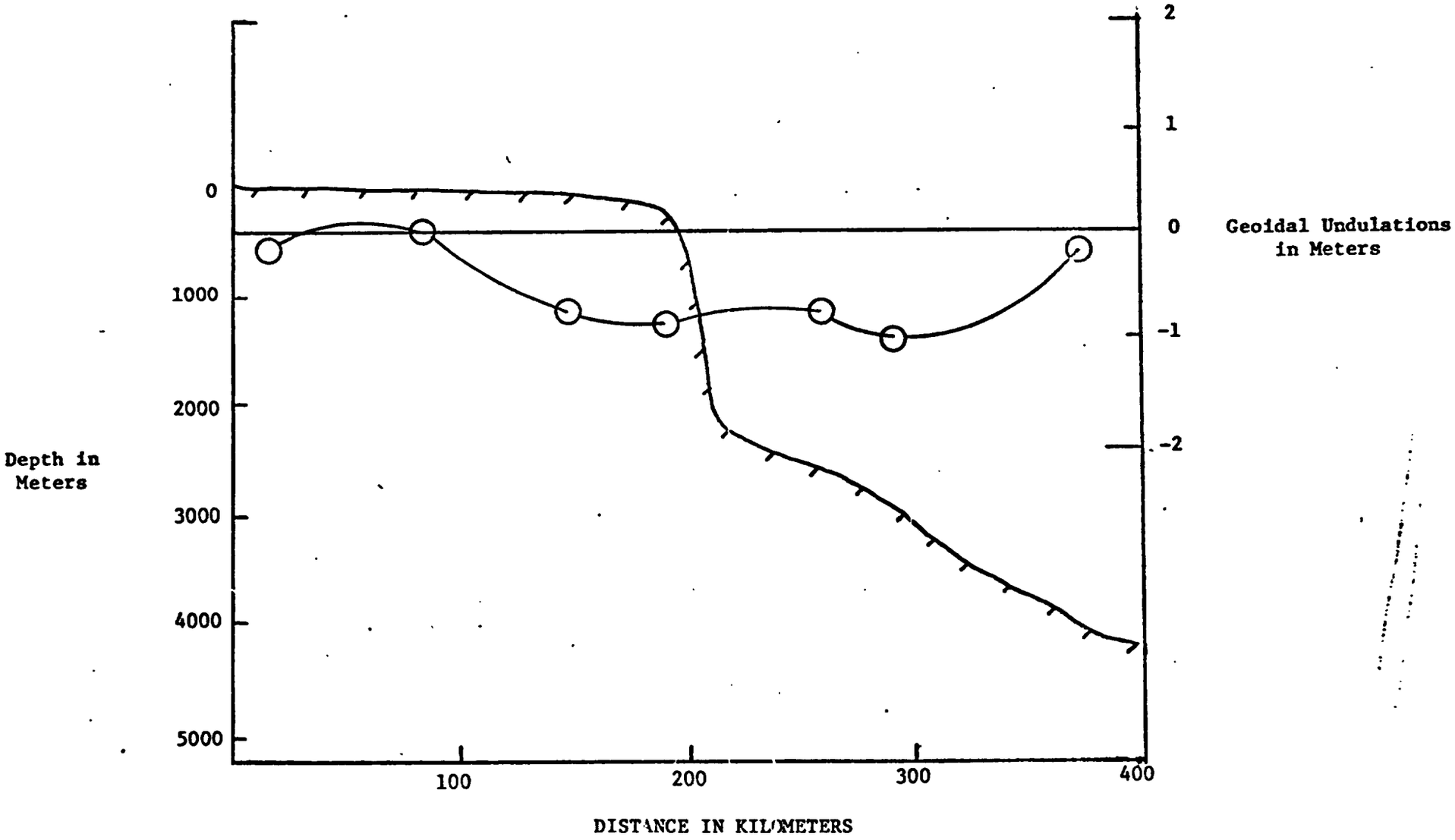

Figure 4.6 Bottom topography and the geoid off of Cape May (Transect I, Fig. 4.1).

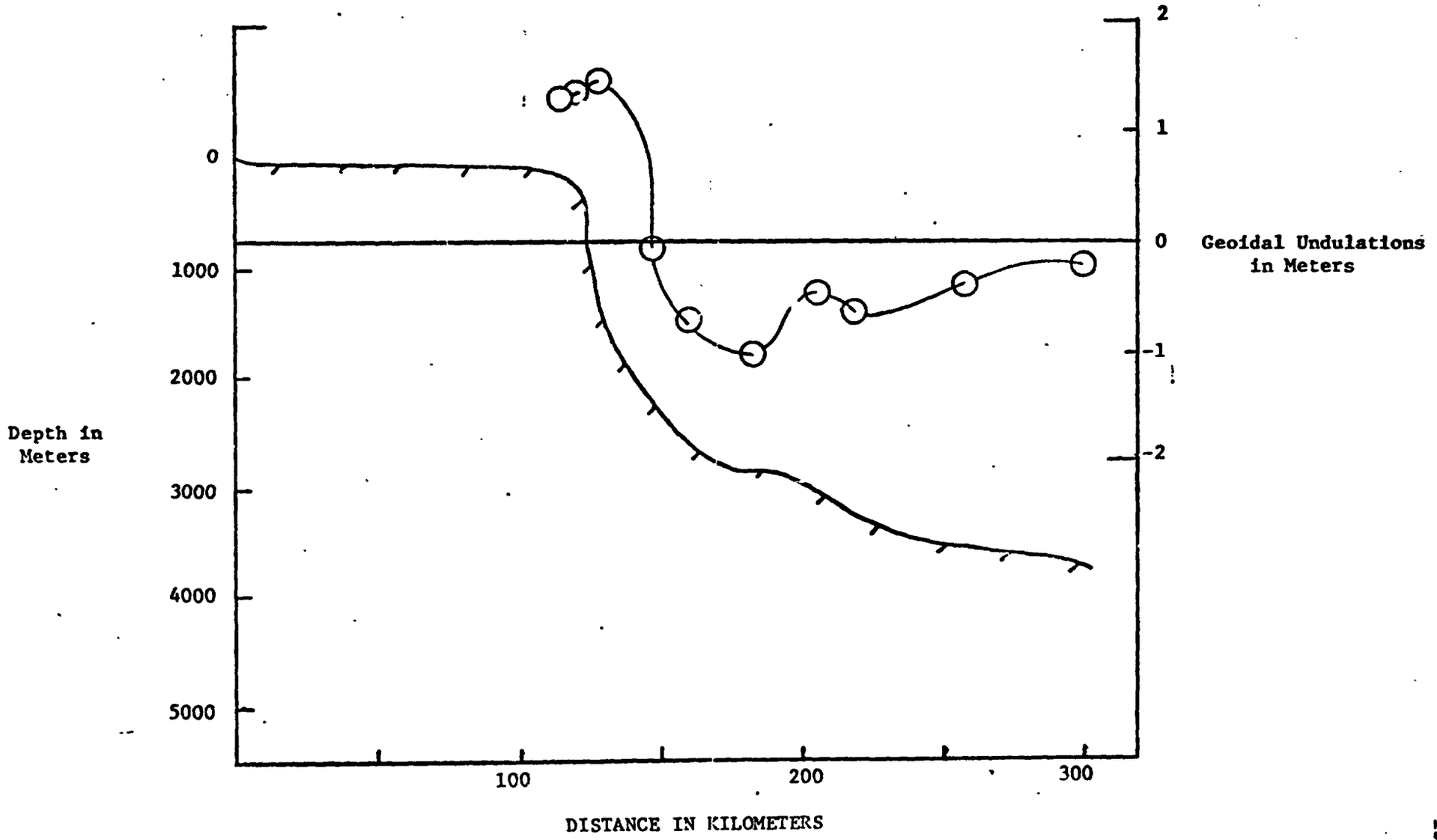

Figure 4.7 Bottom topography and the geoid off of Cape Henry (Transect III, Fig. 4.1).

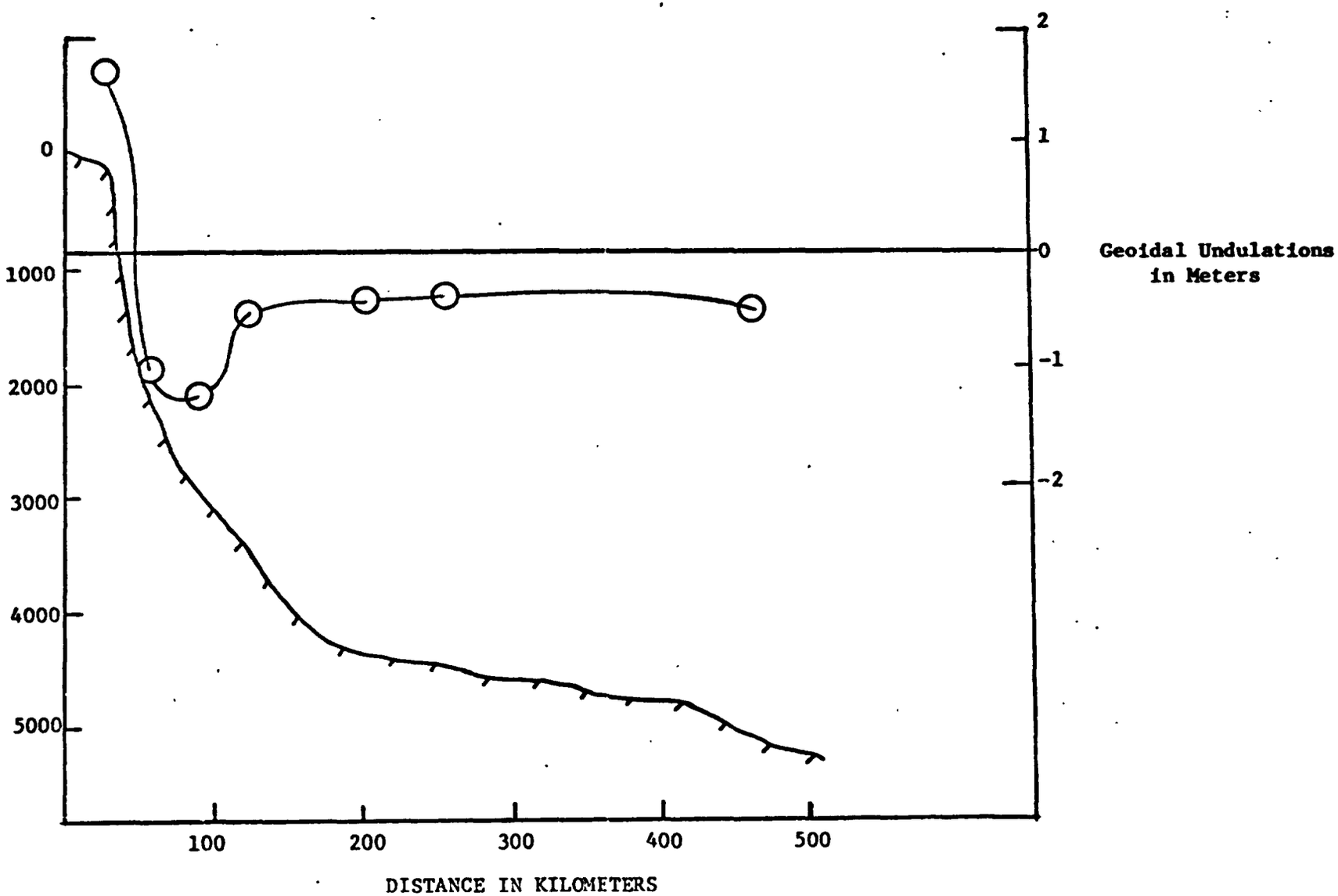

Figure 4.8 Bottom topography and the geoid off of Cape Hatteras (Transect IV, Fig. 4.1).

5. DISCUSSIONS AND RECOMMENDATIONS

5.1 DISCUSSIONS

Based on the results of this study, the following points are of special interest:

(a) Contrary to the accepted view, there are fluctuations of the Gulf Stream occurring over extremely short periods of time of the order of several days. Such changes can easily be observed from Figures 3.32 to 3.36. Qualitatively, such changes are independently confirmed by infrared imagery as shown by Stumpf (1974) in Figures 5.1 and 5.2. It is not clear what the cause of such short time change may be. Local wind stress seems improbable both from the energy argument of Stommel (1966) and from actual field data presented in Chapter 3 which shows low correlation between local wind and the Gulf Stream location and strength. A possible cause is the instability of the stream which causes some Gulf Stream water masses to spin off in an apparent energy relieving process. Such "eddies," "shingles" or "sausages" would show up in hydrographic data as well as infrared imagery as reported by Rao, Strong and Koffler (1971). These phenomena are impossible to study using only shipboard instruments and methods. This can be further demonstrated by the following example. Let curve 1 in Figure 5.3 be the Gulf Stream at time T_1, and curve 2 be the Gulf Stream at time T_2. If a ship set out to study the phenomenon at T_1 and finished the study at T_2. The data that the ship actually collected would result in the solid curve which is not true at any time. Of course if the time scale of the phenomenon is relatively long compared to the cruise time, the ship's data will be more accurate. Unfortunately, high frequency changes do occur. Such mobility of the Gulf Stream immediately leads to the question not only of the fidelity of the data, but also of the geostrophic assumption

which depends crucially on steady state conditions. The influence of short period variations on dynamic calculations has been discussed by Seiwell (1939). The implication seems to be that for highly variable, large scale motions, such as world current systems, remote sensing may be the only practical tool to use in a synoptic sense.

(b) The seasonal variations of the Gulf Stream are considerable. Due to the seasonal changes of t e global wind field, the Gulf Stream ill have to change accordingly. This problem has been studied by Fuglister (1951) and he concluded: "The maximum current speeds occur during the summer in the southern segments of the Gulf Stream system and during the winter in the north segments. The minimum speeds occur during the fall months throughout the system." The results are presented graphically in Figures 5.4 and 5.5. The fluctuations are, of course, due to the global wind field and are not directly related to the local wind field. Fuglister found, however, that the Gulf Stream strength correlated directly with the trade winds but only partially with the local mean wind.

(c) Beyond the seasonal fluctuations, nothing can be said about year to year changes. The existing data are too sparse to be of any use in addressing long term variational patterns. However, since long term meteorological cycles do exist, it stands to reason that there may be similar cycles which the Gulf Stream observes. Fluctuations at these scales can not be studied by traditional methods because for such long term meteorological cycles, the temporal scales are of sufficiently large enough size that the Global circulation systems (Figure 5.6) might interact with each other. Such interaction will, in turn, influence long term weather cycles. This phenomenon should be one of the most important and unique tasks for remote sensing oceanography to address itself to.

(d) Due to the discussion above, it becomes obvious that a single Gulf Stream model, good for all time, is impossible. Though a mean is still possible, as reported by Keondzhyan (1973), the model should be used judiciously.

(e) The undulations caused by topography and isostasy in the region of the continental shelf break would appear to be of the order of several meters excursion which is at least as large in magnitude as any change in sea surface height as a function of the Gulf Stream. Since the solid earth based causes for geoidal undulations are not time dependent, then it would be of considerable worth to be able to simply delete such cause and effect from the data. The implication is that subtracting out the effects of crossing the shelf rise would allow one to look at ocean systems directly.

5.2 RECOMMENDATIONS

Based on the study, the following recommendations can be made:

(a) The remote sensing method should be used to cover the global ocean continuously for an extensive period of time so that the temporal and spatial variations can be determined over all ranges. It is granted that there are limitations of remote sensing methods and, therefore, comparisons with available in situ field data should be made complementarily with each other.

(b) Since most strong current systems in the world occur as western boundary flows, e.g., the Gulf Stream and Kuroshio, care should be taken when we are trying to infer current conditions from altimeter measurements and geostrophic theory, since part of the Gulf Stream generally follows the continental shelf where the geoid perturbation caused by the continental rise could be mistaken as part of the stream. Therefore, a detailed study of geoid perturbation along the continental shelf should be one of the most crucial tasks to be worked on.

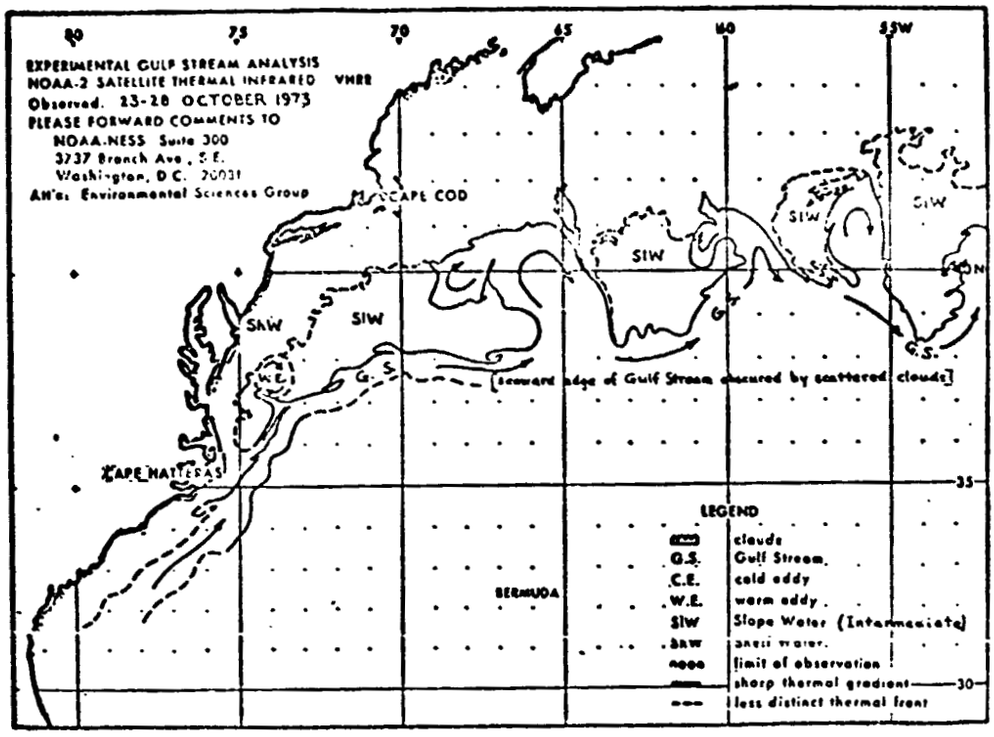

Figure 5.1 Facsimile chart for October 23-28, 1973 (Stumpf, 1974).

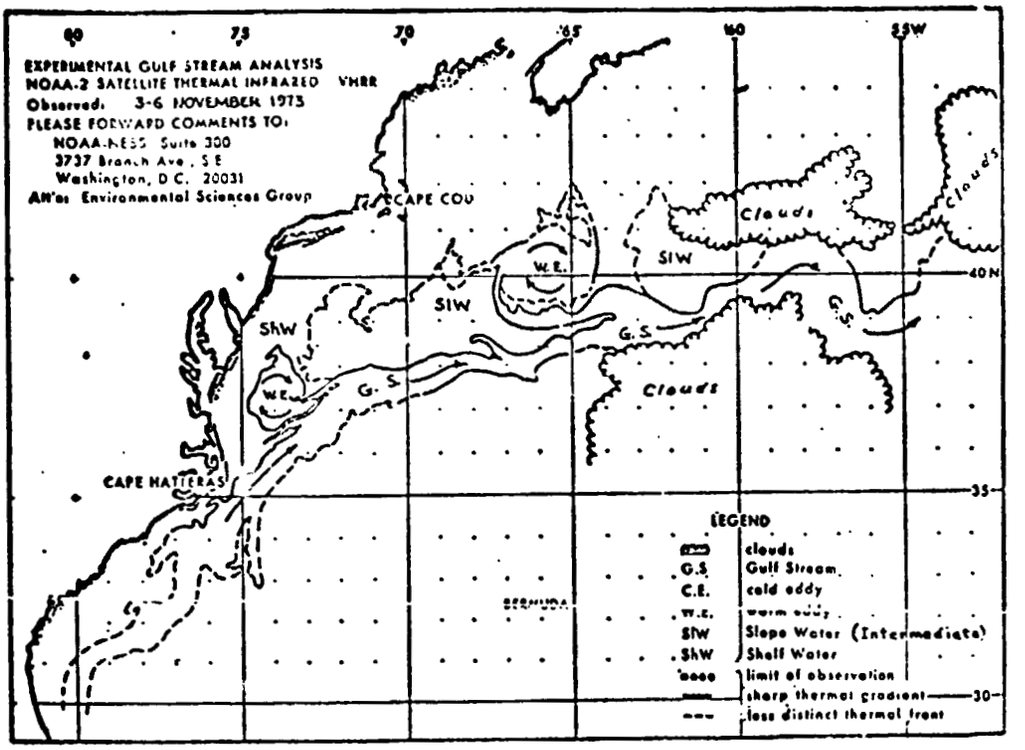

Figure 5.2 Facsimile chart for November 3-6, 1973 (Stumpf, 1974).

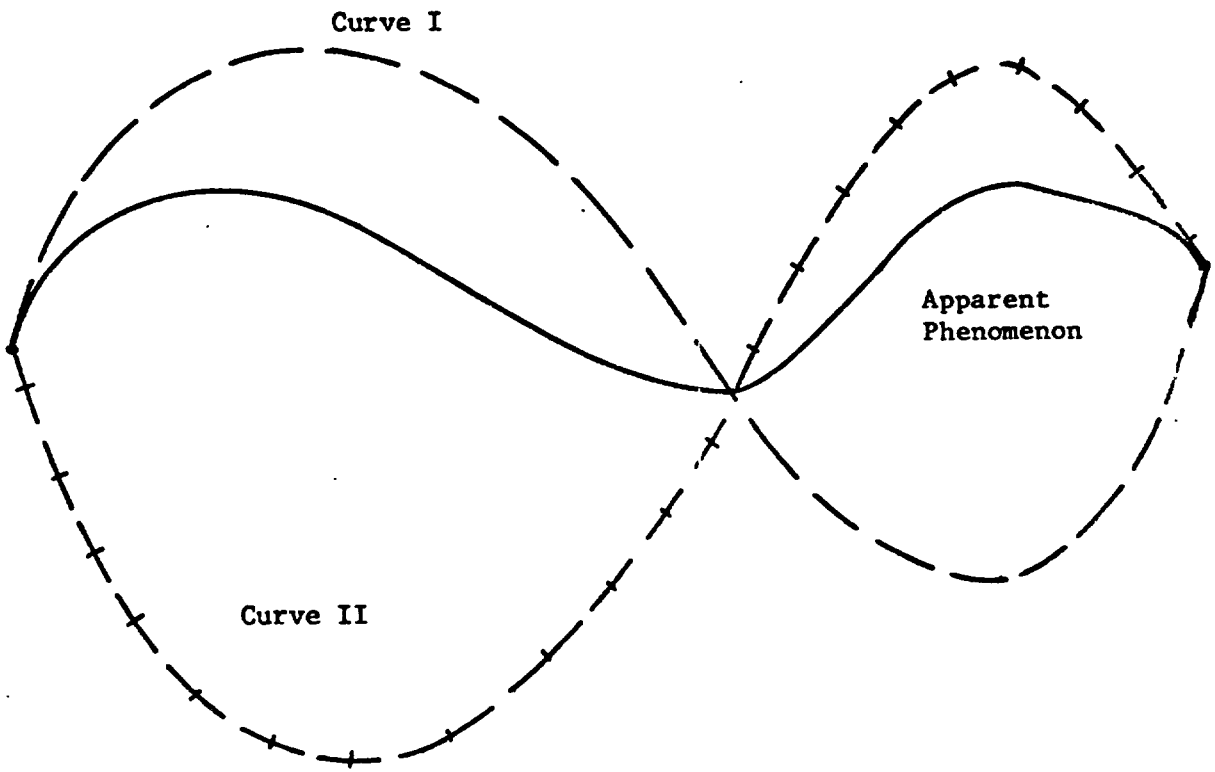

Figure 5.3 The result of a slow ship survey in a fast changing field.

Figure 5.4 Location of segments of the Gulf Stream system used to calculate annual variations in current speeds. Arrows show resultant current directions (Fuglister, 1951).

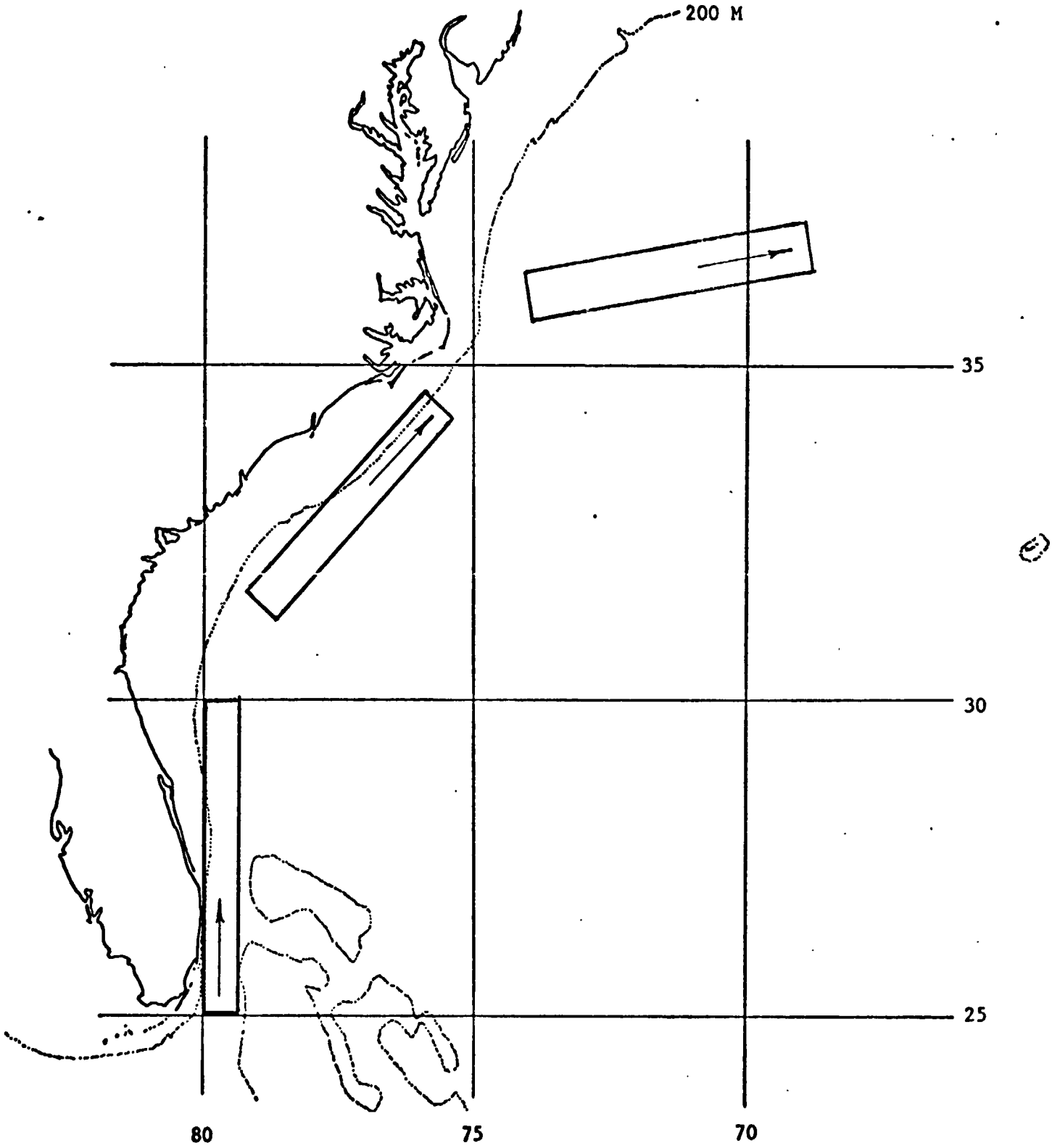
200 M
35
30
25
80
75
70

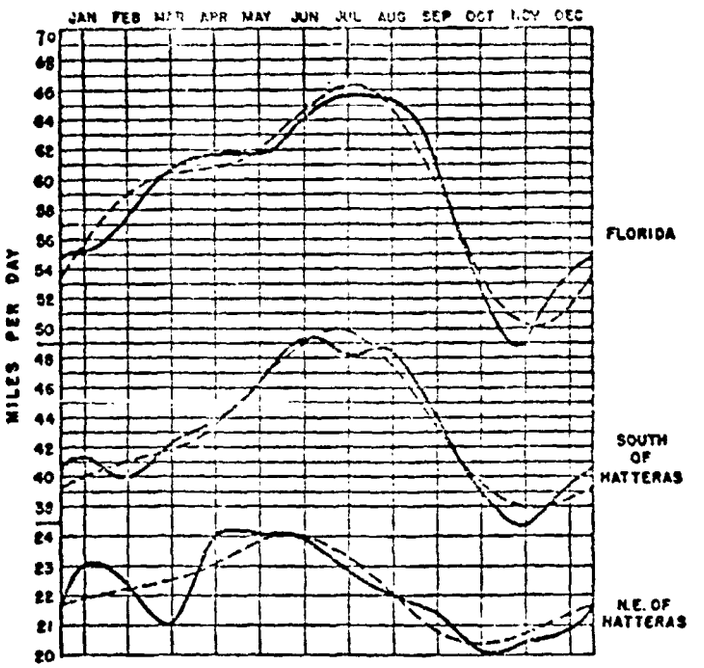

Figure 5.5 Annual variation in the current speed in three segments of the Gulf Stream system. Observed data, solid lines calculated combination of annual and semi-annual periods, dashed lines (Fuglister, 1951).

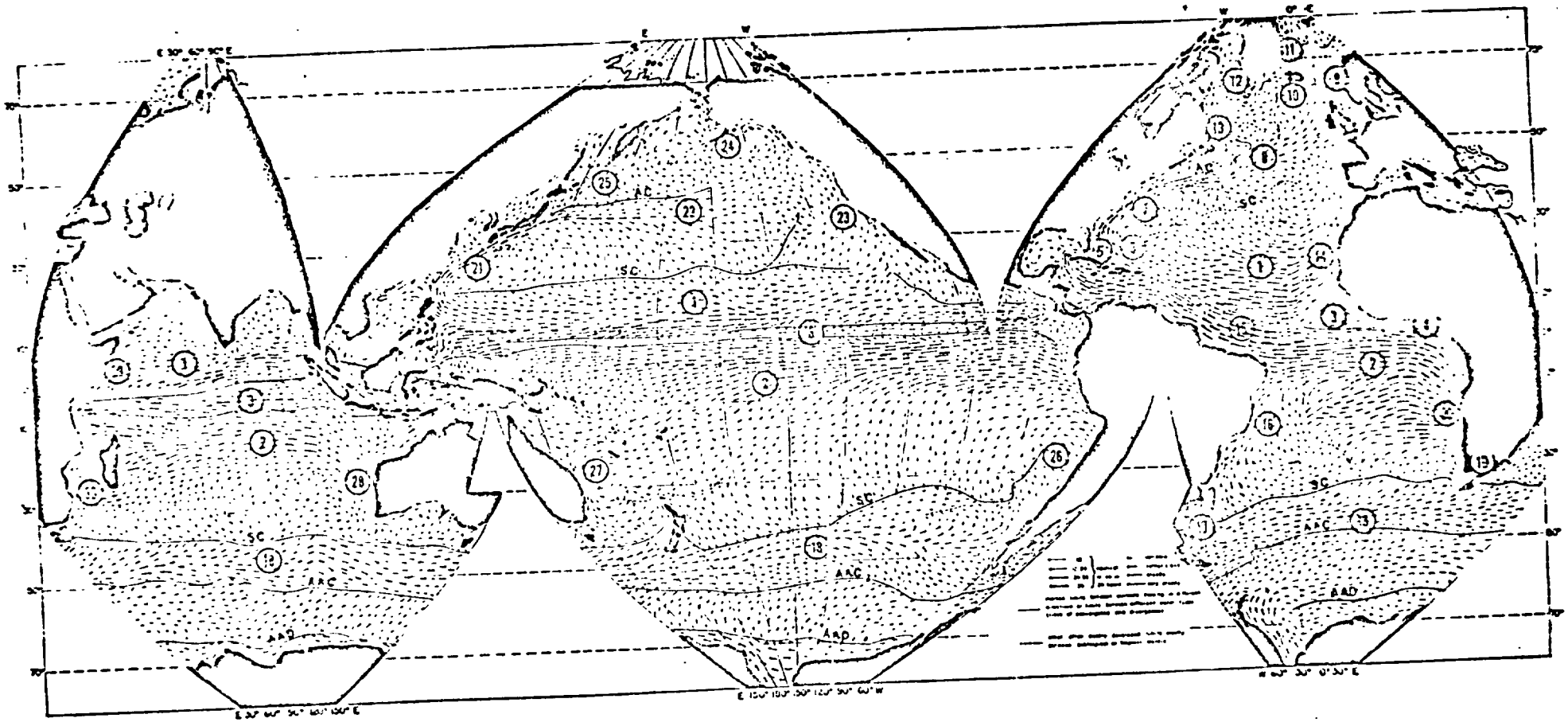

Figure 5.6 World ocean current systems (based on Neuman, 1968).

Legend: *1* = North Equatorial Current; *2* = South Equatorial Current; *3* = Equatorial Countercurrent; *4* = Guinea Current; *5* = Antilles Current; *6* = Florida Current; *7* = Gulf Stream; *8* = North Atlantic Current; *9* = Norwegian Current; *10* = Irminger Current; *11* = East Greenland Current; *12* = West Greenland Current; *13* = Labrador Current; *14* = Canary Current; *15* = Guiana Current; *16* = Brazil Current; *17* = Falkland Current; *18* = Antarctic Circumpolar Current; *19* = Agulhas Current; *20* = Benguela Current; *21* = Kuroshio; *22* = North Pacific Current; *23* = California Current; *24* = Aleutian Current; *25* = Oya Shio; *26* = Peru Current; *27* = East Australian Current; *28* = West Australian Current; *29* = Somali Current; *30* = Mozambique Current; *31* = (Indian) Monsoon Current (Northern Hemisphere summer).

REFERENCES

Banks, E. R., 1972. Isostatic and Bouguer Gravity Anomalies along the Inside Passage of Alaska and British Columbia. M.S. thesis, Oregon State Univ., 56 numb. leaves.

Bjerknes, V., 1900. Das dynamische Prinzip. der Zirkulations be wegung in der Atmosphare. Meteorol. Z., p. 97.

Bowie, W., 1912. Effect of Topography and Isostatic Compensation upon the Intensity of Gravity. U.S. Coast and Geodetic Survey Spec. Pub. No. 12.

Bowie, W., 1917. Investigations of gravity and isostasy. Wash., D. C., 196 pp. (U.S. Coast and Geodetic Survey Pub. No. 40).

Bowie, W. 1924. Isostatic investigations and data for gravity stations in the U.S. established since 1915. Wash. D. C., 91 pp. (U.S. Coast and Geodetic Survey Pub. No. 99).

Bryan, K., 1969. A numerical method for the study of the circulation of the World Ocean. J. Computational Phys., 4, 347-376.

Bryan, K. and D. Cox, 1967. A numerical investigation of the oceanic general circulation. Tellus 19, 54-80.

Bryan, K. and D. Cox, 1968. A nonlinear model of an ocean driven by wind and differential heating I, II. J. Atmos. Sci. 25, 945-967, 968-978.

Charney, J. G., 1955. The Gulf Stream as an inertial boundary layer. Proc. National Academy of Sci., 41, 731-740.

Coulomb, J. and G. Jobert, 1963. The Physical Constitution of the Earth. New York, N. Y., Hafner Press, 328 pp.

Defant, A., 1941. Die absolute Topographie des physikalischen Meeresniveaus und der Druckflachen, sowie Wasserbewegungen in Atlantischen Ozean. "Meteor"-Werk 6, 191-260.

Fofonoff, N. P., 1954. Steady flow in a frictionless homogeneous ocean. J. Marine Res., 13, 254.262.

Fomin, L. M., 1964. The Dynamic Method in Oceanography. Elsevier, Amsterdam, 212 pp.

Fuglister, F. C., 1951. Annual variations in current speeds in the Gulf Stream System. J. Marine Res., 11, 119-127.

Garland, G. D., 1965. The Earth's Shape and Gravity. Pergamon Press Ltd., London, 183 pp.

Grant, F. S. and G. F. West, 1965. Interpretation Theory in Applied Geophysics McGraw-Hill, New York, N.Y., 584 pp.

Gutenberg, B., 1959. Physics of the Earth's Interior. New York, N.Y., Academic Press, 240 pp.

Harkness, W., 1891. The solar parallax and its related constants including the figure and density of the earth. U.S. Congress. House. 51st Congress, 1st session, Miscellaneous Document., Vol. 38, Wash., D. C., 1963 pp.

Hayford, J. F. and W. Bowie, 1912. The effect of topography and isostatic compensation upon the intensity of gravity. U.S. Coast and Geodetic Survey, Spec. Pub. No. 10.

Heiskanen, W., 1928. Ist die Erde ein dreiaxchsiges Ellipsoid? Gerlands Beitr. Geophys., V. 19, pp. 356-377.

Heiskanen, W. A., 1938. New isostatic tables for the reduction of gravity values calculated on the basis of Airy's hypothesis. Helsinki, 42 p. (International Assoc. of Geodesy, Isostatic Inst. Pub. No. 2)

Heiskanen, W., 1966. Extension of the Gravity Net to the Unsurveyed Areas of the Earth; Geophysical Methods. (paper given at Ohio State Univ. Sym. on Nov. 18-20, 1964) in Gravity Anomalies; Unsurveyed Areas. Geophys. Mono. Series No. 9, American Geophys. Union pub.

Heiskanen, W. A. and F. A. Vening Meinesz, 1958. The Earth and Its Gravity Field. New York, McGraw-Hill.

Heiskanen, W. A. and H. Moritz, 1967. Physical Geodesy. San Francisco, W. H. Freeman Co.

Helland-Hansen, B., 1934. The Sognefjord section. James Johnstone Memorial Volume, Liverpool.

Helland-Hansen, B. and I. W. Sandstrom, 1903. Uber die Berechnung von Meeresstromungen. Rept. Norway Fish. and Mar. Inst.

Iselin, C. O'D., 1940. Preliminary report on long-period variations in the transport of the Gulf Stream system. Papers Phys. Oceanog. Meteorol., 8, 40 pp.

Karki, P., L. Kivioja, and W. A. Heiskanen, 1961. Topographic-isostatic reduction maps for the world for the Hayford zones 18-1, Air-Heiskanen System, T = 30 KM. Helsinki Pub. Isostat., Inst. Int. Assoc. Geod., No. 35.

Keondzhyan, V. P., 1973. Diagnostic Calculations of Current Velocities at 16 Depths in the North Atlantic. Izv. Atmos. and Ocean Phys., 8, 1297-1307.

Lineykin, P. S., 1957. On the dynamics of the baroclinic layer in the ocean. Dokl. Akad. Nank S.S.S.R., 177, 971-974.

Mohn, H., 1885. Die Stromungen des Europaischen Nordmeers. Petermanns Geogr. Mitt., Erganzungsheft, no. 79.

Morgan, G. W., 1956. On the wind-driven ocean circulation. Tellus, 8, 301-320.

Munk, W. H., 1950. On the wind driven ocean circulation. J. Meteorol., 7, 79-93.

Neumann, G., 1968. Ocean Currents. Amsterdam, Elsevier, 352 pp.

Niskanen, Effki, 1945. On the deformation of the earth's crust under the weight of a glacial ice-load and related phenomena. Isostatic Inst. Pub. No. 12.

Rao, P. K., A. E. Strong and R. Koffler, 1971. Gulf Stream meanders and eddies as seen in satellite infrared imagery. J. Phy. Oceanog., 1, 237-239.

Sarkisyan, A. S., 1969. Deficiencies of barotropic models of oceanic circulation. Izv. Atmo. Ocean Phys., 5, 818-835.

Sarkisyan, A. S., and Keondzhyan, V. P., 1972. Circulation of the surface level and total mass transport function for the North Atlantic. Izv. Atmo. Ocean Phys., 8, 1202-1215.

Seiwell, H. R., 1939. The effect of short period variations of temperature and salinity on calculations in dynamic oceanography. Papers in Phy. Oceanog. Meteorol., 7, 32 pp.

Stefannson, U. and L. P. Atkinson, 1967. Physical and chemical properties of the shelf and slope waters of North Carolina. Tech. Report, Duke Univ. Marine Lab, N. C.

Stommel, H., 1948. The westward intensification of wind-driven ocean currents. Trans. Amer. Geophys. Union, 29, 202-206.

Stommel, H., 1961. Geophysical fluid dynamics at WHOI. Ref. no. 61-39, Woods Hole, Mass.

Stommel, H., 1966. The Gulf Stream. Berkeley, U. C. Press, 248 pp.

Stumpf, H. G., 1974. Satellite-derived experimental Gulf Stream Analysis. NOAA-NESS Reports, p. 149-152.

Sturges, W., 1974. Sea level slope along continental boundaries. J. Geophys. Res., 79, 825-830.

Tsuboi, C., 1940. Isostasy and maximum earthquake energy. Proc. of the Imperial Acad. 16, 449-454.

Walcott, R. I., 1967. The Bouguer anomaly map of S. W. British Columbia. Vancouver, 74 pp., Univ. of British Columbia, Sci. Rept. No. 15.

Wertheim, G. K., 1954. Studies of the electrical potential between Key West Florida and Havana, Cuba. Trans. Am. Geophys. Union, 35, 872-882.

Worzel, J. L. and G. F. Shurbet, 1955. Gravity anomalies at continental margins. Proc. National Acad. Sci., 41, 458-469.

Zubov, N. N., 1957. Oceanological Tables.

```
C     PROGRAM DYNSAT
C     TWO STATIONS TO BE RUN AT A TIME.

      DIMENSION D(500),T(500),S(500),DD(1000),TT(1000),SS(1000)
     1,DI(550),TI(550),SI(550),KI(1000),P(1000),DYN(2,550),ALPH(1000)
     2,NSTA(3),FLA(3),FLO(3),ALP(1000),ANOM(550),DYA(550),DEAN(550)
     3,SIGT(550
.100  FORMAT (1H ,3F20.5)
 101  FORMAT(13,2F10.5)
 102  FORMAT(1H1,37HGEOSTROPHIC VELOCITY BETWEEN STATION ,I3,2H (,F5.2
     1,4H S, .F6.2,3H W),13H AND STATION , I3,2H (,F5.2,4H S .F6.2,3H W))
 1021 FORMAT(1HO.16HMEAN LATITUDE = ,F5.2,4H S , ,17HMEAN LONGITUDE =
     1,F6.2,2H W)
 1022 FORMAT(1HO,28HDISTANCE BETWEEN STATIONS = ,F8.0,8H METERS·,24H DIR
     1ECTION OF CURRENT = ,F5.1,8H DEGREES)
 103  FORMAT(1H ,F12.1,24X,F10.3)
 104  FORMAT(1HO,16H DEPTH IN METERS,10X,34HVELOCITY IN CENTIMETERS PER
     1SECOND)
 105  FORMAT(1HO)
 106  FORMAT(1H1,14HSTATION NUMBER,I3)
 107  FORMAT(1HO.8X,11HD IN METERS,3X,14HT IN DEGREES C,6X,9HS IN 0/00,
     19X,7HSIGMA T.6X,14HDYNAMIC METERS,6X,7HANOMALY,7X,11HANOMALY SUM)
 108  FORMAT(1H ,1F16.1,6F17.4)
      NINTL=10000
      DIN=10.
      II=0
 1    II=II+1
      READ 101,NSTA(II),FLA(II),FLO(II)

      IF(NSTA(II)) 201,200,201
 201  I=1
      PRINT 106,NSTA(II)

C     VALUE ESTIMATING
 2    READ 100,D(I),T(I),S(I)
      IF(S(I))4,4,3
 3    I=I+L
      GO TO 2
 4    MAXI=I-1
      D.(1)=0.0
      T.(1)=T(1)
```

```
      SI(1)=S(1)
      DD(1)=0.0
      TT(1)=T(1)
      SS(1)=S(1)
      K=1
      LI=2
      DMAX=D(MAXI)
      NINT=DMAX/DIN+1.
      XNINT=NINT
      IF(DMAX/DIN+1.-XNINT)11,12,11
11    LAST=NINT+1
      GO TO 13
12    LAST=NINT
13    DI(LAST)=D(MAXI)
      TI(LAST)=T(MAXI)
      SI(LAST)=S(MAXI)
      DO 5 I=2,NINT
      XIM=I-1
      DINT=XIM*DIN
      IF(MAXI-LI)5,61,61
61    DO 6 J=LI,MAXI
      IF(D(J)-DINT)7,8,9
7     K=K+1
      DD(K)=D(J)
      TT(K)=T(J)
      SS(K)=S(J)
      GO TO 6
8     K=K+1
      DD(K)=D(J)
      TT(K)=T(J)
      SS(K)=S(J)
      TI(1)=TT(K)
      SI(I)=SS(K)
      DI(I)=DINT
      KI(I)=K
      LI=J+1
      GO TO 5
9     K=K+1
      DD(K)=DINT
      TT(K)=((T(J)-T(J-1))*(DINT-D(J-1)))/(D(J)-D(J-1))+T(J-1)
      SS(K)=((S(J)-S(J-1))*(DINT-D(J-1)))/(D(J)-D(J-1))+S(J-1)
      TI(I)=TT(K)
```

```
      SI(I)=SS(K)
      DI(I)=DINT
      KI(I)=K
      LI=J
      GO TO 5
 6    CONTINUE
 5    CONTINUE
      IF(MAXI-LI)52,51,51
 51   DO 10 J=LI,MAXI
      K=K+1
      DD(K)=D(J)
      TT(K)=T(J)
      SS(K)=S(J)
 10   CONTINUE
 52   KI(1)=1
      KI(LAST)=K
C     IMPLICATION OF DYNAMIC DEPTH
      P(1)=0.0
      DEAN(1)=0.0
      ANOM(1)=0.0
      ALP(1)=ALPHA(0.0,0.0,35.0)
      DYA(1)=0.0
      ALPH(1)=ALPHA(P(1),TT(1),SS(1))
      DYA(1)=0.0
      ALPH(1)=ALPHA(P(1),TT(1),SS(1))
      SIGT(1)=(1./ALPH(1)-1.)*1000.
      DYN(II.1)=0.0
      DO 15 I-2,LAST
      DYA(I)=DYA(I-1)
      DYN(II,I)=DYN(II,I-1)
      KS=KI(I-1)+1
      KF=KI(I)
      IF(KF-KS)15,161,161
 161  DO 16 J=KS,KF
      P(J)=1.009785*DD(J)+2.293478E-6*DD(J)*DD(J)
      ALP(J)=ALPHA(P(J),0.0,35.0)
      DYA(I)=DYA(I)+(ALP(J)+ALP(J-1))*(P(J)-P(J-1))/2.
      ALPH(J)=ALPHA(P(J),TT(J),SS(J))
      DYN(II,I)=DYN(II,I)+(ALPH(J-1))*(P(J-1)-P(J-1))/2.
 16   CONTINUE
      ANOM(I)=(DYN(II,I)-DYA(I)*100000.
      DEAN(I)=ANOM(I)-ANOM(I-1)
```

```
      SIGT(I)=(1./ALPHA(0.0,TI(I),SI(I))-1.)*1000.
 15   CONTINUE
      PRINT 107
      PRINT 105
      DO 20 I=1.LAST
      PRINT 108,DI(I),TI(I),SI(I),SIGT(I),DYN(II,I),DEAN(I),ANOM(I)
 20   CONTINUE
      IF (NINT-NINTL)203,1,1
 203  NINTL=NINT
      GO TO 1
 200  CONTINUE
C     CALCULATION OF GEOSTROPHY
      GLAT=(FLA(1)+FLA(2))/2.
      GLON=(FLO(1)+FLO(2))/2.
      DLON=(FLO(2)-FLO(1))*COS(GLAT/57.29578)
      DLAT=FLA(2)-FLA(1)
      IF(DLON)21,22,23
 21   IF(DLAT)24,25,25
 24   DIR=90.+ATAN(DLAT/DLON)*57.29578
      GO TO 30
 25   DIR=180.-ATAN(DLAT/DLON)*57.29578
      GO TO 30
 23   IF(DLAT)26,26,27
 26   DIR=-ATAN(DLAT/DLON)*57.29578
      GO TO 30
 27   DIR=270.+ATAN(DLAT/DLON)*57.29578
      GO TO 30
 22   IF(DLAT)28,29,29
 28   DIR=90.
      GO TO 30
 29   DIR=270.
 30   DLAA=FLA(1)/57.29578
      DLAB=FLA(2)/57.29578
      DLOA=FLO(1)/57.29578
      DLOB=FLO(2)/57.29578
      CDIST=-COS(DLAA)*COS(DLAB)*(1.-COS(DLOA-DLOB))+COS(DLAA-DLAB)
      DIST=ARCOS(CDIST)*6371004.2
      PRINT 102,NSTA(1),FLA(1),FLO(1),NSTA(2),FLA(2),FLO(2)
      PRINT 1021,GLAT,GLON
      PRINT 1022,DIST,DIR
      PRINT 104
      PRINT 105
```

```
      COR=6856710./(DIST*SIN(GLAT/57.29578))
      DO 19 I=1,NINTL
      DVELC=COR*(DYN(1,I)-DYN(2,I))
      PRINT 103,DI(I),DVELC
19    CONTINUE
      END
```